# การออกแบบและการวิเคราะห์หน่วยฟลูอิดคะตะไลติกแครกกิงเพื่อการผลิตแก๊สโซลีน

นายอานนท์ ฉั่วชื่นสุข

วิทยานิพนธ์นี้เป็นส่วนหนึ่งของการศึกษาตามหลักสูตรปริญญาวิศวกรรมศาสตรดุษฎีบัณฑิต
สาขาวิชาวิศวกรรมเคมี ภาควิชาวิศวกรรมเคมี
คณะวิศวกรรมศาสตร์ จุฬาลงกรณ์มหาวิทยาลัย
ปีการศึกษา 2555

# DESIGN AND ANALYSIS OF FLUID CATALYTIC CRACKING UNIT FOR GASOLINE PRODUCTION

Mr. Anon Chuachuensuk

A Dissertation Submitted in Partial Fulfillment of the Requirements
for the Degree of Doctor of Engineering Program in Chemical Engineering
Department of Chemical Engineering
Faculty of Engineering
Chulalongkorn University
Academic Year 2012

| | |
|---|---|
| Thesis Title | DESIGN AND ANALYSIS OF FLUID CATALYTIC CRACKING UNIT FOR GASOLINE PRODUCTION |
| By | Mr. Anon Chuachuensuk |
| Field of Study | Chemical Engineering |
| Thesis Advisor | Assistant Professor Amornchai Arpornwichanop, D.Eng. |

Accepted by the Faculty of Engineering, Chulalongkorn University in Partial Fulfillment of the Requirements for the Doctoral Degree

…….…….Dean of the Faculty of Engineering
(Associate Professor Boonsom Lerdhirunwong, Dr.Ing.)

THESIS COMMITTEE

……..Chairman
( Associate Professor Muenduen Phisalaphong, Ph.D.)

……..Thesis advisor
(Assistant Professor Amornchai Arpornwichanop, D.Eng.)

……..Examiner
(Assistant Professor Apinan Soottitantawat, D.Eng.)

……..Examiner
(Assistant Professor Soorathep Kheawhom, Ph.D.)

……..External examiner
(Assistant Professor Woranee Paengjuntuek, D.Eng.)

อานนท์ ฉั่วชื่นสุข : การออกแบบและการวิเคราะห์หน่วยฟลูอิดคะตะไลติกแครกกิงเพื่อการผลิตแก๊สโซลีน. (DESIGN AND ANALYSIS OF FLUID CATALYTIC CRACKING UNIT FOR GASOLINE PRODUCTION) อ.ที่ปรึกษาวิทยานิพนธ์หลัก : ผศ.ดร.อมรชัย อาภรณ์วิชานพ, 133 หน้า.

งานวิจัยนี้มุ่งเน้นการออกแบบและการวิเคราะห์ประสิทธิภาพของหน่วยฟลูอิดคะตะไลติกแครกกิงซึ่งประกอบไปด้วยเครื่องปฏิกรณ์และหน่วยฟื้นฟูประสิทธิภาพตัวเร่งปฏิกิริยา และสามารถแบ่งออกได้เป็นสามส่วนหลักดังนี้ ส่วนแรกเป็นการศึกษาการวิเคราะห์อย่างเป็นระบบโดยอ้างอิงจากแบบจำลองของหน่วยฟื้นฟูประสิทธิภาพตัวเร่งปฏิกิริยาชนิดไหลลงเพื่อใช้ในการฟื้นฟูประสิทธิภาพของตัวเร่งปฏิกิริยาของกระบวนการฟลูอิดคะตะไลติกแครกกิง แบบจำลองทางคณิตศาสตร์แบบหนึ่งมิติของหน่วยฟื้นฟูประสิทธิภาพตัวเร่งปฏิกิริยาที่ใช้ประกอบไปด้วยลักษณะของการไหลและจลนศาสตร์ของการฟื้นฟูสภาพตัวเร่งปฏิกิริยา ผลลัพธ์ที่ได้จากวิเคราะห์พบว่าตัวเร่งปฏิกิริยาที่มีปริมาณคาร์บอนสูงทำให้อุณหภูมิที่ใช้ในการฟื้นฟูสภาพตัวเร่งปฏิกิยามีค่าสูง อัตราส่วนของตัวเร่งปฏิกิริยาหมุนเวียนต่อตัวเร่งปฏิกิริยาที่ผ่านการใช้งานแล้วในช่วง 1.0-3.5 และอุณหภูมิของตัวเร่งปฏิกิริยาที่ผ่านการใช้งานแล้วในช่วง 703.15-803.15 เคลวิน ไม่มีผลต่อประสิทธิภาพโดยรวมของหน่วยฟื้นฟูสภาพตัวเร่งปฏิกิริยา ความเร็วของก๊าซที่และอัตราการไหลของตัวเร่งปฏิกิริยาที่ผ่านการใช้งานแล้วที่เหมาะสมมีค่าในช่วง 4-7 เมตรต่อวินาที และ 20-40 กิโลกรัมต่อตารางเมตรต่อวินาที ตามลำดับ งานต่อมาได้ทำการศึกษาประสิทธิภาพของการฟื้นฟูสภาพตัวเร่งปฏิกิริยาในกระบวนการฟลูอิดคะตะไลติกแครกกิงโดยการพิจารณาปฏิกิริยาการแก๊สซิฟิเคชันด้วยไอน้ำร่วมกับปฏิกิริยาการเผาไหม้โดยใช้แบบจำลองทางคณิตศาสตร์ในหนึ่งมิติของหน่วยฟื้นฟูสภาพตัวเร่งปฏิกิริยาชนิดไหลลงซึ่งประกอบไปด้วยลักษณะทางการไหลและจลนศาสตร์ของปฏิกิริยา ผลจากการจำลองกระบวนการแสดงให้เห็นว่าปฏิกิริยาแก๊สซิฟิเคชันด้วยไอน้ำซึ่งเป็นปฏิกิริยาดูดความร้อนสามารถช่วยลดอุณหภูมิของการฟื้นฟูสภาพตัวเร่งปฏิกิริยาลงได้และให้ไฮโดรเจนเป็นผลพลอยได้ที่มีมูลค่าสูง และตอนท้ายได้ทำการศึกษาประสิทธิภาพของระบบร่วมของเครื่องปฏิกรณ์ชนิดไหลลงและหน่วยฟื้นฟูสภาพตัวเร่งปฏิกิริยาชนิดไหลขึ้น โดยใช้แบบจำลองทางคณิตศาสตร์ในหนึ่งมิติของเครื่องปฏิกรณ์ชนิดไหลลงและหน่วยฟื้นฟูสภาพตัวเร่งปฏิกิริยาชนิดไหลขึ้น ผลจากการจำลองกระบวนการโดยศึกษาอิทธิพลของอัตราส่วนของตัวเร่งปฏิกิริยาต่อน้ำมันซึ่งเป็นตัวแปรหลักที่ใช้ในการออกแบบเครื่องปฏิกรณ์แสดงให้เห็นว่าที่อัตราส่วนของตัวเร่งปฏิกิริยาต่อน้ำมันมีค่าเท่ากับ 20 ระบบร่วมจะสามารถทำงานได้อย่างมีประสิทธิภาพโดยจะมีค่าการเปลี่ยนเท่ากับ 0.85 และผลได้ของแก๊สโซลีนเท่ากับ 0.55 และยังสามารถรักษาสมดุลทางความร้อนไว้ได้

ภาควิชา วิศวกรรมเคมี ลายมือชื่อนิสิต .....

สาขาวิชา วิศวกรรมเคมี ลายมือชื่อ อ.ที่ปรึกษาวิทยานิพนธ์หลัก .....

ปีการศึกษา 2555 .....

# # 5071830621 : MAJOR CHEMICAL ENGINEERING
KEYWORDS : DOWNER REGENERATOR / DOWNER REACTOR / RISER REGENERATOR / SIMULATION

ANON CHUACHUENSUK : DESIGN AND ANALYSIS OF FLUID CATALYTIC CRACKING UNIT FOR GASOLINE PRODUCTION. ADVISOR : ASST. PROF. AMORNCHAI ARPORNWICHANOP, D.Eng., 133 pp.

This study concentrated on the design and analysis of a fluid catalytic cracking process consisting of a reactor and a regenerator and can be divided into three main parts. Firstly, the performance improvement of a catalytic regenerator in the fluid catalytic cracking (FCC) process for gasoline production to achieve a higher burning efficiency was focused. This study performed a systematic model-based analysis of a downer-type regenerator to recover the activity of FCC catalyst by using a one-dimensional model of the regenerator coupled with its hydrodynamic characteristics and the kinetics of catalyst regeneration. The results of a sensitivity analysis showed that higher carbon content on spent catalyst causes a higher regeneration temperature. Ratio of the recycled-to-spent catalyst flow rate in range of 1.0-3.5 and temperatures of the spent catalyst in range of 703.15-803.15 K have insignificant effects on the overall performance of the regenerator. The suitable superficial gas velocity and the spent catalyst flow rate are in range of 4-7 m $s^{-1}$ and 20-40 kg $m^{-2}$ $s^{-1}$, respectively. Next, the performance of the regeneration of the FCC catalyst by considering the steam gasification reaction with burning reaction was studied. The simulation results show that the steam gasification reaction which is an endothermic reaction can help reduce the regeneration temperature and gives hydrogen as a valuable byproduct. Finally, an integrated downer reactor and riser regenerator system was studied based on the one-dimensional model of the downer reactor and riser regenerator. The simulation results on the effect of the catalyst-to-oil (CTO) ratio which is the key parameter in designing the FCC reactor reveal that at the CTO ratio of 20, the integrated system can operate efficiently with the conversion of gasoil of 0.85 and the yield of gasoline of 0.55. Moreover, the heat balance of the system can be maintained under this operating condition.

Department : Chemical Engineering Student's Signature .....

Field of Study : Chemical Engineering Advisor's Signature .....

Academic Year : 2012 .....

# ACKNOWLEDGEMENTS

I wish to express my foremost and deep sense of gratitude to Assistant Professor Amornchai Arpornwichanop for his considerable encouragement, meticulous guidance, and continuous support throughout the period of study. I am very fortunate to have such an expert academician who has been a source of inspiration and perseverance in completing of this research work.

I am very sincerely acknowledged to the member of examiners, Associate Professor Muenduen Phisalaphong, Assistant Professor Apinan Soottitantawat, Assistant Professor Soorathep Kheawhom, and Assistant Professor Woranee Paengjuntuek for their valuable comments and helpful suggestions.

Much appreciation is extended to Professor Jesse Zhu, Particle Technology Research Center (PTRC), Department of Chemical and Biochemical Engineering, Faculty of Engineering, The University of Western Ontario who give me the excellent opportunity to join his research group. His helpful discussion, encouraging guidance, and wonderful ideas are great of benefit to me and these bring great understanding and improvement of comprehensive skills in the gas-solid fluidization area.

I am thankful to PTT public company limited for their grant support during my study and the Graduate School of Chulalongkorn University for giving the 90th Anniversary of Chulalongkorn University Fund (Ratchadaphiseksomphot Endowment Fund), Conference Grant for Ph.D. Student and Ph.D. Scholarship for research abroad. Financial support from the Computational Process Engineering research group, the Special Task Force for Activating Research (STAR), Chulalongkorn University Centenary Academic Development Project is also gratefully acknowledged.

My sincere thanks are due to Dr. Yaneeporn Patcharavorachot, Dr. Dang Saebea, and Dr. Suthida Authayanan who always encourage, advice, and assist me both morally and technically. I would thank my fellow students in the Control and Systems Engineering Research Center; especially Aritsara Saengchan, Narissara Chatrattanawet, Bhawasut Chutichai, Phanicha Tippawan and Prathak Jienkulsawad for their help, friendship and encouragement.

Finally and most importantly, I wish to express my greatest appreciation toward my beloved father, mother and sister for their endless love and continuous support. They are the source of inspiration and encouragement. This research work cannot be accomplished without them.

# CONTENTS

PAGE

CHAPTER PAGE

CHAPTER PAGE

CHAPTER PAGE

CHAPTER PAGE

# LIST OF TABLES

# LIST OF FIGURES

FIGURE PAGE

FIGURE PAGE

FIGURE PAGE

# LIST OF ABBREVIATIONS

| | |
|---|---|
| $API$ | API gravity |
| $a$ | Recycled to spent catalyst flow rate ratio (= $G_{sr}/G_{ss}$) |
| $A$ | Cross-sectional area [$m^2$] |
| $A_{lg}$ | Coefficient of the Antoine equation for gasoil feedstock |
| $A_p$ | Effective interface heat transfer area per unit volume between catalyst and gas phases in reactor [$m^2\ m^{-3}$] |
| $B_{lg}$ | Coefficient of the Antoine equation for gasoil feedstock |
| $C$ | Concentration [kg kg catalyst$^{-1}$ ; kmol $m^{-3}$] |
| $C_{Cs}$ | Carbon content on spent catalyst [kg kg catalyst$^{-1}$] |
| $C_D$ | Drag coefficient |
| $C_{Ds}$ | Standard drag coefficient |
| $C_{lg}$ | Coefficient of the Antoine equation for gasoil feedstock |
| $C_p$ | Heat capacity [kJ $kg^{-1}$ $K^{-1}$] |
| $C_{pm}$ | Mean heat capacity [kJ $kg^{-1}$ $K^{-1}$] |
| $d_p$ | Diameter of catalyst particle [m] |
| $D$ | Diameter of riser or downer [m] |
| $E_a$ | Activation energy [kJ $kmol^{-1}$] |
| $E_\beta$ | Activation energy for $CO/CO_2$ ratio at surface (given in the form of E/R) [K] |

$E_{3c}$ Activation energy for catalytic CO combustion (given in the form of E/R) [K]

$E_c$ Activation energy for overall coke combustion (given in the form of E/R) [K]

$f_g$ Friction coefficient between gas and wall

$f_s$ Friction coefficient between solid and wall

$F$ Mass flow rate [kg $s^{-1}$]

$F_D$ Drag force between gas and particle [kg m $s^{-2}$]

$F_{fg}$ Friction force between gas and wall [kg m $s^{-2}$]

$F_{fs}$ Friction force between solid and wall [kg m $s^{-2}$]

$Fr$ Froude number, $Fr = U\mathrm{g} / \left( g\, d_{\mathrm{p}} \right)^{1/2}$

$g$ Acceleration due to gravity [m $s^{-2}$]

$G_g$ Gas flow rate (based on cross-sectional area of downer) [kg $m^{-2}$ $s^{-1}$]

$G_s$ Total solid flow rate (based on cross-sectional area of downer $(= G_{ss} + G_{sr})$ [kg $m^{-2}$ $s^{-1}$]

$G_{sr}$ Recycled catalyst flow rate (based on cross-sectional area of downer) [kg $m^{-2}$ $s^{-1}$]

$G_{ss}$ Spent catalyst flow rate (based on cross-sectional area of downer) [kg $m^{-2}$ $s^{-1}$]

$h_p$ Interface heat transfer coefficient between the catalyst and gas phases in the reactor [kJ $m^2$ $s^{-1}$ $K^{-1}$]

| | |
|---|---|
| $k_1$ | Rate constant for incomplete burning reaction [$kPa^{-1}\ s^{-1}$] |
| $k_2$ | Rate constant for incomplete burning reaction [$kPa^{-1}\ s^{-1}$] |
| $k_{3c}$ | Rate constant for catalytic combustion of CO reaction [kmol $m^{-3}\ s^{-1}$] |
| $k_{3c,0}$ | Pre-exponential factor for catalytic CO combustion reaction [kmol $kg^{-1}$ $kPa^{-2}\ s^{-1}$] |
| $k_{3h}$ | Rate constant for homogeneous combustion reaction [kmol $m^{-3}$ $kPa^{-2}$ $s^{-1}$] |
| $k_{3h,0}$ | Pre-exponential factor for homogeneous CO combustion reaction [kmol $m^{-3}$ $kPa^{-2}\ s^{-1}$] |
| $k_4$ | Rate constant for hydrogen burning reaction [$kPa^{-1}\ s^{-1}$] |
| $k_{4,0}$ | Pre-exponential factor for hydrogen burning reaction [$kPa^{-1}\ s^{-1}$] |
| $k_C$ | Carbon combustion reaction constant [$kPa^{-1}\ s^{-1}$] |
| $k_{C,0}$ | Pre-exponential factor for overall coke combustion [$kPa^{-1}\ s^{-1}$] |
| $k_g$ | Thermal conductivity of hydrocarbon [kJ $s^{-1}$ $m^{-1}$ $K^{-1}$] |
| $k_{gf}$ | Rate constant for gasification reaction [ $s^{-1}$] |
| $k_H$ | Hydrogen combustion reaction constant [$kPa^{-1}\ s^{-1}$] |
| $K_f$ | Watson characterization factor [$K^{1/3}$] |
| $M_w$ | Molecular weight [kg $kmol^{-1}$] |
| $M_{wm}$ | Mean molecular weight [kg $kmol^{-1}$] |
| $n_t$ | Total mole [mol] |
| $p_{O_2}$ | Partial pressure of oxygen [kPa] |

| | |
|---|---|
| $P$ | Pressure [kPa] |
| $P_{pc}$ | Pseudo-critical pressure [kPa] |
| $P_{pr}$ | Pseudo-reduced pressure [kPa] |
| $Q_{react}$ | Rate of heat generation of removal by reaction [kJ $s^{-1}$] |
| $r$ | Reaction rate [$s^{-1}$; kg kg $catalyst^{-1}$ $s^{-1}$] |
| $r_1$ | Reaction rate of incomplete burning reaction [kg kg $catalyst^{-1}$ $s^{-1}$] |
| $r_2$ | Reaction rate of complete burning reaction [kg kg $catalyst^{-1}$ $s^{-1}$] |
| $r_{3c}$ | Reaction rate of catalytic CO combustion reaction [kmol $m^{-3}$ $s^{-1}$] |
| $r_{3h}$ | Reaction rate of homogeneous CO combustion reaction [kmol $m^{-3}$ $s^{-1}$] |
| $R$ | Ideal gas constant (=8.314) [ kJ $kmol^{-1}$ $K^{-1}$] |
| $R_{AN}$ | Aromatics to naphthenes ratio in a liquid feedstock |
| $\mathrm{Re}_g$ | Reynolds number defined by $\mathrm{Re}_g = \dfrac{\rho_g U_g D}{\mu_g}$ |
| $\mathrm{Re}_r$ | Reynolds number defined by $\mathrm{Re}_r = \dfrac{d_p \rho_g \left\lvert \bar{V}_g - \bar{V}_s \right\rvert}{\mu_g}$ |
| $S_g$ | Specific gravity |
| $T$ | Temperature [K] |
| $T_a$ | Air temperature at inlet [K] |
| $T_g$ | Regenerated catalyst temperature [K] |
| $T_{MABP}$ | Molal average boiling temperature [K] |
| $T_{MeABP}$ | Mean average boiling temperature [K] |

| | |
|---|---|
| $T_{pc}$ | Pseudo-critical temperature [K] |
| $T_{pr}$ | Pseudo-reduced temperature [K] |
| $T_s$ | Spent catalyst temperature [K] |
| $T_v$ | Normal boiling point [K] |
| $T_{VABP}$ | Volume average boiling temperature [K] |
| $U_g$ | Superficial gas velocity [m $s^{-1}$] |
| $\bar{V}$ | Cross-sectionally averaged velocity [m $s^{-1}$] |
| $y_i$ | Weight fraction |
| $z$ | Reactor or regenerator length [m] |

**Greek letters**

| | |
|---|---|
| $\alpha$ | Mass ratio of hydrogen to carbon in coke |
| $\alpha_c$ | Catalyst deactivation coefficient |
| $\alpha_{C0}$ | Pre-exponential factor of catalyst deactivation coefficient |
| $\alpha_C^*$ | Exponent for representing $\alpha_C$ |
| $\beta$ | Molar ratio of $CO_2$ to CO in the flue gas |
| $\beta_C$ | Initial ratio of $CO/CO_2$ at catalyst surface |
| $\beta_{C,0}$ | Pre-exponential factor for $CO/CO_2$ ratio at surface |
| $\Delta H_C$ | Enthalpy due to carbon combustion [kJ $kg^{-1}$] |
| $\Delta H_f$ | Heat of formation [kJ $kmol^{-1}$] |
| $\Delta H_H$ | Enthalpy due to hydrogen combustion [kJ $kg^{-1}$] |
| $\Delta H_i$ | Heat of reaction for four-lump cracking reaction [kJ $kg^{-1}$] |

| | |
|---|---|
| $\Delta H_r$ | Heat of reaction [kJ kmol$^{-1}$] |
| $\Delta H_{v\lg}$ | Heat of vaporization of liquid feedstock [kJ kg$^{-1}$] |
| $\overline{\varepsilon}_g$ | Cross-sectionally averaged voidage |
| $\overline{\varepsilon}_s$ | Cross-sectionally averaged solid holdup |
| $\eta$ | Correction factor for drag coefficient |
| $\mu$ | Viscosity [Pa s] |
| $\mu_m$ | Mean viscosity [Pa s] |
| $\mu_{pc}$ | Pseudo-critical viscosity [Pa s] |
| $\mu_{pr}$ | Pseudo-reduced viscosity [Pa s] |
| $\rho$ | Density [kg m$^{-3}$] |
| $\phi_c$ | Catalyst deactivation function |

**Subscripts**

| | |
|---|---|
| 0 | Initial condition |
| *ck* | Coke |
| *C* | Carbon atom |
| *CL* | Catalyst transport line |
| *CO* | Carbon monoxide |
| $CO_2$ | Carbon dioxide |
| *ds* | Disperse steam |
| *FS* | Feed vaporization section |
| *g* | Gas phase |

| | |
|---|---|
| *gf* | Gasification |
| *gl* | Gasoline |
| *go* | Gas oil |
| *gs* | $C_1$-$C_4$ gases |
| *H* | Hydrogen atom |
| $H_2O$ | Water |
| *lg* | Liquid feedstock (gas oil) |
| *out* | Outlet condition |
| *ref* | Reference condition (273.15 K) |
| *reg* | Regenerator |
| *rxt* | Reactor |
| *s* | Gas phase |
| *wv* | Water vapor |

# CHAPTER I

# INTRODUCTION

## 1.1 Background and motivation

A fluid catalytic cracking (FCC) is an important process in oil refinery industries. The purpose of this process is to crack low-value heavy hydrocarbons (e.g., gas oil) to valuable light products (e.g., gasoline). It is known that FCC and its ancillary units provide about 45% of the total gasoline production and the revenue about 40% of the total refinery's income (Sadeghbeigi, 2000; Ramachandran et al., 2007; Roman et al., 2009). Due to environmental awareness and requirement of high-quality products, a further improvement of FCC performance is still needed.

In general, an FCC process is composed of two major units: a reactor and a regenerator. The strong interaction between these two units causes the complexity of the process. Cracking reactions of long-chain hydrocarbons are carried out in the FCC reactor. In the past, it was mostly operated in a riser mode in which hydrocarbon feedstock and catalyst were fed at the bottom of the reactor. Presently, a gas-solid concurrent down-flow reactor, which is also known as a downer, is found to be a promising reactor for the FCC process because it can overcome the drawback of a conventional up-flow reactor (or the riser) caused by the catalyst back-mixing (Talman and Reh, 2001; Chen et al., 2005; Qi et al., 2008; Wu et al., 2008). In the downer, gas and solid catalyst move downward; this can avoid the back-mixing of catalyst and reduce hot spots that may occur in the riser reactor (Zhu et al., 1995). Many previous studies showed that the operation of the downer reactor nearly reaches the plug-flow condition (Wei and Zhu, 1996; Talman et al., 1999; Liu et al., 2006; Cheng et al., 2008; Qi et al., 2008; Wu et al., 2010; Zhao et al., 2010). In addition, both experimental and simulated results suggest that using the downer as a reactor in a fluid catalytic cracking process can improve both yield and selectivity of the desired products (Abul-Hamayel, 2004; Wu et al., 2009). However, the knowledge of the

downer reactor in the literature usually considers only the downer itself, with only a few studies give details about the accompanying regenerator (Shaikh et al., 2008). Since the reactor and the regenerator are operated simultaneously, the study of the integrated system would be beneficial for understanding the behaviour of the system.

In the FCC regenerator, coke deposited on catalyst's surface is eliminated by combustion reactions (Sadeghbeigi, 2000). The recent trend of using low-quality feedstock for the FCC process causes high carbon content on the spent catalyst surface. This leads to the rapid deactivation of catalyst and extreme regeneration operation with high temperatures, which will deactivate the catalyst permanently. Different types of the FCC regenerator have been proposed to improve its burning efficiency. An example of a regenerator design is a high-efficiency regenerator in which the bottom chamber of the regenerator is operated in the turbulent fluidized bed state, thereby resulting in a better gas-solid contact efficiency and smaller vessel. A regenerator with two-stage combustion is another design. The first stage combustion is used to burn most of the hydrogen-rich compounds and also the majority of the carbon deposited on the catalyst surface at low temperatures within a short time, whereas the second one is applied to combust the remaining carbon at high temperatures with a longer time. This prevents the exposure of catalyst to high temperature steam occurred from the burning of hydrogen-rich components that may cause the permanent deactivation of the catalyst (Avidan and Shinnar, 1990).

The other new developed regenerator is referred to as a riser regenerator because it operates in the riser mode having the advantages of high heat and mass transfers and high solid-gas contact efficiency (Bai et al., 1997, 1998). However, the operation of the riser in which gas and solid flowing against the direction of gravity suffers from the severe back-mixing and non-uniform flow structure causing the wide residence time distribution of the gas and solid phases (Werther and Hirschberg, 1997; Jin et al., 2002). Since the radial distributions of gas and solid in a downer is more uniform than that in a riser, the use of the downer as a regenerator would be a promising approach.

Another approach for enhancing of regeneration is considering the reactions, some research works have been done on studying the possibility of the coke steam gasification reaction for converting some part of coke into hydrogen in the regeneration environment while the another part is still eliminated by burning for maintaining the system heat balance. Consideration of gasification reaction together with the burning reaction has the benefit of temperature reduction. Since the steam reforming reaction is the endothermic reactor, thereby, it can help reduce the high temperature caused by burning high amount of carbon deposited on spent catalyst from reactor.

In this study, the performance of a downer regenerator of FCC process is analyzed based on a systematic model-based approach. A one-dimensional model of the downer regenerator, which consists of mass and energy conservative equations, hydrodynamic characteristics, and regeneration kinetics of FCC catalyst under steady state condition, is employed to perform a sensitivity analysis of the regenerator with respect to key operating parameters such as recycled and spent catalyst flow rates, superficial gas velocity, carbon content on spent catalyst, and spent catalyst temperature, on the catalyst regeneration performance.

However, the steam gasification can proceed at the limited condition. Therefore, this work also investigates the steam gasification together with combustion for regeneration of the FCC catalyst in a downer-type regenerator via simulation study.

Moreover, this work carries out a theoretical analysis of an integrated system between downer reactor and riser regenerator in the FCC process for investigation of the performance of this integrated system.

## 1.2 Objective of Research

The objective of this research is mainly focus on a performance analysis and design of a regenerator in the FCC process operated with the down-flow operation as well as the theoretical investigation on an integrated system of a downer reactor and a riser regenerator.

## 1.3 Scopes of Research

The scopes of this research are listed as follow:

- Analyze the performance of the downer regenerator using a systematic model-based process analysis.
- Investigate the steam gasification reaction together with combustion reaction for regeneration of the FCC catalyst in the downer regenerator using one-dimensional model of hydrodynamic characteristics and kinetic models including burning and gasification reactions.
- Analyze the performance of the integrated system of a downer reactor and a riser regenerator using one-dimensional model of hydrodynamic characteristics of both riser and downer incorporated with kinetic models of cracking reactions and coke burning reactions.

# CHAPTER II

# LITERATURE REVIEWS

This chapter presents the literature review about the researches focusing on the fluid catalytic cracking (FCC) unit and its crucial characteristics in various aspects. The content begins with the investigation on riser reactor model. Next, the evolution of FCC regenerator is discussed. Then, the works on downers in FCC process as well as the steam reforming process were reviewed.

## 2.1 Investigation on riser reactor models

Riser has been used as a reactor in the fluid catalytic cracking for a long time (Avidan and Shinnar, 1990). Numerous models have been published to predict and analyze the performance of the riser and even the whole process including steady-state model (Araujo-Monroy and Lopez-Isunza, 2005; Heydari et al., 2010), dynamic model (Han and Chung, 2001; Bollas et al., 2007; Fernandes et al., 2007; Roman et al., 2009), computational fluid dynamic model (CFD) (Theologos et al., 1996; Das et al., 2003; Lan et al., 2009; Lopes et al., 2011; Ahsan, 2012), computational fluid dynamic model with discrete particle technique (CFD-DEM) (Wu et al., 2010), model for controlling purpose (Jia et al., 2003; Roman et al., 2009) and model of other relevance behavior (Han et al., 2004; Hernandez-Barajas et al., 2006). These models contain different degrees of assumptions and simplifications.

A crucial assumption affecting to the yield prediction of the model is kinetic of cracking reaction. In FCC process, the pseudo-component or lump technique has been used to represent the group of hydrocarbon with close boiling points.

The simplest kinetic of cracking reaction for the purpose of modeling was developed by Weekman and Nace, (1970). This scheme has divided the components involving in the reactions into three groups, i.e., gas oil, gasoline, and gas+coke , and was used to predict the conversion and gasoline yield in isothermal fixed, and fluid

bed reactors. However, The three-lump model of Weekman and Nace, (1970) contains major disadvantage of predicting coke yield, since coke yield is predicted together with the gas yield. The four-lump cracking reaction model has been introduced to overcome this situation (Lee et al., 1989). The four-lump scheme separates the coke yield to be an independent lump, therefore; this scheme is more useful for predicting the cracking reactions. Since the coke yield prediction is needed for prediction in characteristics of burning reactions in the regenerator which are the source of heat needed for cracking reactions. Models of cracking reactions with more lumps have been proposed and used in the literature for example five-lump model (Larcoca et al., 1990; Jaurez et al., 1999; Bollas et al., 2007), six-lump model (Coxon and Bischoff, 1987; Takatsuka et al., 1987), seven-lump model (Ou-guan et al., 2006), nine-lump model (Hongjun et al., 2006), ten-lump model (Jacob et al., 1976), twelve-lump model (Cerqueira et al., 1997) and the nineteen-lump model presented by Pitault at al. 1994. The advantage of these schemes is the ability of predicting the details of cracking products, however; more the kinetic parameters need to be evaluated and cause the complexity of calculation.

Other important assumptions used for FCC riser modeling in the literature are shown in Table 2.1.

## 2.2 Investigation on FCC regenerators

The regenerator used in the conventional operation of FCC is operated in turbulent or bubbling fluidization regime. This causes the slow burning reactions that entail the long residence time of the catalyst in the regenerator. Due to the characteristics of the operating regime of the conventional of the regenerator. The behavior of the conventional regenerator was usually described by the two-regime (dense bed and freeboard) and two-phase (emulsion and bubble) behavior model (Han and Chung, 2000; Alaradi and Rohani, 2002; Cristea et al., 2003).

**Table 2.1** Important aspects of FCC riser model.

| | Vaporization | Temperature variation | Gas and catalyst velocity | Gas expansion | Kinetic model | Catalyst deactivation |
|---|---|---|---|---|---|---|
| Ali et al., 1997 | Instantaneous | Adiabatic | Not considered | Constant | Four-lump | Constant |
| Araujo-Monroy and Lpez-Isunza, 2006 | Vaporization followed by cracking | Adiabatic | Constant slip factor | Included | Six-lump | Non-selective based on time on stream |
| Fernandes et al., 2007 | Instantaneous | Adiabatic | Momentum balance for solid, continuity for gas | Included | Six-lump | Non-selective based on coke content |
| Ahari et al., 2008 | Instantaneous | Adiabatic | Use slip factor | Included | Four-lump | Non-selective based on time on stream |
| Haydari et al., 2010 | Instantaneous | Adiabatic | Constant | Included | Four-lump | Non-selective based on time on stream |
| Han and Chung, 2011 | Vaporization followed by cracking | Considered heat loss | Momentum balance | Included | Four-lump | Non-selective based on coke content |

A number of regenerators have been designed and implemented to FCC processes globally to improve the burning efficiency. Therefore, the modeling works of these designs are needed for prediction, monitoring and control of the FCC processes. An example of the regenerator design is the high-efficiency regenerator which is operated in the fast-fluidized followed by the plug flow as shown in Figure 3.2. This enables the better gas-solid contact efficiency. In this design, the bottom part of the regenerator acts as a mixing chamber. The burning reactions occur in the lift pipe and the upper chamber. The bottom part and lift pipe are modeled as a plug-flow where the upper chamber is modeled as CSTR (Fernandes et al., 2007). Another design is a two-regenerator R2R technology that uses for processing the high coke content in the residual cracking. In this configuration, the first regenerator (located at the bottom part) uses for burning 40-70% of the coke on the catalyst in a lower temperature. Then, the partially regenerated catalyst is transport to the second regenerator (located at the position above the first regenerator) using air. The partially regenerate catalyst will be burned using higher temperature with low steam partial pressure and slightly air excess to eliminate the remaining coke without catalyst deactivation. The dense bed of this regenerator was modeled using the CSTR model and the lift pipe was modeled as a plug flow reactor (Gauthier et al, 2000; Fernandes et al., 2007).

Due to the trend of using more resid feedstock which causes more carbon content on the spent catalyst, some researchers have investigated the using of the alternative configurations of the regenerator to cope with this issue. Considering the burning reactions that occur in the lift pipe, this part is in the fast fluidization regime in which particles are transferred from the bottom to the top of the pipe. This pipe can be categorized as a riser type reactor.

Since riser has several advantages (i.e., high gas-solid contact efficiency, high heat and mass transfer and high throughput) compared to the conventional turbulent bed, it is a promising type of a reactor for using as a regenerator. Bai et al. (1998) developed models for steady-state simulation of riser regenerator in plug flow mode and CSTR mode. Their models include the hydrodynamic model and kinetics of regeneration model as well as mass and energy balance. This model was validated

with the riser section in the industrial high-efficiency regenerator and found that the models and the industrial data were in a good agreement. Moreover, the same authors (Bai et al., 1997) further simulated the performance of the FCC riser regenerator by proposing two designs of riser regenerators to improve the performance and the flexibility of the single riser regenerator. The first design separates the supplied air to feed at several levels along the axial distance of the riser. The simulation results revealed that this design improves the operation performance, flexibility and stability with higher solids inventory and longer solids residence time. The second design is a two-stage riser regenerator where two riser regenerators are connected in series. This design couple the advantages of the riser regenerator and the conventional two-stage turbulent bed regeneration. This double-stage regeneration can separately control air flow rates and temperatures. The simulation results showed that the second stage regenerator can operate at a much higher temperature without hydrothermal catalyst deactivation because most of the hydrogen is burnt in the first stage and this leads to high regeneration efficiency and flexibility.

## 2.3 Investigation on downers in FCC processes

Due to the disadvantages of the riser such as particle back-mixing and particle clustering leading to widely distribution of the solids residence time, therefore; a down-flow operation which can overcome the drawbacks of the riser such as less back-mixing, more uniform particle distribution in radial direction, shorter residence time and closer to plug flow operation is now in attention (Wang et al., 1992; Zhu et al., 1995).

Both experimental and simulated studies have been conducted for clarifying the hydrodynamic characteristics and the cracking reactions in the downers.

### 2.3.1 Experimental studies

The very first catalytic cracking in the downer has been performed using cumene as a feedstock in a bench-scale downer with high catalyst-to-oil ratio. It is found that the measured conversion is lower than that of predicted by a plug-flow

model at this high catalyst-to-oil ratio. This is because high solids flux operation results in the cluster flow of particles. Moreover, the incomplete break-up of the solids entering the downer causes lower surface area and resistant of mass transfer resulting in the lower conversion. (Talman and Reh, 2001).

The experimental study of the downer reactor showed that the downer improves the selectivities and yields of desired products, i.e., propylene and gasoline, significantly while the unwanted product yields, i.e., dry gas and coke, were suppressed in comparison with the operation of the riser at the same condition. The flow patterns of the gas and solids in the downer that almost reach plug flow condition enable the suitable condition for the DCC process (Deng et al., 2002).

The pilot-plant scale of 0.1 b/d. and the demonstration plant of 30 b/d. of the high severity FCC process were successful operated in Saudi Arabia. These two processes aim at increasing in light olefin production. The comparison of the riser and downer operations have been performed and found that the FCC downer provided the increased yield of gasoline and reduced coke and dry gas. The main reason behind these results is the reduction of back-mixing that causes the gasoline over cracking. Despite the yield of light olefin in the downer reactor is lower than that in the riser due to suppression of back-mixing, the yields of useful products including gasoline and light olefin in the downer is higher. However, with the use of catalyst with light olefin maximizing additive namely ZSM-5, the yield of light olefin can be increased from 28.7 wt.% to 39.3 wt.% in pilot-plant and 25.7 wt.% to 43.9 wt.% in demonstration plant (Abul-Hamayel, 2004; Abul-Hamayel et al., 2005; Fujiyama et al., 2005) .

Though the downer reactor offers advantages, the disadvantages were also reported i.e., sensitivity to hydrodynamics, limited mixing of gas and solids, very dilutes gas-solids flow causing limited catalytic capability. Therefore, some works have studied on designing a downer to riser (DtoR) reactor (Deng et al., 2005; Liu et al., 2005; Liu et al., 2008; Wu et al., 2008, 2009) for extending the advantages of the downer reactor with the riser reactor. This type of reactor is used for controlling of reactions pathway by reducing olefin content in the gasoline yield. They firstly

studied the hydrodynamic and mixing behavior in the coupling reactor. Riser reactor used in the DtoR was the annular riser which offers the more uniform radial structure than the conventional riser. Then, they simulated the reactions and conducted the hot experiment and finally the test in industrial pilot plant for residual fluid catalytic cracking had been done. This process increases the yield of LPG and propylene by 8.15 and 4.30 wt.% and reduces the content of olefin in gasoline by 17 wt.% in comparison with the riser reactor.

### 2.3.2 Simulated studies

Apart from simulation studies that were mentioned in the experimental works above. The modeling and simulated work on downers have been proposed to clarify their behavior and performance.

Bolkan-Kenny et al. (1994) developed a novel hydrodynamic model of a downer, that combines the hydrodynamic of the downer with the reaction kinetic of the FCC process, to simulated the performances of the downer FCC. The simulated results are in the range of industrial FCC units. Moreover, the calculated results also showed that the downer introduces more uniform flow, better reaction control, shorter residence times with narrower residence time distributions (RTD), and higher catalyst/oil ratios compared to the riser. The operation of the downer can improve the conversions, yields as well as the selectivities of the FCC in case of using the commercial silica-alumina catalysts.

Shaikh et al. (2008) developed the mathematical model and performed the simulations of the downer in a pilot plant scale that operate under high severity conditions. The model consists of the steady-state non-isothermal model of the heavy oil cracking in a down-flow reactor and a catalyst regeneration in fluidized-bed reactor. The model based on the four-lump kinetics of the cracking reactions and the complete combustion kinetics for the regenerator reactions. Model predictions of the conversion, product yields, and temperatures in the downer reactor are satisfactory when they are partially validated with the data from the pilot plant that was operated in the high-severity mode.

Due to the advance in computational technology, the more complex model has been used to simulated the behavior of the downer reactor. The computational fluid dynamics (CFD) technique has been used to simulate the downer reactor. Liu et al. (2006) used this technique to incorporate the effect of molar expansion due to cracking reactions in the non-reactive flow model of Zheng et al. (2002). Wu et al. (2009) proposed the two-dimensional model based on the empirical study for revealing the performance of the downer reactor in comparison with the riser reactor. Their model can capture the key characteristics of the gas-solids flow with reactions in the riser and downer reactor. The results provided the better understanding of both types of reactors. Moreover, Wu et al., (2010) use the CFD with discrete element method (DEM) to simulate the reactive flow in the riser and downer reactor by considering the particle-scale behavior in a discrete manner which provides several advantages i.e., the catalyst activity can be calculated in time, therefore; the effect of residence time distribution on the catalyst activity should be well revealed.

As mentioned above, several works have been performed on the studying of the downer due to its potential for fast reaction which intermediates are desired products. However, most works focusing on the use of the downer do not address the accompanying regenerator.

## 2.4 Steam reforming in FCC processes

Generally, the regeneration of the spent catalyst has been done by oxidization reaction of coke with air. There is a work that performed a study on reduction of coke on FCC catalyst by the steam gasification reaction and found that coke on zeolite-type spent catalyst could undergo the reaction with steam at temperature about 810-922 K. This produced hydrogen, carbon dioxide, carbon monoxide and methane as products. (Hsing and Mudra , 1993).

A catalyst activity is also one of the main factors that affects to the performance of the FCC operation. The main feature of the cracking catalyst is to maximize the yield of the desired products and reduce the yield of undesired product. However, some catalyst additives have been used to promote the coke combustion

reaction in regenerator (Luo et al., 2007). There is a research work on the synthesis of a steam gasification catalyst for using in regenerator (Corma et al., 2011), since this reaction is advantage in reducing carbon on catalyst and the temperature of the regenerator in case of high coke content on spent catalyst.

# CHAPTER III

# THEORY

## 3.1 Fluid Catalytic Cracking (FCC)

Fluid catalytic cracking (FCC) is a main conversion unit in the petrochemical industry. This unit is used for cracking of high-boiling point petroleum fractions, i.e., heavy gas oil to lower-boiling point, e.g., gasoline using a microspheroidal catalyst (i.e., zeolite), which behaves like a fluid when properly aerated by air.

### 3.1.1 Technology of the fluid catalytic cracking (Sadeghbeigi, 2000)

A large number of fluid catalytic cracking units (also called cat cracker) are operating in the petrochemical process worldwide with the different configurations and licensers. However, the main objective of each FCC units is to upgrade the low-value petroleum fraction into the more valuable product fractions. It is also known that the 45% of the gasoline pool comes from the FCC and its ancillary units, such as alkylation unit.

Since the first commercial FCC unit was started up in 1942, the configuration of the FCC unit has always been adapted to meet the demands of the market. The improvements are aimed to upgrade the mechanical reliability and the capability of handling heavier feedstocks.

The typical FCC unit configuration of some licensers, namely Exxon's flexicracker, UOP FCC and SWEC stacked FCC unit are shown in Figure 3.1 through Figure 3.3.

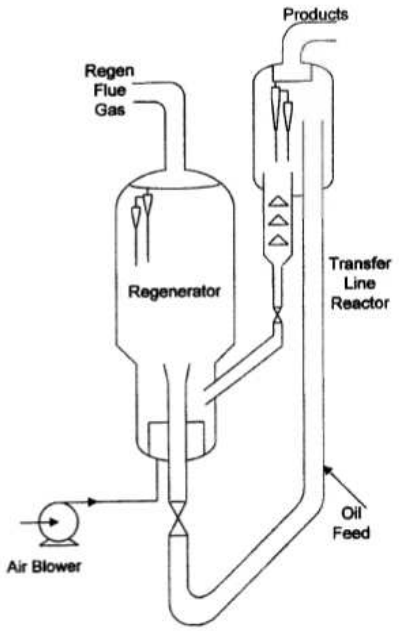


**Figure 3.1** Typical schematic diagram of Exxon's flexicracker (Sadeghbeigi, 2000).

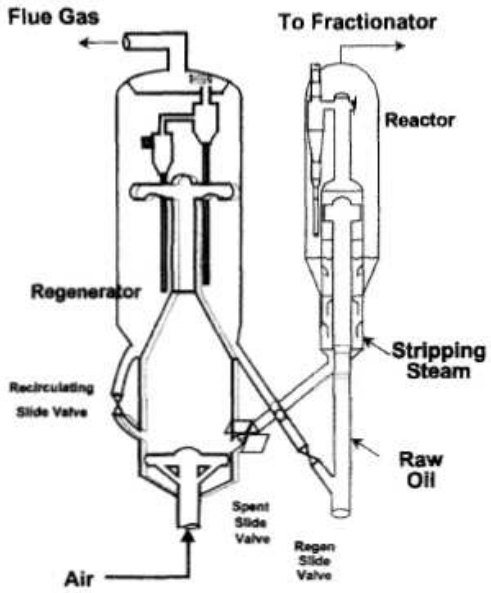


**Figure 3.2** Typical schematic diagram of UOP FCC (Sadeghbeigi, 2000).

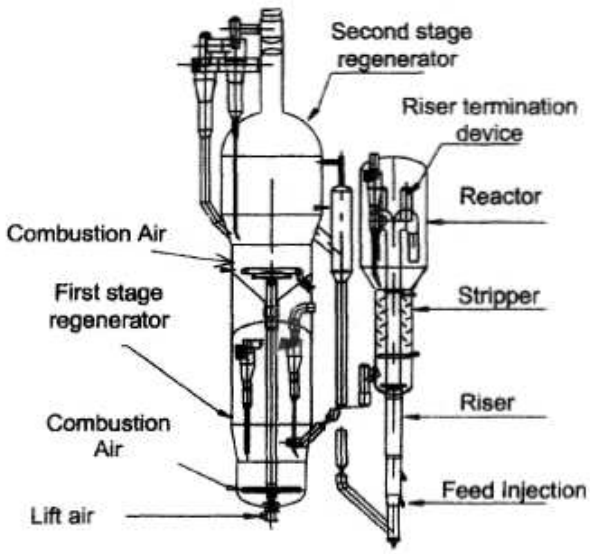


**Figure 3.3** Typical schematic diagram of SWEC stacked FCC unit (Sadeghbeigi, 2000).

## 3.1.2 Fluid catalytic cracking process description (Sadeghbeigi, 2000)

In petroleum refinery, there are lots of processing units using for convert raw crude oil into the products such as gasoline, diesel, and fuel oil. Generally, crude oil contains water, inorganic salts, suspended solids, and water-soluble trace metals. In order to prevent corrosion, plugging, and fouling of equipment and poisoning of the catalysts in the process, the contaminants must be removed by desalting (dehydration) before processing of crude oil.

The desalted crude oil is sent to the atmospheric distillation tower for distilling into several intermediate products; naphtha, kerosene, diesel, and gas oil (Figure 3.4). The heavy fraction that cannot be distilled in the atmospheric tower will be heated and sent to the vacuum distillation tower. Here, the heavy fraction is split into gas oil and tar.

Then tar will be sent to be processed in a delayed coker, deasphalting unit, or visbreaker, or be sold as fuel oil or road asphalt. The gas oil will be used as the feed

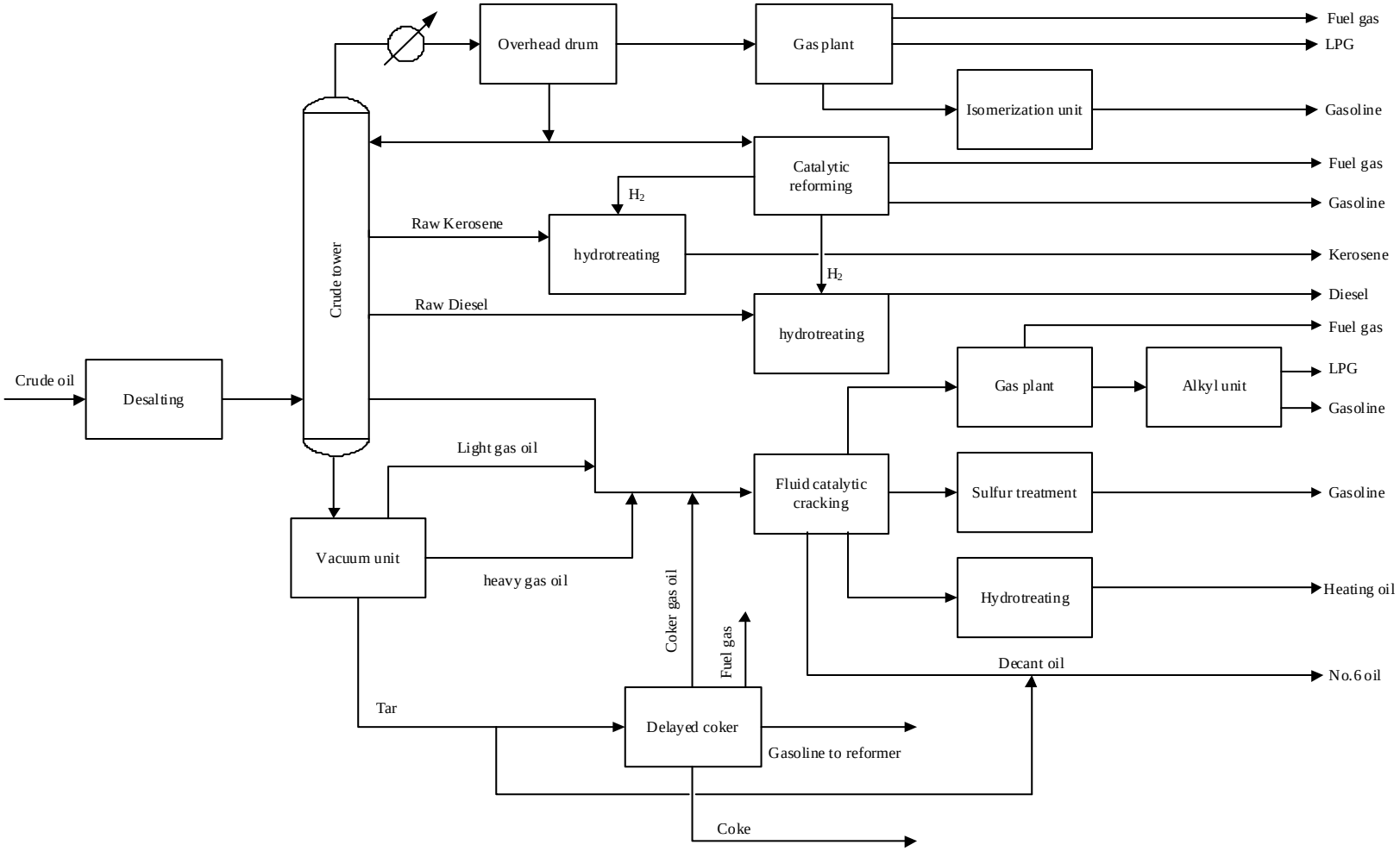


**Figure 3.4** A typical high conversion refinery (Sadeghbeigi, 2000).

for the fluid catalytic cracking unit. However, the feedstocks for the fluid catalytic cracking unit are also derived from the atmospheric tower and the delayed coker.

The FCC process is a complex process and consists of many parts. Therefore, the process has been separated into six sections for better understanding including, feed preheat, riser-reactor-stripper, regenerator-heat/catalyst recovery, main fractionators, gas plant and treating facilities.

### 3.1.2.1 Feed preheat

Generally, the gas oil produced in the any refinery is sufficient for providing to the FCC unit. However, some refineries cannot produce the gas oil to meet the capacity of the FCC unit. Therefore, it would be economical to blending some residue to the feedstocks or purchasing the gas oil from the other sources. These feedstocks including the gas-oil and the supplement feedstocks are mixed and sent to the surge drum. The surge drum is used in order to offer the steady flow of the feed to the pump. Moreover, this surge drum can be used for separate the water and vapor in the feedstocks (Figure 3.5).

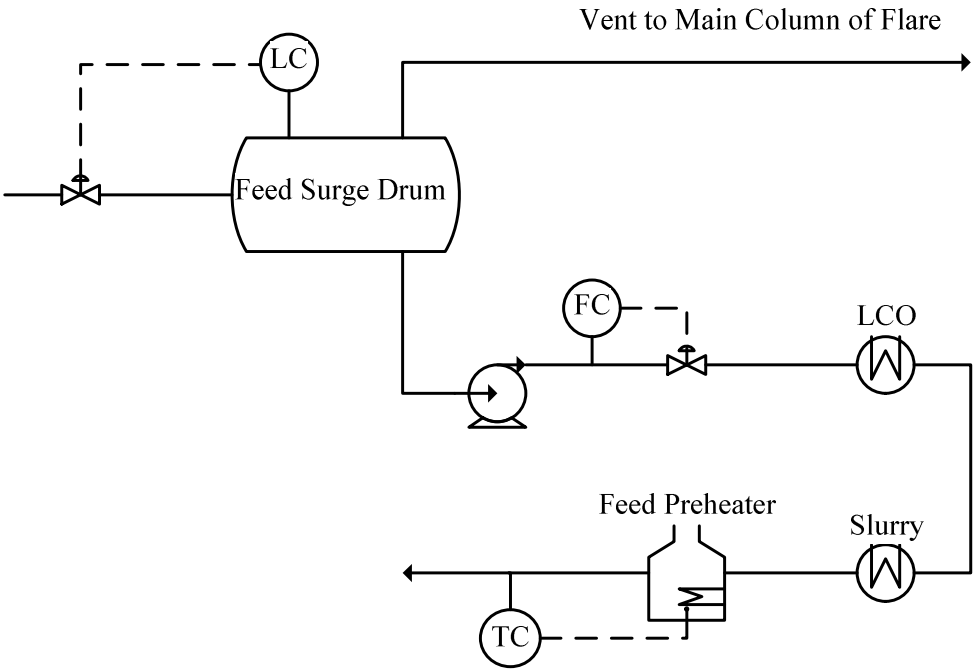


**Figure 3.5** Typical feed preheat system (Sadeghbeigi, 2000).

Then, the feed from the surge drum is heated with the main fractionators pumparound and fired heaters to the temperature of 260°C to 370°C. The feed is pumped through heat exchangers to heat up by the hot streams from the main fractionators, i.e., top pumparound of light cycle oil product and the bottoms pumparound. It can be noted that the process of removing heat from the main fractionators is as important as preheating of the feed.

The fired heaters are commonly use for the final preheat of the FCC unit. The feed preheater provides control over the catalyst-to-oil ratio which is a key variable of the process. The increasing of the preheat temperature enables the increasing of the throughput in the FCC unit that the air blower is constrained.

### 3.1.2.2 Riser-reactor-stripper

In the modern FCC process, it can be stated that the reactor and the regenerator are the main units. The cracking reactions take place in the reactor for 1.5-3.0 s before separation by cyclones.

The feedstock from preheater is fed to the riser reactor near the base and contacts with the hot regenerated catalyst flowing from the regenerator (temperature ranges from 677-732°C) and then vaporized (Figure 3.6). The catalyst from the regenerator acts as the heat carrier transferring the heat from regenerator to the reactor. The hot regenerated catalyst provides heat for vaporization of the feed, for heating the feed to the desired reactor temperature and for endothermic cracking reactions in the riser. The typical range of the catalyst-to-oil ratio used in the riser reactor is in the range of 4-9 by weight.

The vaporization of the feed causes the expanding volume of gases which is the main driving force that carry the catalyst up along the riser reactor. The cracking reactions occur in the riser reactor while the catalyst moves upward with the gases.

The riser reactor is a vertical pipe with a 10-13 cm thick refractory lining for insulation and abrasion resistance. The typical diameter of the riser is 60-180 cm and

25-30 m in length. The ideal operation of the riser is in a plug flow mode. The gas and catalyst travel up along the length of the riser without or minimum back mixing.

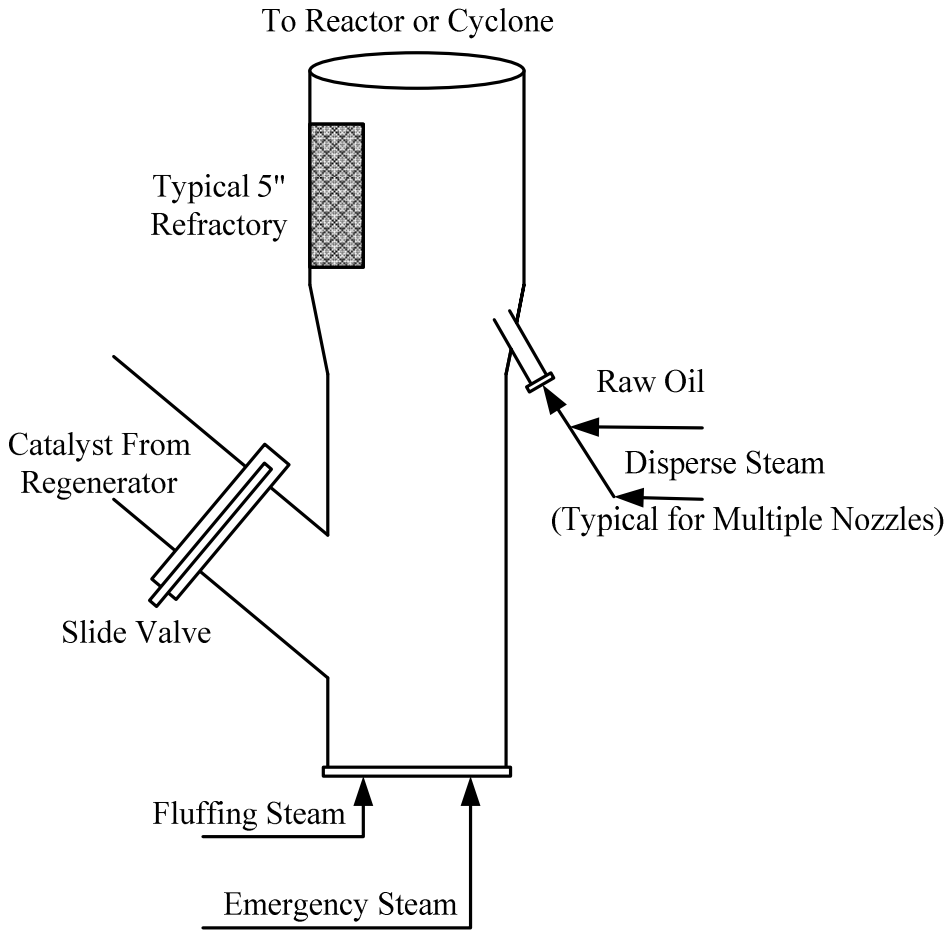


**Figure 3.6** Typical riser (Sadeghbeigi, 2000).

At the entrance of the riser reactor, steam is used to atomize the feed into smaller oil droplets. Because the efficient contacting of the feed and the active site of catalyst is crucial for achieving the desired cracking reactions, the small droplets increase the possibility of feed to act with the reactive acid sites on the catalyst. Nowadays, the cracking reactions take 3 seconds or less, with the highly active zeolite catalyst.

The outlet vapor velocity of riser reactor is about 15.2-22.8 m/s based on the outlet conditions. As cracking reactions proceed, a hydrogen-deficient material which is called coke will deposite on the surface of the catalyst and reducing the catalytic

activity of catalyst. Therefore, the catalyst needs to eliminate the coke for restoring the cracking activity.

The catalyst and gases that are composed of cracked products and uncracked feed are quickly separated in the cyclones. The cyclones are installed in the cyclone housing at the top of the riser reactor. The typical FCC units use single or two-stage cyclones to separate the catalyst from the gas (Figure 3.7). The spent catalyst from cyclones will drop to the stripper and the gases will be sent to the main fractionators for splitting into various fraction. The efficiency of a typical two-stage cyclone system is more than 99%.

The catalyst and vapors need to be separated as soon as they exit the riser reactor because the extended contact time of catalyst and the vapors will cause the over-cracking of the desirable products into unwanted products. Moreover, the extended contact time also causes the thermal cracking of the desirable products.

In the stripper (Figure 3.8), the steam at a rate of 0.2-0.5 wt. % will be used to remove the entrained hydrocarbon vapors locating between the catalyst particles. However, not only the entrained hydrocarbons are carried with the spent catalyst but the hydrocarbons that adsorbed on the catalyst surface or fill in the catalyst pores are also went into the stripper. Here, the stripping steam does not address hydrocarbon desorption and hydrocarbons filling the catalyst pore.

In the stripper, there are some cracking reactions which are driven by the temperature and the residence time of catalyst in the regenerator still occur. They are the cracking reactions of the adsorbed hydrocarbon into the clean lighter product. The stripper is usually designed to allow the efficient contact between the catalyst and the steam with the superficial gas velocity of 0.23 m/s and a flux of catalyst ranges between 2.4 to 3.4 kg $m^{-2}$ $s^{-1}$. If the operation is in the high flux state, the falling catalyst will entrain steam causing the reduction of the stripping steam efficiency.

The stripping steam cannot remove all the hydrocarbon vapors in the catalyst pores. Therefore, some of hydrocarbon vapors will be carried with the spent catalyst to the regenerator. It should be noted that the amount of hydrocarbon vapors entrained

to the regenerator need to be minimized. Since these hydrocarbons have a higher hydrogen-to-carbon ratio than the coke, the disadvantages of allowing these hydrocarbons to the regenerator are:

- Loss of the valuable product. This fraction of hydrocarbon should be recovered in the main fractionator as the product instead of burning in the regenerator.

- Loss of throughput. Since the burning of hydrogen to water gives the heat higher than combustion of carbon to carbon dioxide about 3.7 times. Burning of these hydrocarbons causes higher temperature of regeneration. This will affect to the regenerator internals. Therefore, the unit will be forced to operate in the lower feed rate.

- Loss of catalyst activity. The higher regenerator temperature and the steam at high temperature would destroy the catalyst's crystalline structure causing the permanent deactivation of the catalyst.

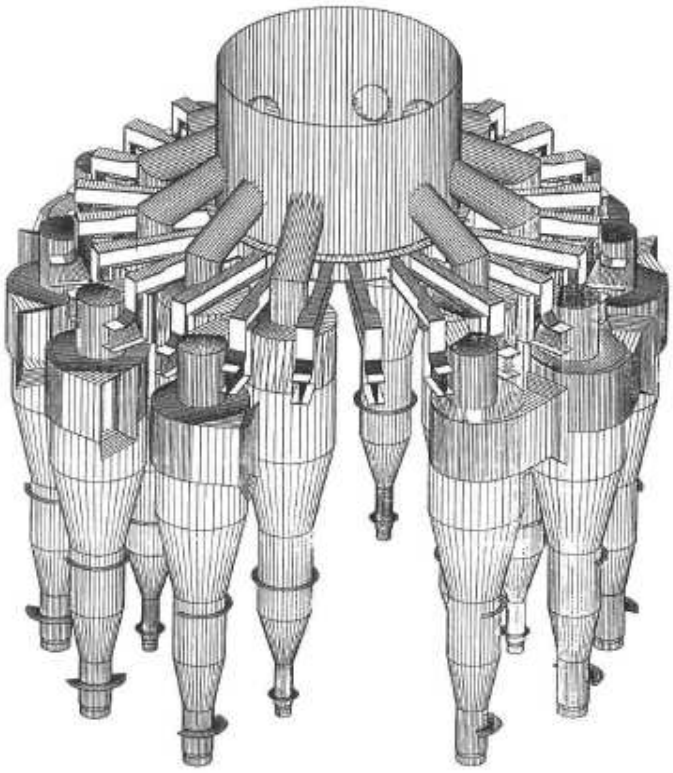

**Figure 3.7** A two-stage cyclone system (Sadeghbeigi, 2000).

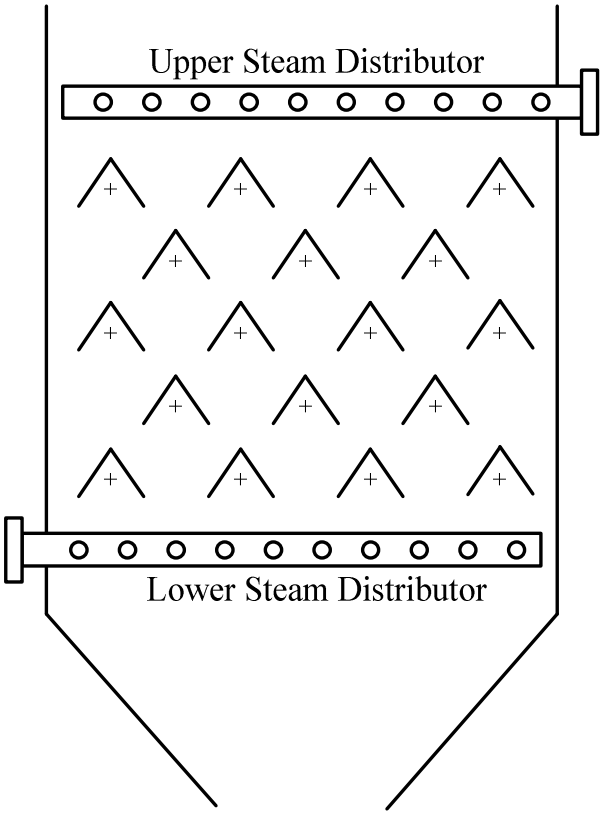


**Figure 3.8** An example of a two-stage stripper (Sadeghbeigi, 2000).

In the earlier FCC unit, the transport of spent catalyst from the reactor to the regenerator is designed to use lift air. Presently, the flow of spent catalyst is usually controlled by a slide valve which is controlled by the level of catalyst in the stripper. The catalyst height in the stripper causes the pressure head that push the spent catalyst to flow to the regenerator. The surface of the slide valve is lined with the refractory to resist erosion.

### 3.1.2.3 Regenerator-heat/catalyst recovery

The burning of coke in the regenerator is not only designed for restoring the catalyst activity but also for providing heat to the endothermic cracking reaction in the reactor. Typically, the coke content on spent catalyst flowing to the regenerator is in the range of 0.4-2.5 wt%. This amount of coke depends on the quality of feedstock. The main compositions of coke are carbon, hydrogen, and trace amounts of sulfur and nitrogen. These burn according to the reactions as shown in Table 3.1.

**Table 3.1** Reactions occur in the regenerator (Sadeghbeigi, 2000).

| Reactions | Heat of reaction (kcal/kg of C, $H_2$ or S) |
|---|---|
| $C+1/2O_2 \rightarrow CO$ | 2,200 |
| $CO+1/2O_2 \rightarrow CO_2$ | 5,600 |
| $C+O_2 \rightarrow CO_2$ | 7,820 |
| $H_2+1/2O_2 \rightarrow HO_2$ | 28,900 |
| $S+xO \rightarrow SO_x$ | 2,209 |
| $N+xO \rightarrow NO_x$ | |

Air from one or more blowers is supplied to the regenerator in order to provide oxygen to the system. Oxygen is used in the combustion reactions of coke containing carbon, hydrogen, sulfur and nitrogen. The air is fed to the regenerator from the bottom and the air blowers need to supply sufficient air velocity and pressure to maintain fluidized bed of the catalyst in the regenerator. The air distributor at the bottom of the regenerator is important to the regeneration, since the efficient contact of air and catalyst depends on the configuration of the air distributors. In typical design of air distributors, the pressure drop is 7-15 kPa for ensuring that air flow through all nozzles.

In general, the regenerator operating with the air velocity of 0.6-1.2 m/s and can be divided into two regions: the dense phase and the dilute phase. The dense phase is located from the air distributor to the top of the bed and the dilute phase is in the region above the dense phase up to the cyclone inlet. The bulk of catalyst is in the dense phase and the small amount of catalyst is in the dilute phase.

After regeneration, the catalyst called regenerated catalyst contains the coke level of 0.05%. The regenerated catalyst flows down a standpipe which is a transfer line. In the standpipe, the pressure head of the catalyst allows the circulation of the catalyst from the regenerator to the reactor.

Some standpipes are designed to extend into the regenerator with the hopper at the top section. The hopper is the inverted cone design which is used for providing extra time for the regenerated catalyst to be de-bubbled before entering the standpipe.

The typical size of the standpipes is designed for the catalyst flux of 500-1,500 kg $m^{-2}$ $s^{-1}$and the bulk density of catalyst in the range of 560 to 720 kg/$m^3$.The flue gas will be carried down with the regenerated catalyst to keep fluidized state in the standpipes. External aeration of air, steam, nitrogen, or fuel gas may be used in the long standpipes to ensure the fluidization.

The flow of regenerated catalyst from the regenerator to the reactor is controlled by the pressure differential between the reactor and the regenerator. The flow rate of the catalyst is regulated by a slide or plug valve which is controlled by the reactor temperature. The function of this valve is to supply the catalyst for heating feed to the desired reactor temperature.

Some of catalysts are entrained with the flue gas from dense phase to the dilute phase. The flue gas superficial velocity is determined the amount of entrained catalyst. The particles with the size of 50-90 $\mu$m can fall back to the dense bed while the small particle (0-50 $\mu$m) will flow up to cyclones.

In FCC regenerator, 4-16 sets of primary and secondary cyclones are used to recover the entrained catalyst particles with a diameter greater than 20 $\mu$m. The catalyst particles captured by cyclones are returned to the regenerator through the diplegs.

The centerline of the inlets of the primary cyclones should be higher than the distance referred to as the transport disengaging height (TDH). This height is the distance above the dense catalyst bed which the flue gas velocity is stabilized. Moreover, the catalyst concentration in the flue gas at this height is constant as no catalyst return to the dense phase. Therefore, if the centerline of the primary cyclone inlets is lower than the TDH, a large amount of catalyst will be taken away with flue gas. This causes the extremely loss of catalyst.

Regeneration of the catalyst can be done in the different temperatures and different compositions of products. There are two modes of operations for burning of the coke on catalyst: partial combustion mode and complete combustion mode. In partial combustion, oxygen fed to the system is limited so carbon is in excess condition. An increased in coke content would allow more CO to be formed. In complete combustion, oxygen will be fed to the system in the excess condition, therefore; the combustion of carbon in coke will form $CO_2$ as a product. This condition would allow more combustion and would generate more heat. in case of high coke yield

In another approach, the FCC regeneration can be divided into three types based on the ranges of temperature, i.e., low, intermediate, and high temperature. The low temperature operation (about 640°C) cannot undergo the complete combustion. Therefore, the gaseous products in flue gas that is mainly composed of $O_2$, CO, and $CO_2$ are in the high level. This operation was used in the early design of FCC process.

Then, the high temperature regeneration was invented. The high temperature regeneration is aimed to burn all of the oxygen and low carbon on the regenerated catalyst. The flue gas of this operation mode contains either no oxygen and small amount of CO or no CO and small amount of oxygen. However, if high level of CO presents in the flue gas, it will be called partial combustion.

The intermediate temperature regeneration is developed with the combustion promoter. It is used to reduce the temperature of regeneration while the combustion is still in full combustion mode. The reduction of regeneration temperature can be done by promoting of CO combustion in dense phase. However, without the combustion promoter, the intermediate temperature is not stable. Table 3.2 summarizes various aspects of regeneration. The columns of regeneration temperatures and the operating modes illustrate the limitations of each operating regions. The regeneration can be operated in partial or complete combustion mode at low, intermediate, or high temperatures. At low temperature operation, the regeneration proceeds only in the partial combustion mode with quite high carbon content on spent catalyst. The

afterburn occurs when the combustion air is increased. At intermediate temperature, the carbon content on regenerated catalyst is reduced.

**Table 3.2** Aspects of regeneration (Sadeghbeigi, 2000).

| **Operating region regenerator combustion** | **Partial combustion mode** | **Full combustion mode** |
|---|---|---|
| Low temperature (nominally 640°C) | Stable (small afterburning) $O_2$, CO, and $CO_2$ in the flue gas | Not achievable |
| Intermediate temperature (nominally 690°C) | Stable (with combustion promoter); tends to have high carbon on regenerated catalyst | Stable with combustion promoter |
| High temperature (norminally 730°C) | Stable operation | Stable operation |

It can be seen that the full combustion mode tends to show the better regeneration performance than the partial combustion mode. However, this mode contains some disadvantages. The advantages and disadvantages associated with full combustion mode are shown:

Advantages of full combustion mode:

- Energy efficient
- Heat-balances at low coke yield
- Minimum hardware (no CO boiler)
- Better yields from clean feed

Disadvantages of full combustion:

- Narrow range of coke yields unless some heat removal system is incorporated.
- Greater afterburn, particularly with an uneven air or spent catalyst distribution system.

- Low cat/oil ratio

The mode of regeneration is based upon the feed quality. The full combustion mode is suitable for clean feed and the partial combustion mode with the heat removal system is suitable for low quality feed or the resid feed.

### 3.1.2.4 Main fractionators

The main fractionators or main column is used to recover the liquid products from reactor vapors. The hot vapors of the products from the reactor flow to the main fractionators at the base of the column, then the vapors will be condensed and re-vaporized. The hydrocarbon components will be separated as they flow upward through the trays in the main fractionators.

The operation of the main fractionation contains two different points differing from the crude distillation unit. First, the feed is the vapors from FCC reactor and need to be cooled before the fractionation can be started. Second, a large amount of gases will travel overhead with the unstabilized gasoline that is needed to be separated in other process.

## 3.2 Downer Reactor and equipments (Zhu et al., 1995)

Beside of a long tubular shape, operation of a downer reactor requires the auxiliary equipments for example a gas and solids distributor and a gas and solids separator. The following section describes the function and operation of the downer reactor and the accessories.

### 3.2.1 Gas and solids distributor (Zhu et al., 1995)

The operation of a downer reactor greatly relies on the uniform distribution of the solids at entrance since solids acceleration in a downer depends on gravity and drag. This is clearly different from the operation of the riser. In riser, uniform distribution of gas is more important because the acceleration of solids is totally depends on gas drag.

The gas and solids feeding system of the downer is shown in Figure 3.9. It can be seen that there is a fluidized bed on the top of the feeding system. A lot of small vertical tubes are placed in the fluidized bed for transportation of the solids to the downer column. The fluidized bed is kept around minimum fluidization without any bubbles because the bubbles will block the flowing of the solids into the tubes. The solids flow rate can be controlled by adjusting the bed height and the flow rate of the fluidization air. Solids that flow to the top of the distributor may come from the transport lines or other solids flow controls such as a vibratory feeder.

Apart from the solids distribution system as shown in Figure 3.9, there are other alternatives for feeding the solids to the downer such as using a set of interchangeable distribution plates with different number of holes to provide different solids feed rates. The main air can be feed into the downer through the same small distributor tubes of solids distribution or can be fed into the downer directly using the horizontal tubes located below the distributor.

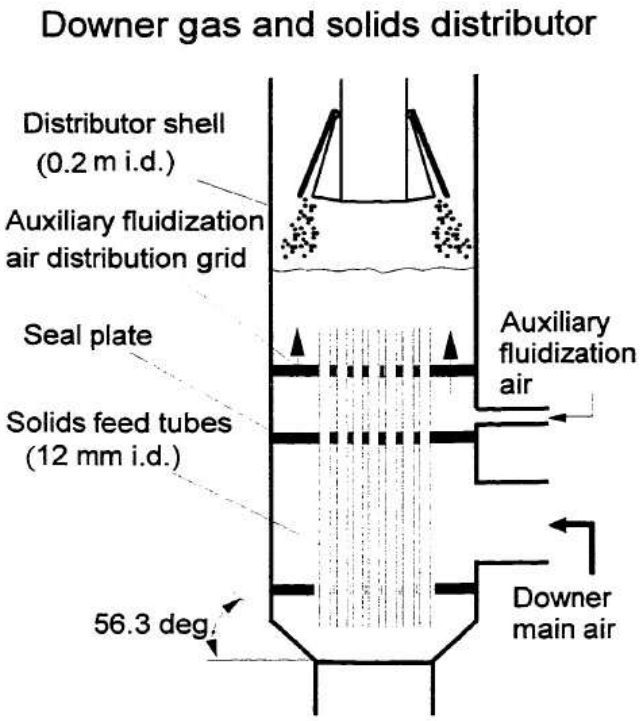


**Figure 3.9** Downer gas and solids distributor (Zhang, 1999).

### 3.2.2 Downer reactor (Zhu et al., 1995)

A downer reactor is composed of a vertical column with a gas and solids distributor at the top and a gas and solids separator at the bottom. In the fluid catalytic cracking process, the catalyst need to be regenerated in the regenerator and re-circulated back to the distributor of the downer reactor. However, in a cold model of downer reactor, the recirculation and down flow of catalyst will be performed in a concurrent downflow circulating fluidized bed (CDCFB). In this system, the solids and gas will be separated at the bottom of the downer and solids are re-circulated upward in an accompanying riser to the distributor at the top of the downer as shown in the equipment in Figure 3.10.

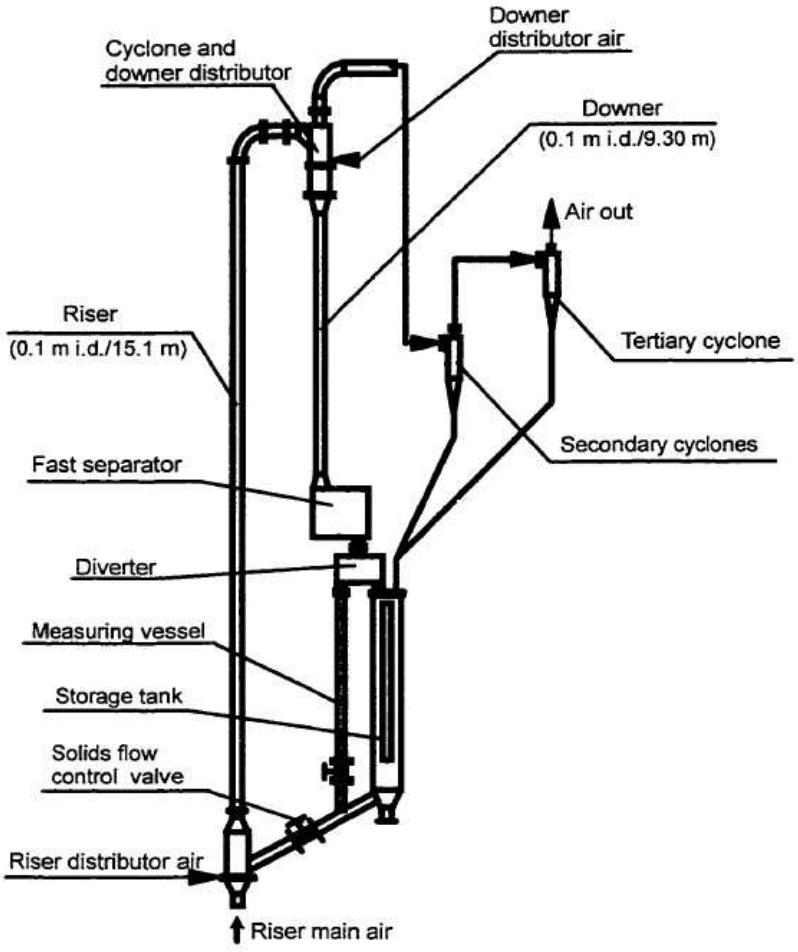


**Figure 3.10** Schematic diagram of a concurrent down-flow circulating fluidized bed (CDCFB) (Zhang, 1999).

The operation of the CDCFB in Figure 3.10 starts at the point that the solids in the storage tank located at the bottom of the downer flow to the riser base and then they are entrained upward along the riser length. Next, solids and gas are separated using a cyclone. Solids flow into the gas and solids distributor at the top of the downer and then flow into the downer as shown in Figure 3.9. The superficial gas velocity and solids flux in the downer are controlled by the condition in the riser for simplicity. At the bottom of the downer, the gas and solids are separated by the quick inertial separator as shown in Figure 3.11. However, detailed of the quick separator will be discussed in the next topic. Most of the solids are captured by the quick separator. Moreover, the three stages of cyclones are used to recover the remaining solids before they flow into the storage tank. The solids circulation rate can be measured by switching the solid to the measuring tank instead of the storage tank.

### 3.2.1 Gas-solids separator (Zhu et al., 1995)

Typically downer is designed to use with the fast reaction that the intermediate is the desired product. Therefore, a fast separation is extremely important. It is not appropriate in the case that the residence time of the gas and solids in the downer is lower that a second while a cyclone use 1-2 seconds to separate gas and solids.

In some hydrocarbon process, a short residence time of reaction can be achieved by quenching the products from reactor. The quenching of the total mass is needed for a slow gas and solids separation. The Stone and Webster hold a patent of a novel one-quarter turn cyclone. This cyclone takes 30 ms for separation of gas and solids with the efficiency of 98%. Therefore, there is 2% left for quenching which is safer than quenching of the total mass.

As described above, another type of a quick gas-solids separator has been invented as shown in Figure 3.11. It is a inertial separator that the gas and solids will pass through a specially designed nozzle and then move on a curved guiding plate. This separator can be separated more than 96% to 99% of the solids and take about 0.05-0.3s.

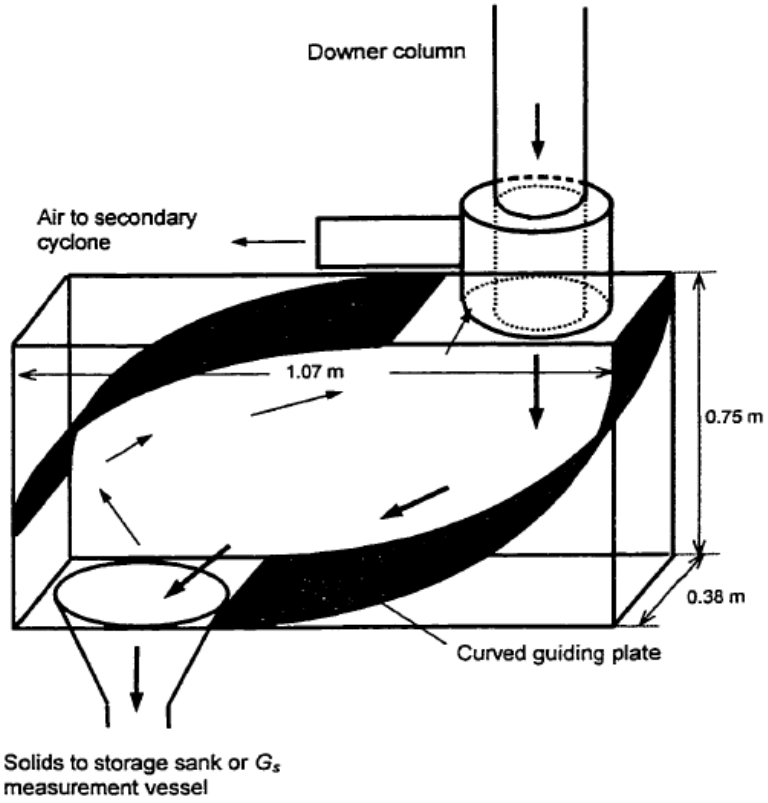


**Figure 3.11** Gas-solids separator (Zhang, 1999).

## 3.3 Reforming of coke-on-catalysts with steam or carbon dioxide (Corma et al., 2011)

In the regenerator, there are possibilities of reactions to proceed with different heat of reactions. Therefore, each reaction offers a different impact on heat balances of the FCC system. The main reactions are the coke burning reactions which are generally considered to be composed of C and H in the different ratio. The burning reactions are:

$$C + \frac{1}{2}O_2 \rightarrow CO \quad \Delta H = -110\ kJ\ mol^{-1} \tag{3.1}$$

$$CO + \frac{1}{2}O_2 \rightarrow CO_2 \quad \Delta H = -283\ kJ\ mol^{-1} \tag{3.2}$$

$$H + \frac{1}{4}O_2 \rightarrow \frac{1}{2}H_2O \quad \Delta H = -121\ kJ\ mol^{-1} \tag{3.3}$$

However, with the high amount of steam and hydrogen pressure in the regenerator, there are reactions that are promoted i.e., steam reforming, water-gas shift (WGS) ,methanation ana Boudouard as shown:

Gasification reaction: $C + H_2O \rightarrow CO + H_2 \quad \Delta H = +131\, kJ\ mol^{-1}$ (3.4)

Water-gas shift reaction: $CO + H_2O \rightarrow CO_2 + H_2 \quad \Delta H = -41\, kJ\ mol^{-1}$ (3.5)

Methanation reaction: $C + 2H_2 \rightarrow CH_4 \quad \Delta H = -75\, kJ\ mol^{-1}$ (3.6)

Boudouard reaction: $C + CO_2 \rightarrow 2CO \quad \Delta H = +172\, kJ\ mol^{-1}$ (3.7)

# CHAPTER IV

# MATHEMETICAL MODEL

In order to analyze the performance the riser and the regenerator, the mathematical model is needed. This chapter presents the mathematical model used in this study including the hydrodynamic model of riser, hydrodynamic model of downer, kinetic model of cracking reactions, kinetic model of regeneration, i.e., burning and steam gasification reactions.

## 4.1 Hydrodynamic model of downer

Hydrodynamic model is derived based on the conservations of mass and momentum to estimate solid holdup and pressure variation along the axial direction of the downer regenerator at steady state condition (Wu et al., 2008). It is assumed that variations in the radial direction can be neglected due to the characteristics of the downer regenerator (Deng et al., 2002).

Steady state continuity equations for the gas and solid phases are:

Gas phase:

$$\frac{d(\bar{\varepsilon}_g \rho_g \bar{V}_g)}{dz} = 0 \text{ , where } G_g = \bar{\varepsilon}_g \rho_g \bar{V}_g = \text{constant} \tag{4.1}$$

Solid phase:

$$\frac{d(\bar{\varepsilon}_s \rho_s \bar{V}_s)}{dz} = 0 \text{ , where } G_s = \bar{\varepsilon}_s \rho_s \bar{V}_s = \text{constant} \tag{4.2}$$

The relationship of the two phases is: $\bar{\varepsilon}_g + \bar{\varepsilon}_s = 1$

The momentum conservation equations are:

Gas phase:

$$\frac{d(\bar{\varepsilon}_g \rho_g \bar{V}_g^2)}{dz} = -\frac{dP}{dz} - F_D - F_{fg} + \bar{\varepsilon}_g \rho_g g \tag{4.3}$$

Solid phase:

$$\frac{d(\bar{\varepsilon}_s \rho_s \bar{V}_s^2)}{dz} = F_D - F_{fs} + \bar{\varepsilon}_s(\rho_s - \rho_g)g \tag{4.4}$$

The drag force, $F_D$, can be expressed as:

$$F_D = \frac{3}{4}\frac{C_D}{d_p}\bar{\varepsilon}_s \rho_g \left|\bar{V}_g - \bar{V}_s\right|\left(\bar{V}_g - \bar{V}_s\right) \tag{4.5}$$

where $C_D$ is the drag coefficient which can be determined by the following expression.

$$\frac{C_D}{C_{Ds}} = \frac{14.1\left[1 + 2.78\left(G_g / G_s\right)\right]}{Fr} \tag{4.6}$$

The drag force and drag coefficient can be used in the range of $1.3 < U_g < 10$ m/s and $30 < G_s < 180$ kg/m$^2$s.

The Froude number ($Fr$) can be expressed as:

$$Fr = \frac{U_g}{\sqrt{g d_p}} \tag{4.7}$$

The standard drag coefficient ($C_{Ds}$) can be determined by:

$$C_{Ds} = \frac{24}{\mathrm{Re}_r}\left(1 + 0.15\,\mathrm{Re}_r^{\,0.687}\right) \text{ for } \mathrm{Re}_r \le 1000 \tag{4.8}$$

$$C_{Ds} = 0.44 \text{ for } \mathrm{Re}_r > 1000 \tag{4.9}$$

The Reynolds number ($\mathrm{Re}_r$) is defined as:

$$\mathrm{Re}_r = \frac{\rho_g d_p \left|\bar{V}_g - \bar{V}_s\right|}{\mu_g} \tag{4.10}$$

The friction force between gas and wall ($F_{fg}$) can be expressed as:

$$F_{fg} = \frac{2 f_g \bar{\varepsilon}_g \rho_g \bar{V}_g^2}{D} \tag{4.11}$$

where $f_g$ is the gas and wall friction coefficient expressed as:

$$f_g = \frac{16}{\mathrm{Re}_g}, \text{ when } \mathrm{Re}_g \le 2300 \tag{4.12}$$

$$f_g = \frac{0.079}{\mathrm{Re}_g^{\,0.313}}, \text{ when } \mathrm{Re}_g > 2300 \tag{4.13}$$

The Reynolds number ($\mathrm{Re}_g$) is defined as:

$$\mathrm{Re}_g = \frac{\rho_g U_g D}{\mu_g} \tag{4.14}$$

The friction force between particle and wall ($F_{fs}$) is:

$$F_{fs} = \frac{2 f_s \bar{\varepsilon}_s \rho_s \bar{V}_s^2}{D} \tag{4.15}$$

where $f_s$ is the particle and wall friction coefficient which can be defined as:

$$f_s = \frac{0.0285\sqrt{gD}}{\left(G_s / \rho_s \bar{\varepsilon}_s\right)} \tag{4.16}$$

The superficial gas velocity and the solid velocity are defined as:

$$\bar{V}_g = \frac{U_g}{\bar{\varepsilon}_g} = \frac{G_g}{\rho_g \bar{\varepsilon}_g} \tag{4.17}$$

$$\bar{V}_s = \frac{G_s}{\rho_s \bar{\varepsilon}_s} \tag{4.18}$$

The change in superficial gas velocity is calculated by the changing in the total molar flow rate of gas as:

$$U_g = \frac{n_t R T_g}{PA} \tag{4.19}$$

The hydrodynamic model of the downer regenerator is validated against the experimental data reported by Deng et al. (2004). Figure 4.1 shows the comparison of the simulation results and experimental data at $U_g$ = 4.33 and 6.14 m s$^{-1}$. It can be seen that the prediction results agree very well with the experimental data. This ensures the validity of the hydrodynamic model used in this simulation. It is noted that the model can be used to explain the FCC regenerator operated under the solid flux ($G_s$) and superficial gas velocity ($U_g$) in a range of 30-180 kg m$^{-2}$ s$^{-1}$ and 1.3-10 m s$^{-1}$, respectively.

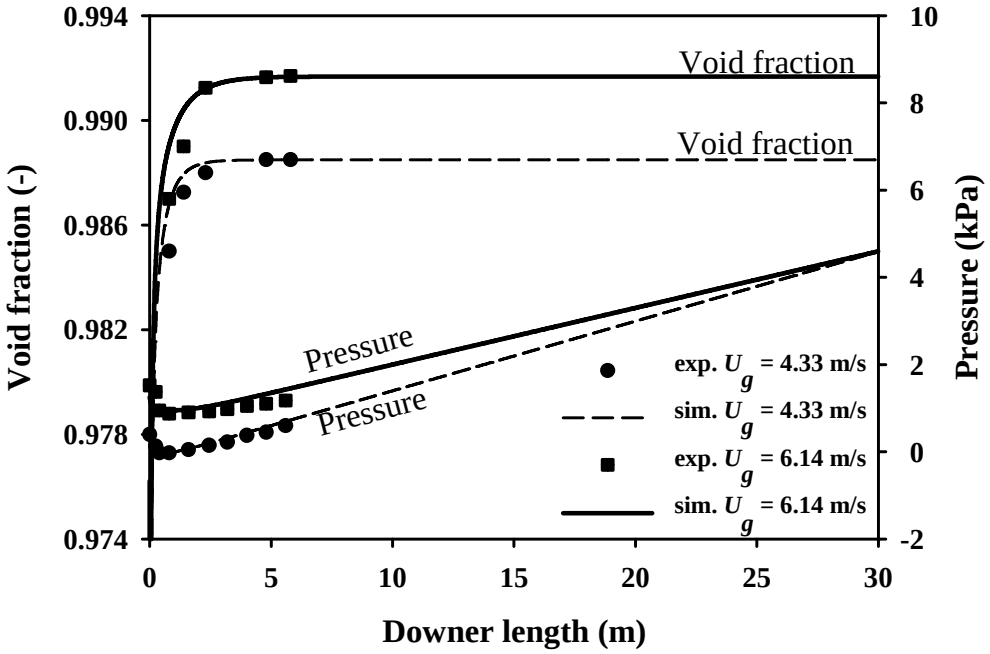


**Figure 4.1** Comparison between simulation results and experimental data at $U_g$ = 4.33 and 6.14 m $s^{-1}$.

## 4.2 Hydrodynamic model of riser

Hydrodynamic model of the riser reactor is similar to that of the downer and some equations are identical to the model for downer. The difference of these two models is the calculation of drag force and drag coefficient.

Steady state continuity equations for the gas and solid phases are:

Gas phase:

$$\frac{d(\bar{\varepsilon}_g \rho_g \bar{V}_g)}{dz} = 0 \text{, where } G_g = \bar{\varepsilon}_g \rho_g \bar{V}_g = \text{constant} \tag{4.20}$$

Solid phase:

$$\frac{d(\bar{\varepsilon}_s \rho_s \bar{V}_s)}{dz} = 0 \text{, where } G_s = \bar{\varepsilon}_s \rho_s \bar{V}_s = \text{constant} \tag{4.21}$$

The momentum conservation equations are:

Gas phase:

$$\frac{d(\bar{\varepsilon}_g \rho_g \bar{V}_g^2)}{dz} = -\frac{dP}{dz} - F_D - F_{fg} - \bar{\varepsilon}_g \rho_g g \tag{4.22}$$

Solid phase:

$$\frac{d(\bar{\varepsilon}_s \rho_s \bar{V}_s^2)}{dz} = F_D - F_{fs} - \bar{\varepsilon}_s (\rho_s - \rho_g) g \tag{4.23}$$

The drag force, $F_{D,rxt}$ , can be expressed as:

$$F_D = \frac{3}{4}\frac{C_D}{d_p}\bar{\varepsilon}_s \rho_g \left(\bar{V}_g - \bar{V}_s\right)^2 \tag{4.24}$$

The drag coefficient ( $C_D$ ) used in this work is a modified drag coefficient can be expressed as:

$$\frac{C_D}{C_{Ds}} = 1.405\eta\left(\bar{\varepsilon}_g\right)^{2.322}\left(\frac{\mathrm{Re}_r}{\mathrm{Re}_t}\right)^{-0.932}\left(\frac{d_p}{D}\right)^{0.105} \tag{4.25}$$

The correlation factor due to column diameter ( $\eta$ ) is shown below:

$$\eta = 1 - \frac{0.5e^{8(D-0.8)}}{1+e^{8(D-0.8)}} \tag{4.26}$$

The standard drag coefficient ( $C_{Ds}$ ) can be determined by:

$$C_{Ds} = \frac{24}{\mathrm{Re}_r}\left(1 + 0.15\,\mathrm{Re}_r^{\,0.687}\right) \text{ for } \mathrm{Re}_r \le 1000 \tag{4.27}$$

$$C_{Ds} = 0.44 \text{ for } \mathrm{Re}_r > 1000 \tag{4.28}$$

The Reynolds number ( $\mathrm{Re}_r$ ) is defined as:

$$\mathrm{Re}_r = \frac{\rho_g d_p \left|\bar{V}_g - \bar{V}_s\right|}{\mu_g} \tag{4.29}$$

The friction force between gas and wall ( $F_{fg}$ ) can be expressed as:

$$F_{fg} = \frac{2 f_g \bar{\varepsilon}_g \rho_g \bar{V}_g^2}{D} \tag{4.30}$$

where $f_g$ is the gas and wall friction coefficient expressed as:

$$f_g = \frac{16}{\mathrm{Re}_g}, \text{ when } \mathrm{Re}_g \le 2300 \tag{4.31}$$

$$f_g = \frac{0.079}{\mathrm{Re}_g^{0.313}}, \text{ when } \mathrm{Re}_g > 2300 \tag{4.32}$$

The Reynolds number ( $\mathrm{Re}_g$ ) is defined as:

$$\mathrm{Re}_g = \frac{\rho_g U_g D}{\mu_g} \tag{4.33}$$

The friction force between particle and wall ( $F_{fs}$ ) is

$$F_{fs} = \frac{2 f_s \bar{\varepsilon}_s \rho_s \bar{V}_s^2}{D} \tag{4.34}$$

where $f_s$ is the particle and wall friction coefficient which can be defined as:

$$f_s = \frac{0.0285\sqrt{gD}}{\left(G_s / \rho_s \bar{\varepsilon}_s\right)} \tag{4.35}$$

The superficial gas velocity and the solid velocity are defined as:

$$\bar{V}_g = \frac{U_g}{\bar{\varepsilon}_g} = \frac{G_g}{\rho_g \bar{\varepsilon}_g} \tag{4.36}$$

$$\bar{V}_s = \frac{G_s}{\rho_s \bar{\varepsilon}_s} \tag{4.37}$$

The change in superficial gas velocity is calculated by the changing in the total molar flow rate of gas as:

$$U_g = \frac{n_t R T_g}{PA} \tag{4.38}$$

Due to the limited availability of the data in the literature, he hydrodynamic model of riser is validated against the experimental data (Zhang et al., 1999) as shown in Figure 4.2. The results reveal that the model prediction and the experimental data of solid holdup in riser reactor are in good agreement.

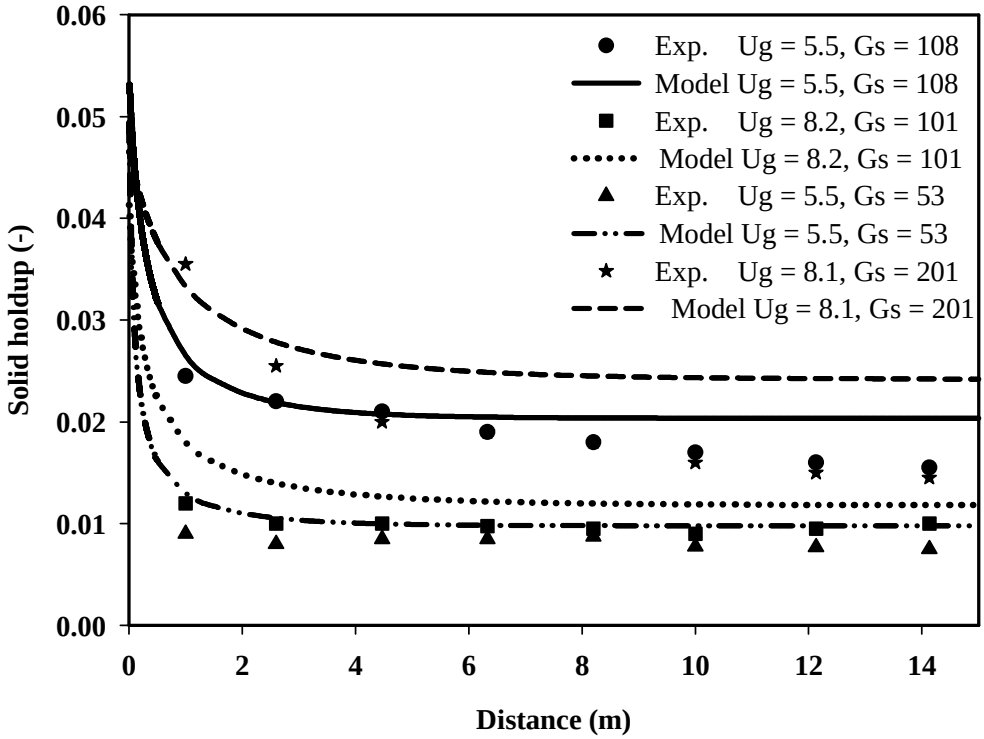


**Figure 4.2** Comparison between simulation results and experimental data of riser reactor.

## 4.3 Burning reaction model

### 4.3.1 Complete burning reaction

#### 4.3.1.1 Kinetics model

A regeneration of spent catalyst is the process that involves the burning of carbon and hydrogen depositing on the catalyst surface and the combustion of CO adsorbing on the catalyst surface as shown in the following expression:

$$CH_{12\alpha} + \left( \frac{\beta + 0.5}{\beta + 1} + 3\alpha \right) O_2 \longrightarrow \frac{\beta}{\beta + 1} CO_2 + \frac{1}{\beta + 1} CO + 6\alpha H_2O \qquad (4.39)$$

where $\alpha$ is the mass ratio of hydrogen to carbon and $\beta$ is the molar ratio of $CO_2$ to CO in the flue gas.

Here, the regeneration is assumed to be in a complete combustion mode, therefore the value of $\beta$ reaches infinity and the above reaction can be shown as:

$$CH_{12\alpha} + (1+3\alpha)O_2 \longrightarrow CO_2 + 6\alpha H_2O \tag{4.40}$$

In this case, the regeneration of coke ($CH_{12\alpha}$) that contains carbon and hydrogen is found to be two steps: carbon burning and hydrogen burning. The reaction kinetics of the two burning processes obtained from fitting with experimental data are given as (Wang et al., 1986):

$$r_C = k_C p_{O_2} C_C \tag{4.41}$$

$$r_H = k_H p_{O_2} C_H \tag{4.42}$$

$$k_C = 1.65\times10^8 \exp\left(-\frac{1.612\times10^5}{RT}\right) \tag{4.43}$$

$$k_H = \begin{cases} 2.44\times10^8 \exp\left(-1.577\times10^5/(RT)\right), T < 973\text{K} \\ 2.44\times10^8 \exp\left(-1.577\times10^5/(RT)\right)\left[1-2.67\times10^{30}\exp(-7.34\times10^4/T)\right], T \geq 973\text{K} \end{cases} \tag{4.44}$$

The partial pressure of oxygen is calculated from the ideal gas law as:

$$p_{O_2} = C_{O_2} RT \tag{4.45}$$

## 4.3.1.2 Mass and energy balances

In this study, coke is considered to be mainly composed of carbon and hydrogen. Sulfur and nitrogen are neglected due to a small portion in coke formation. Mass and energy balances along the length of a downer regenerator at steady state condition can be expressed as:

Coke:

$$\frac{dC_C}{dz} = \frac{-r_C \rho_s (1-\bar{\varepsilon}_g)}{G_s} \tag{4.46}$$

Hydrogen:

$$\frac{dC_H}{dz} = \frac{-r_H \rho_s (1-\bar{\varepsilon}_g)}{G_s} \tag{4.47}$$

Oxygen:

$$\frac{dC_{O_2}}{dz} = \frac{-(r_C/12 + r_H/4)\rho_s(1-\bar{\varepsilon}_g)}{U_g} \tag{4.48}$$

Carbon dioxide:

$$\frac{dC_{CO_2}}{dz} = \frac{(r_C/12)\rho_s(1-\bar{\varepsilon}_g)}{U_g} \tag{4.49}$$

Water:

$$\frac{dC_{H_2O}}{dz} = \frac{(2r_H/4)\rho_s(1-\bar{\varepsilon}_g)}{U_g} \tag{4.50}$$

Energy:

$$\frac{dT}{dz} = \frac{\rho_s(1-\bar{\varepsilon}_g)(r_C\Delta H_C + r_H\Delta H_H)}{U_g\rho_g C_{p,g} + G_s C_{p,s}} \tag{4.51}$$

The concentration of carbon and hydrogen on the catalyst and the feed temperature at the regenerator inlet can be determined by the following relations:

$$C_{C,0} = \frac{G_{ss}C_{Cs} + G_{sr}C_{C,out}}{G_{ss} + G_{sr}} \tag{4.52}$$

$$C_{H,0} = \frac{\alpha G_{ss}C_{Cs} + G_{sr}C_{H,out}}{G_{ss} + G_{sr}} \tag{4.53}$$

$$T_0 = \frac{G_{ss}C_{p,s}T_s + G_{sr}C_{p,s}T_{g,out} + U_g\rho_g C_{p,g}T_a}{G_{ss}C_{p,s} + G_{sr}C_{p,s} + U_g\rho_g C_{p,g}} \tag{4.54}$$

## 4.3.2 Partial burning reactions

### 4.3.2.1 Kinetics model

The main objective of the regeneration process is to recover the cracking activity of the FCC catalyst caused by the deposition of coke. Generally, coke is considered to be composed of carbon and hydrogen atoms at a different ratio. This ratio is obtained by a laboratory determination and found that H/C ratio in coke ranges from 0.5 to 1.0 (Wang et al., 1986). Burning reactions involve with the burning of carbon and hydrogen atom in coke as well as the combustion of carbon monoxide to

carbon dioxide which are shown below: (Arbel et al., 1995; Han and Chung, 2001a; Affum et al., 2011).

Reaction 1: $$C+\frac{1}{2}O_2 \xrightarrow{k_1} CO \tag{4.55}$$

Reaction 2: $$C+O_2 \xrightarrow{k_2} CO_2 \tag{4.56}$$

Reaction 3 (heterogeneous): $$CO+\frac{1}{2}O_2 \xrightarrow[heterogeneos]{k_{3c}} CO_2 \tag{4.57}$$

Reaction 3 (homogeneous): $$CO+\frac{1}{2}O_2 \xrightarrow[homogeneous]{k_{3h}} CO_2 \tag{4.58}$$

Reaction 4: $$H+\frac{1}{4}O_2 \xrightarrow{k_4} \frac{1}{2}H_2O \tag{4.59}$$

The initial ratio of $CO/CO_2$ at catalyst surface which relates to burning rate of carbon to CO and $CO_2$ can be expressed by;

$$\frac{CO}{CO_2}=\frac{k_1}{k_2}=\beta_C=\beta_{C,0}\exp(-E_\beta/RT) \tag{4.60}$$

The rate constant for complete and incomplete burning reaction (Reaction 1 and 2) can be explained in term of overall coke burning rate as shown:

$$k_1=\frac{\beta_C k_C}{\beta_C+1} \tag{4.61}$$

$$k_2=\frac{k_C}{\beta_C+1} \tag{4.62}$$

where $k_C=k_1+k_2=k_{C,0}\exp(-E_c/RT)$.

The rate constant for catalytic and homogeneous combustions of CO as well as the rate constant for hydrogen burning can be express as:

$$k_{3c}=k_{3c,0}\exp(-E_{3c}/RT) \tag{4.63}$$

$$k_{3h}=k_{3h,0}\exp(-E_{3h}/RT) \tag{4.64}$$

$$k_4=\begin{cases} k_{4,0}\exp\left(-E_4/(RT)\right), & T<973\,\mathrm{K} \\ k_{4,0}\exp\left(-E_4/(RT)\right)\left[1-2.67\times10^{30}\exp(-7.34\times10^4/T)\right], & T\geq 973\,\mathrm{K} \end{cases} \tag{4.65}$$

The rates of all burning reactions are shown below:

$$r_1 = k_1 P_{O_2} C_C \tag{4.66}$$

$$r_2 = k_2 P_{O_2} C_C \tag{4.67}$$

$$r_{3c} = \bar{\varepsilon}_s \rho_s k_{3c} P_{O_2} P_{CO} \tag{4.68}$$

$$r_{3h} = \bar{\varepsilon}_g k_{3h} P_{O_2} P_{CO} \tag{4.69}$$

$$r_4 = k_4 P_{O_2} C_H \tag{4.70}$$

### 4.3.2.2 Mass balance

Therefore, mass balances of species concentration in the downer regenerator are:

Carbon:

$$\frac{dC_C}{dz} = \frac{-(r_1 + r_2)\rho_s \bar{\varepsilon}_s}{G_s} \tag{4.71}$$

Hydrogen:

$$\frac{dC_H}{dz} = \frac{-r_H \rho_s \bar{\varepsilon}_s}{G_s} \tag{4.72}$$

Oxygen:

$$\frac{dC_{O_2}}{dz} = \frac{1}{U_g}\left[\left(-\frac{1}{2}\frac{r_1}{12} - \frac{r_2}{12} - \frac{r_4}{4}\right)\rho_s \bar{\varepsilon}_s + \left(-\frac{1}{2} r_{3c} - \frac{1}{2} r_{3h}\right)\right] \tag{4.73}$$

Carbon monoxide:

$$\frac{dC_{CO}}{dz} = \frac{1}{U_g}\left[\left(\frac{r_1}{12}\right)\rho_s \bar{\varepsilon}_s + (-r_{3c} - r_{3h})\right] \tag{4.74}$$

Carbon dioxide:

$$\frac{dC_{CO_2}}{dz} = \frac{1}{U_g}\left[\left(\frac{r_2}{12}\right)\rho_s \bar{\varepsilon}_s + (r_{3c} + r_{3h})\right] \tag{4.75}$$

Steam:

$$\frac{dC_{H_2O}}{dz} = \frac{1}{U_g}\left[r_4 \rho_s \bar{\varepsilon}_s\right] \tag{4.76}$$

In regeneration process, the recycled stream is used, therefore; the initial condition for carbon, hydrogen and temperature can be calculated using the relations as shown below:

$$C_{\mathrm{C},0} = \frac{G_s C_C + G_{sr} C_{\mathrm{C,out}}}{G_s + G_{sr}} \tag{4.77}$$

$$C_{\mathrm{H},0} = \frac{\alpha G_s C_C + G_{sr} C_{H,out}}{G_s + G_{sr}} \tag{4.78}$$

$$T_0 = \frac{G_s C_{p,s} T_{s,rxt} + G_{sr} C_{p,s} T_{g,\mathrm{out}} + U_{g,0} \rho_{g,0} C_{p,g,0} T_a}{G_s C_{p,s} + G_{sr} C_{p,s} + U_{g,0} \rho_{g,0} C_{p,g,0}} \tag{4.79}$$

**Table 4.1** The kinetic parameters for regeneration reaction (Arbel et al.,1995)

| Parameters | Value |
|---|---|
| Pre-exponential factor for CO/$CO_2$ ratio at surface, $\beta_{C,0}$ (-) | $9.53\times10^{-4}$ |
| Activation energy for CO/$CO_2$ ratio at surface, $E_\beta$ (given in the form of E/R, K) | 6795.56 |
| Pre-exponential factor for overall coke combustion, $k_{C,0}$ (1/(kPa s)) | $1.055\times10^{6}$ |
| Activation energy for overall coke combustion, $E_C$ (E/R, K) | 18889 |
| Pre-exponential factor for catalytic CO combustion, $k_{3c,0}$ (kmol/(kg $kPa^2$ s)) | $1.136\times10^{-2}$ |
| Activation energy for catalytic CO combustion, $E_{3c}$ (E/R, K) | 13889 |
| Pre-exponential factor for homogeneous CO combustion, $k_{3h,0}$ (kmol/($m^3$ $kPa^2$ s)) | $4.932\times10^{10}$ |
| Activation energy for homogeneous CO combustion, $E_{3h}$ (E/R, K) | 35556 |
| Pre-exponential factor for hydrogen burning reaction, $k_{4,0}$ (1/(kPa s)) | $2.44\times10^{8}$ |
| Activation energy for hydrogen burning reaction, $E_4$ (K) | $1.577\times10^{5}$ |

### 4.3.2.3 Energy balance

In this work, we assume that the temperature of the catalyst and gas in the regenerator are in thermal equilibrium so the temperature variation along the regenerator length can be expressed as shown below:

$$\frac{dT}{dz} = \frac{1}{U_g \rho_g C_{p,g} + G_s C_{p,s}} \left\{ \left( \frac{\rho_s \bar{\varepsilon}_s}{12} (r_1 \Delta H_1 + r_2 \Delta H_2) \right) + \ldots \right. \\ \left. + r_{3c} \Delta H_3 + r_{3h} \Delta H_3 + \left( \rho_s \bar{\varepsilon}_s r_4 \Delta H_4 \right) \right\} \quad (4.80)$$

## 4.4 Steam gasification reaction model

### 4.4.1 Kinetics of steam gasification reaction

Gasification reaction is the reaction of coke on spent catalyst with steam to form CO and $H_2O$. Actually, there are four main reactions involving in the gasification reaction including gasification, water-gas shift, methanation, and boudouard reaction.

Gasification reaction: $C + H_2O \rightarrow CO + H_2$ (4.81)

Water-gas shift reaction: $CO + H_2O \rightarrow CO_2 + H_2$ (4.82)

Methanation reaction: $C + 2H_2 \rightarrow CH_4$ (4.83)

Boudouard reaction: $C + CO_2 \rightarrow 2CO$ (4.84)

In this work, we assume that there is only the gasification reaction proceed with burning reaction and the rate of gasification reaction can be expressed as

$$r_{gf} = k_{gf} C_C \quad (4.85)$$

The rate constant obtained from the experimental determination of Corma et al., 2001 can be expressed in the Arrhenius equation form as shown:

$$k_{gf} = 4022530 \exp(-239000 / RT) \quad (4.86)$$

### 4.4.2 Mass and energy balances

In this study, the steam gasification reaction occurs along with the burning reactions (assumed the complete burning reaction). Mass and energy balances along the length of a downer regenerator at steady state condition can be expressed as:

Coke:

$$\frac{dC_C}{dz} = \frac{-(r_C + r_{gf})\rho_s(1-\bar{\varepsilon}_g)}{G_s} \tag{4.87}$$

Hydrogen:

$$\frac{dC_H}{dz} = \frac{-r_H \rho_s(1-\bar{\varepsilon}_g)}{G_s} \tag{4.88}$$

Oxygen:

$$\frac{dC_{O_2}}{dz} = \frac{-(r_C/12 + r_H/4)\rho_s(1-\bar{\varepsilon}_g)}{U_g} \tag{4.89}$$

Carbon dioxide:

$$\frac{dC_{CO_2}}{dz} = \frac{(r_C/12)\rho_s(1-\bar{\varepsilon}_g)}{U_g} \tag{4.90}$$

Carbon monoxide:

$$\frac{dC_{CO}}{dz} = \frac{r_{gf}\rho_s(1-\bar{\varepsilon})}{U_g} \tag{4.91}$$

Water:

$$\frac{dC_{H_2O}}{dz} = \frac{((2r_H/4) - r_{gf})\rho_s(1-\bar{\varepsilon}_g)}{U_g} \tag{4.92}$$

Gas hydrogen:

$$\frac{dC_{H_2}}{dz} = \frac{r_{gf}\rho_s(1-\bar{\varepsilon}_g)}{U_g} \tag{4.93}$$

Energy:

$$\frac{dT}{dz} = \frac{\rho_s(1-\bar{\varepsilon}_g)(r_C\Delta H_C + r_H\Delta H_H + r_{gf}\Delta H_{gf})}{U_g\rho_g C_{p,g} + G_s C_{p,s}} \tag{4.94}$$

The concentration of carbon and hydrogen on catalyst and the feed temperature at the regenerator inlet can be determined by the following relations.

$$C_{C,0} = \frac{G_{ss}C_{Cs} + G_{sr}C_{C,out}}{G_{ss} + G_{sr}} \tag{4.95}$$

$$C_{H,0} = \frac{\alpha G_{ss}C_{Cs} + G_{sr}C_{H,out}}{G_{ss} + G_{sr}} \tag{4.96}$$

$$T_0 = \frac{G_{ss}C_{p,s}T_s + G_{sr}C_{p,s}T_{g,out} + U_g\rho_g C_{p,g}T_a}{G_{ss}C_{p,s} + G_{sr}C_{p,s} + U_g\rho_g C_{p,g}} \tag{4.97}$$

## 4.5 Model of cracking reactions

### 4.5.1 Mass balance and kinetics model

Mass fraction of each lump is calculated based on the four lumps reaction scheme (Figure 4.3) which can be expressed as shown:

$$\frac{dy_i}{dz} = \frac{\rho_s \bar{\varepsilon}_s A \phi_c}{F_g} r_i, \text{ where } i = go, gl, gs, \text{and } ck \tag{4.98}$$

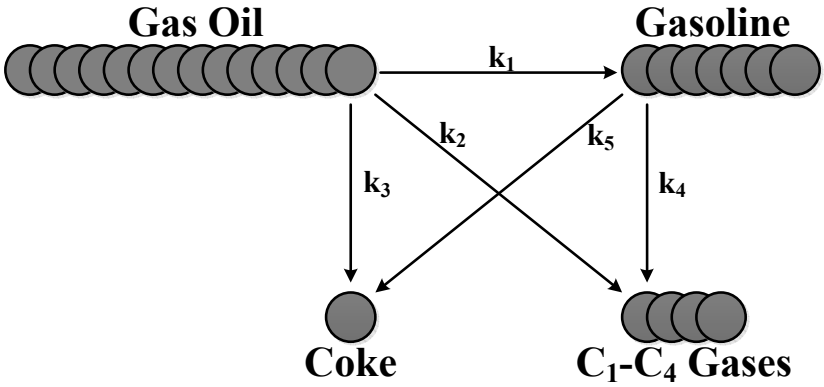


**Figure 4.3** Four-lump cracking reaction scheme.

In this work, we calculated coke deactivation as a function of the coke content on the catalyst while the coke deactivation coefficient ($\alpha_c$) is also a function of temperature and feedstock composition. The deactivation function and the corresponding coefficient can be expressed as:

$$\phi_c = \exp\left(-\alpha_c C_c\right) \tag{4.99}$$

where the coefficient $\alpha_c = \alpha_{c0} \exp\left(\frac{-E_c}{RT_g}\right) R_{AN}^{\alpha_c^*}$

The kinetics parameters of cracking reactions used in this simulation are in the form of Arrhenius equation as shown below:

$$k_i = k_{i,0} \exp\left(\frac{-E_i}{RT_g}\right) \text{ for } i = 1, 2, 3, 4, and\ 5 \tag{4.100}$$

The cracking of gas oil is considered to be second order respect to the gas oil concentration (or fraction of gas oil) while the cracking reactions of other species are first order reactions. The rate of reactions can be described as shown below:

$$r_{go} = -\left(k_1 + k_2 + k_3\right) y_{go}^2 \tag{4.101}$$

$$r_{gl} = k_1 y_{go}^2 - k_4 y_{gl} - k_5 y_{gl} \tag{4.102}$$

$$r_{gs} = k_2 y_{go}^2 + k_4 y_{gl} \tag{4.103}$$

$$r_{ck} = k_3 y_{go}^2 + k_5 y_{gl} \tag{4.104}$$

$$r_{wv} = 0 \tag{4.105}$$

**Table 4.2** The kinetics parameters for four-lump cracking reactions

| Four-lump cracking reactions | Pre-exponential factor (1/s) | Activation energy (kJ/kmol) | Heat of reaction (kJ/kg) |
|---|---|---|---|
| Gasoil to gasoline | 1457.50[a] | 57359[a] | 393[b] |
| Gasoil to $C_1$-$C_4$ gases | 127.59[a] | 52754[a] | 975[b] |
| Gasoil to coke | 1.98[a] | 31820[a] | 1200[b] |
| Gasoline to $C_1$-$C_4$ gases | 256.81[a] | 65733[a] | 1150[b] |
| Gasoline to coke | $6.29\times 10^{-4}$[a] | 66570[a] | 151[b] |
| Deactivation function | $1.1\times 10^{-5}$[a] | 49000[a] | $\alpha_C^* = 0.1177$[a] |

[a]data from Han and Chung, 2001b.

[b]data from Shaikh et al.,2008.

### 4.5.2 Energy balance

At the entrance of the downer reactor, the preheated liquid feedstock will be fed using feed atomization to form small droplets. Those droplets will be assumed to be vaporized instantaneously during contacting with the hot regenerated catalyst. After vaporization, the temperature of vapor hydrocarbon can be calculated using Antoine equation and the temperature of the catalyst can be calculated by the energy balance as shown below:

Gas phase:

$$T_{g,FS} = \frac{B_{\lg}}{A_{\lg} - \log\left(P_{FS} y_{go,FS}\right)} - C_{\lg} \tag{4.106}$$

Solid Phase:

$$T_{s,FS} = T_{s,out} - \frac{1}{F_{s,CL} C_{p,s}} \left[ F_{\lg} C_{p,\lg} \left(T_{g,FS} - T_{\lg}\right) + F_{ds} C_{p,ds} \left(T_{g,FS} - T_{ds}\right) + \ldots F_{\lg} \Delta H_{v\lg} \right] \tag{4.107}$$

Then, we can estimate the temperature profile of both phases along the length the downer reactor from the following energy balance equations:

Gas phase:

$$\frac{dT_g}{dz} = \frac{A}{F_g C_{p,g}} \left[ h_p A_p \left(T_s - T_g\right) + \rho_s \bar{\varepsilon}_s Q_{react} \right] \tag{4.108}$$

Solid Phase:

$$\frac{dT_s}{dz} = \frac{A h_p A_p}{F_s C_{p,s}} \left(T_g - T_s\right) \tag{4.109}$$

The heat of reaction ($Q_{react}$), the interface heat transfer coefficient between phases ($h_p$) and the thermal conductivity of hydrocarbon ($k_g$) can be calculated from the equations below:

Heat of reaction:

$$Q_{react} = -\left(\Delta H_1 k_1 y_{go}^2 + \Delta H_2 k_2 y_{go}^2 + \Delta H_3 k_3 y_{go}^2 + \Delta H_4 k_4 y_{gl} + \Delta H_5 k_5 y_{gl}\right) \phi_c \tag{4.110}$$

Heat transfer coefficient between phases:

$$h_p = 0.03 \frac{k_g}{d_p^{2/3}} \left[ \frac{\left| V_g - V_s \right| \rho_g \bar{\varepsilon}_g}{\mu_g} \right]^{1/3} \tag{4.111}$$

Thermal conductivity of hydrocarbon:

$$k_g = 10^{-6} \times \left( 1.9469 - 0.374 M_{wm} + 1.4815 \times 10^{-3} M_{wm}^2 + 0.1028 T_g \right) \tag{4.112}$$

# CHAPTER V

# A SYSTEMMATIC MODEL-BASED ANALYSIS OF A DOWNER REGENERATOR IN FLUID CATALYTIC CRACKING PROCESSES

## 5.1 Introduction

In the typical FCC regenerator, coke deposited on catalyst's surface is eliminated by combustion reactions in the turbulent bed regenerator. To improve the burning efficiency of the regeneration, the riser regenerator has been invented (Bai et al., 1997, 1998). However, some theoretical and experimental studies indicated that the operation of the riser in which gas and solid flowing against the direction of gravity suffers from the severe back-mixing and non-uniform flow structure causing the wide residence time distribution of the gas and solid phases (Werther and Hirschberg, 1997; Jin et al., 2002). Since the radial distributions of gas and solid in a downer is more uniform than that in a riser, the use of the downer as a regenerator would be a promising approach.

Model-based process analysis is the effective way to understand a process behavior and the obtained data can be employed for design and enhancement of the process. Singh et al. (2009) proposed the model-based, computer-aided system approach for design and analysis of the pharmaceutical process including the monitoring system and this case study was extensively studied by Gernaey et al. (2010). Anenas et al. (2006) used the same approach to design the copolymerization process.

In this study, the performance of a downer regenerator of FCC process is analyzed based on a systematic model-based approach. A one-dimensional model of the downer regenerator, which consists of mass and energy conservative equations, hydrodynamic characteristics and regeneration kinetics of FCC catalyst under steady

state condition, is employed to perform a sensitivity analysis of the regenerator with respect to key operating parameters such as recycled and spent catalyst flow rates, superficial gas velocity, carbon content on spent catalyst, and spent catalyst temperature, on the catalyst regeneration performance.

## 5.2 Systematic model-based analysis

A systematic procedure for model-based analysis and design of processes starts with defining a process objective. This step is important because the designed process has to be satisfied with this process objective. Then, details of the process configuration are considered and a mathematical model is developed for analysis of the process behavior. After the model analysis is performed, a suitable model solution approach is selected for process simulation. A sensitivity analysis is then carried out to determine key process parameters, which are used for optimal design of the process.

### 5.2.1 Process objective

The objective of a FCC downer regenerator is to eliminate coke deposited on the surface of catalyst. Therefore, the required final product is the regenerated catalyst that has low carbon and hydrogen contents. However, a temperature of the regenerated catalyst should not be higher than the refractory limit of the catalyst.

### 5.2.2 Description of a downer regenerator

Figure 5.1 shows an FCC process consisting of a riser reactor and a downer regenerator. The feedstock consisting of heavy hydrocarbons is preheated and then injected with steam at the bottom of the reactor through a distributor. The injected feedstock contacts the hot regenerated catalyst circulated from the regenerator, and then vaporizes. Feedstock vapor and catalyst move upward and cracking reactions occur at the same time, increasing the gas velocity due to a molar expansion. As the cracking reactions occur, coke is deposited on the catalyst surface and is needed to be

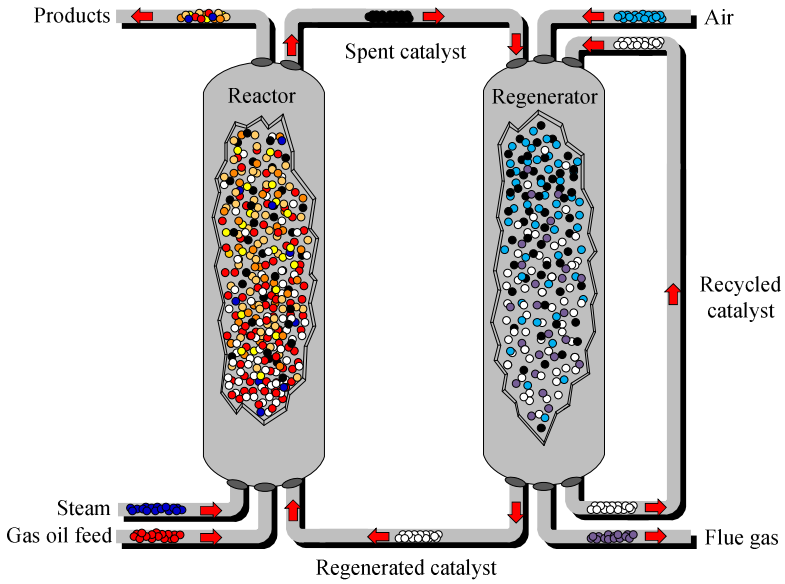


**Figure 5.1** Process flow diagram of the FCC unit.

cleaned out, otherwise it causes the catalyst deactivation. At the top of the riser reactor, the gaseous products and catalyst with coke are separated. Hydrocarbon products and uncracked feedstock are sent to a fractionator to split into various product fractions. A deactivated catalyst is sent to the downer regenerator to burn coke away. The deactivated catalyst and the recycled catalyst along with the preheated air are fed at the top of the regenerator through gas and solid distributors. Then, coke depositing on the surface of the catalyst particles is eliminated by combustion reactions. The heat produced by the burning reactions is transferred to the reactor by the circulation of the catalyst and used for vaporizing the feed stream and raising the temperature of gases for the endothermic cracking reactions occurring in the FCC reactor. It is noted that when gas and catalyst enter a downer, the gas velocity is higher than the catalyst velocity (nearly zero). Then, the catalyst velocity will increase due to the drag force and the gravity. This section is called the first acceleration zone. When the catalyst velocity is equal to the gas velocity, the drag force becomes zero, indicating the end of the first acceleration zone. Once the catalyst velocity is higher than the gas velocity, the drag force changes its direction to be the resistance of the catalyst flow. However, the catalyst is still accelerated by the gravity force with a lower rate. This section is called the second acceleration zone. When the drag force balances the gravity, the particles will flow under the constant velocity

which is called the constant velocity zone (Zhu et al., 1995; Deng et al., 2004; Karimipour et al., 2006). This unique feature of the downer is quite different from that of the riser where the gas velocity is always higher than the particles velocity.

In this study, the downer regeneration is mainly focused. To analyze the performance of the FCC catalyst regenerator, hydrodynamic model, mass and energy balances and kinetics of catalyst regeneration are required.

### 5.2.3 Mathematical model

The details of the models and model validation are described in Section 4.1 and 4.3.1 of Chapter IV. The following table summarizes the equations used in this study.

**Table 5.1** The mathematical model used in chapter V.

| | |
|---|---|
| $\frac{d(\bar{\varepsilon}_g \rho_g \bar{V}_g)}{dz} = 0$ , where $G_g = \bar{\varepsilon}_g \rho_g \bar{V}_g = \text{constant}$ | (5.1) |
| $\frac{d(\bar{\varepsilon}_s \rho_s \bar{V}_s)}{dz} = 0$ , where $G_s = \bar{\varepsilon}_s \rho_s \bar{V}_s = \text{constant}$ | (5.2) |
| $\bar{\varepsilon}_g + \bar{\varepsilon}_s = 1$ | (5.3) |
| $\frac{d(\bar{\varepsilon}_g \rho_g \bar{V}_g^2)}{dz} = -\frac{dP}{dz} - F_D - F_{fg} + \bar{\varepsilon}_g \rho_g g$ | (5.4) |
| $\frac{d(\bar{\varepsilon}_s \rho_s \bar{V}_s^2)}{dz} = F_D - F_{fs} + \bar{\varepsilon}_s (\rho_s - \rho_g) g$ | (5.5) |
| $F_D = \frac{3}{4} \frac{C_D}{d_p} \bar{\varepsilon}_s \rho_g \left\| \bar{V}_g - \bar{V}_s \right\| \left( \bar{V}_g - \bar{V}_s \right)$ | (5.6) |
| $\frac{C_D}{C_{Ds}} = \frac{14.1\left[1 + 2.78\left(G_g / G_s\right)\right]}{Fr}$ | (5.7) |
| $Fr = \frac{U_g}{\sqrt{g d_p}}$ | (5.8) |

**Table 5.1** The mathematical model used in (Continued).

$$C_{Ds}=\begin{cases}\dfrac{24}{\mathrm{Re}_r}\left(1+0.15\,\mathrm{Re}_r^{\,0.687}\right), \mathrm{Re}_r \le 1000\\ 0.44, \mathrm{Re}_r > 1000\end{cases} \tag{5.9}$$

$$\mathrm{Re}_r=\frac{\rho_g d_p \left|\bar{V}_g-\bar{V}_s\right|}{\mu_g} \tag{5.10}$$

$$F_{fg}=\frac{2 f_g \bar{\varepsilon}_g \rho_g \bar{V}_g^2}{D} \tag{5.11}$$

$$f_g=\begin{cases}\dfrac{16}{\mathrm{Re}_g}, \mathrm{Re}_g \le 2300\\ \dfrac{0.079}{\mathrm{Re}_g^{\,0.313}}, \mathrm{Re}_g > 2300\end{cases} \tag{5.12}$$

$$\mathrm{Re}_g=\frac{\rho_g U_g D}{\mu_g} \tag{5.13}$$

$$F_{fs}=\frac{2 f_s \bar{\varepsilon}_s \rho_s \bar{V}_s^2}{D} \tag{5.14}$$

$$f_s=\frac{0.0285\sqrt{gD}}{\left(G_s/\rho_s\bar{\varepsilon}_s\right)} \tag{5.15}$$

$$\frac{dC_{\mathrm{C}}}{dz}=\frac{-r_{\mathrm{C}}\rho_s(1-\bar{\varepsilon}_g)}{G_s} \tag{5.16}$$

$$\frac{dC_{\mathrm{H}}}{dz}=\frac{-r_{\mathrm{H}}\rho_s(1-\bar{\varepsilon}_g)}{G_s} \tag{5.17}$$

$$\frac{dC_{\mathrm{O_2}}}{dz}=\frac{-(r_{\mathrm{C}}/12+r_{\mathrm{H}}/4)\rho_s(1-\bar{\varepsilon}_g)}{U_g} \tag{5.18}$$

$$\frac{dT}{dz}=\frac{\rho_s(1-\bar{\varepsilon}_g)(r_{\mathrm{C}}\Delta H_C+r_{\mathrm{H}}\,\Delta H_{\mathrm{H}})}{U_g\rho_g C_{p,g}+G_s C_{p,s}} \tag{5.19}$$

$$r_{\mathrm{C}}=k_{\mathrm{C}}\,p_{\mathrm{O_2}}C_{\mathrm{C}} \tag{5.20}$$

$$r_{\mathrm{H}}=k_{\mathrm{H}}\;p_{\mathrm{O_2}}C_{\mathrm{H}} \tag{5.21}$$

**Table 5.1** The mathematical model used in (Continued).

$$k_C = 1.65\times10^8 \exp\left(-\frac{1.612\times10^5}{RT}\right) \tag{5.22}$$

$$k_H = \begin{cases} 2.44\times10^8 \exp\left(-1.577\times10^5/(RT)\right), T < 973\,\mathrm{K} \\ 2.44\times10^8 \exp\left(-1.577\times10^5/(RT)\right)\times \\ \quad \left[1-2.67\times10^{30}\exp(-7.34\times10^4/T)\right], T \geq 973\,\mathrm{K} \end{cases} \tag{5.23}$$

$$p_{O_2} = C_{O_2} RT \tag{5.24}$$

$$C_{\mathrm{C},0} = \frac{G_{ss}C_{Cs} + G_{sr}C_{\mathrm{C,out}}}{G_{ss}+G_{sr}} \tag{5.25}$$

$$C_{\mathrm{H},0} = \frac{\alpha G_{ss}C_{Cs} + G_{sr}C_{H,out}}{G_{ss}+G_{sr}} \tag{5.26}$$

$$T_0 = \frac{G_{ss}C_{p,s}T_s + G_{sr}C_{p,s}T_{g,\mathrm{out}} + U_g\rho_g C_{p,g}T_a}{G_{ss}C_{p,s} + G_{sr}C_{p,s} + U_g\rho_g C_{p,g}} \tag{5.27}$$

## 5.2.4 Model analysis

The model of the downer regenerator consists of 21 algebraic equations (Eqs. (5.1)-(5.3), (5.6)-(5.15) and (5.20)-(5.27)) and 6 differential equations (Eqs. (5.4), (5.5) and (5.16)-(5.19)) and the number of variables involved is 50, which can be classified into two groups: known and predicted variables. The known variables are 5 design parameters and 15 process parameters, whereas the predicted variables are 6 differential variables and 24 algebraic variables, as shown in Table 5.2. It can be seen that the number of predicted variables is higher than that of the equations and thus, a iteration solution approach needs to be implemented (Singh et al., 2009).

**Table 5.2** Classification of variables in the FCC regenerator model.

| **Known variables** | | **Predicted variables** | |
|---|---|---|---|
| **Process parameters** | **Design parameters** | **Differential variables** | **Algebraic variables** |
| $\rho_s\ \rho_g\ g\ d_p\ \mu_g$ $D\ \Delta H_C\ \Delta H_H$ $C_{pC}\ C_{pg}\ \alpha\ R$ $T_{air}\ G_g\ G_s$ | $U_g\ G_{ss}\ G_{sr}\ C_{Cs}\ T_s$ | $\bar{\varepsilon}_g\ P\ C_C\ C_H\ C_{O_2}$ $T$ | $\bar{\varepsilon}_s\ V_g\ V_s\ F_{fg}\ F_{fs}\ F_D$ $C_D\ C_{Ds}\ F_r\ \mathrm{Re}_r\ \mathrm{Re}_g$ $f_g\ f_s\ r_C\ r_H\ k_C\ k_H$ $p_{O_2}\ C_{C,out}\ C_{H,out}$ $T_{g,out}\ C_{C,0}\ C_{H,0}\ T_0$ |

## 5.2.5 Model solution

In this work, the mathematical model of the downer regenerator mentioned above is coded by Matlab and numerically solved by Euler's method to determine the variations in solid holdup, pressure, gas compositions and temperature along the length of the regenerator. Figure 5.2 shows the iterative, numerical approach for the model solution. In the figure, initial conditions for void fraction ($\bar{\varepsilon}_g$) and pressure ($P$) are first specified together with initial guesses of the unknown variables: the outlet concentrations of carbon ($C_{\mathrm{C,out}}$) and hydrogen ($C_{\mathrm{H,out}}$) and the outlet temperature ($T_{g,\mathrm{out}}$). To obtain the solution at each length step, a set of differential and algebraic equations describing the hydrodynamic characteristics, species concentrations and temperature within the downer regenerator is solved. The calculation continues until the step reaches the end of the downer and then the unknown variable is recalculated. This procedure is repeated until the difference in the values of the unknown and calculated variables satisfies a desired accuracy ($10^{-6}$).

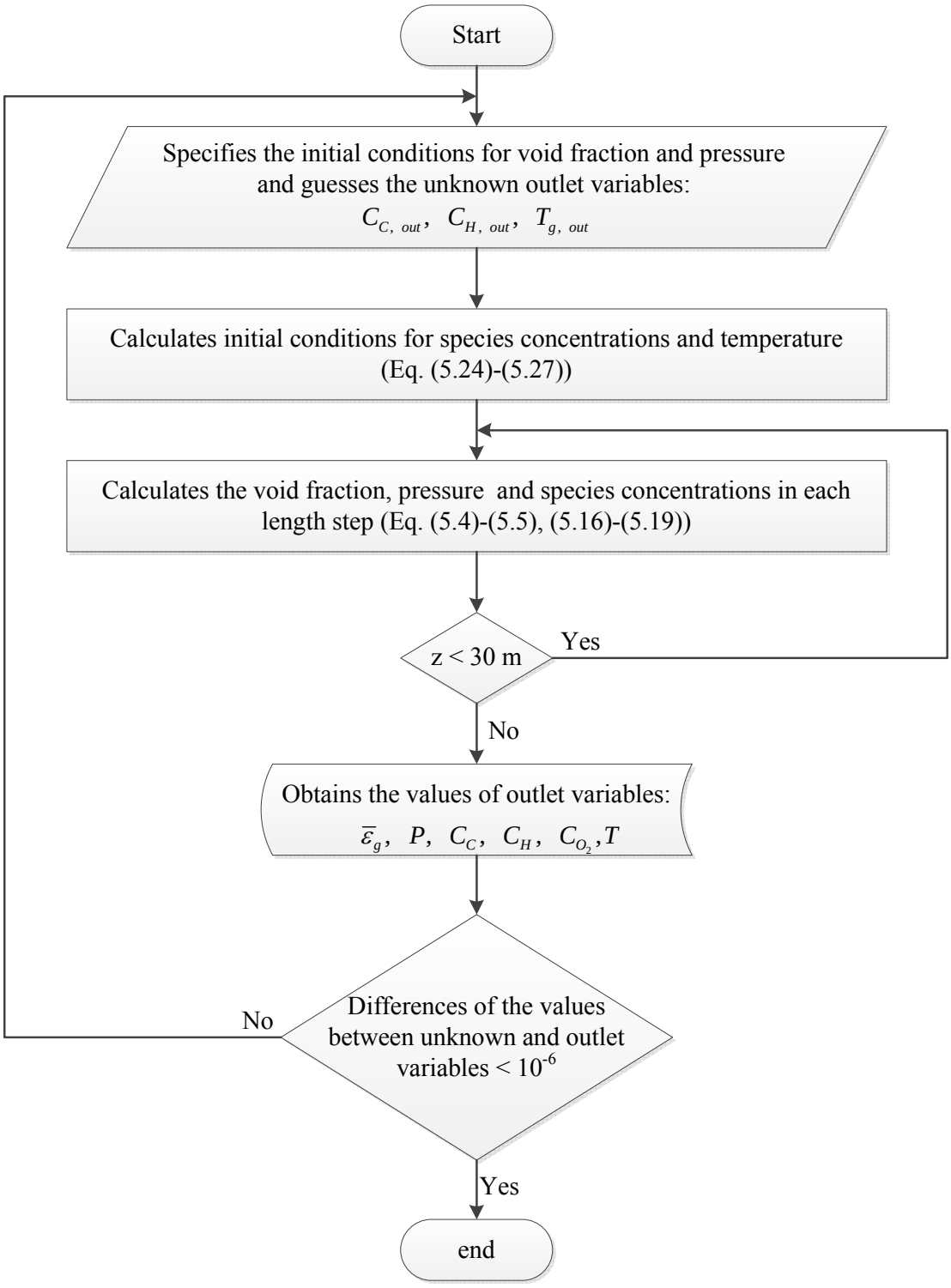


**Figure 5.2** Schematic diagram of numerical model solution.

### 5.2.6 Sensitivity analysis

Simulations of the downer regenerator for a given set of initial conditions are performed to investigate the effect of key operational parameters. Table 5.3 lists the values of model parameters and known initial conditions used in this study. A range of the catalyst flow rate and superficial gas velocity are chosen based on the validity of the hydrodynamic model. Regarding the objective of the downer regenerator to eliminate coke on the surface of catalyst without causing high temperatures, key parameters affecting this effect are investigated. Five scenarios are selected to perform the sensitivity analysis; the regenerator is operated with different recycled catalyst flow rate, spent catalyst flow rate, carbon content on spent catalyst, spent catalyst temperature and superficial gas velocity. The standard conditions of the regenerator and their operational ranges examined in this study are shown in Table 5.4. The results of the analysis are presented in the next section.

**Table 5.3** Parameters used for simulation of a downer regenerator at standard condition.

| | |
|---|---|
| spent catalyst flow rate ($G_{ss}$) | 40 kg $m^{-2}$ $s^{-1}$ |
| recycled catalyst flow rate ($G_{sr}$) | 120 kg $m^{-2}$ $s^{-1}$ |
| total solid flow rate ($G_s$) | 160 kg $m^{-2}$ $s^{-1}$ |
| carbon content on spent catalyst ($C_{Cs}$) | 0.0125 kg carbon kg $catalyst^{-1}$ |
| mass ratio of hydrogen to carbon in coke ($\alpha$) | 0.087 |
| spent catalyst temperature ($T_s$) | 763.15 K |
| inlet air temperature ($T_a$) | 313.15 K |
| superficial gas velocity ($U_g$) | 4 m $s^{-1}$ |
| gas flow rate ($G_g$) | 1.83 kg $m^{-2}$ $s^{-1}$ |
| catalyst density ($\rho_s$) | 1545 kg $m^{-3}$ |
| diameter of catalyst particle ($d_p$) | 0.000059 m |
| downer diameter ($D$) | 0.14 m |
| inlet averaged voidage ( $\bar{\varepsilon}_g$ ) | 0.6 |
| inlet pressure ($P$) | 506.625 kPa |

**Table 5.4** Operating conditions for the downer regenerator.

| Parameters | Standard condition | Operational range |
|---|---|---|
| 1. Recycled catalyst flow rate , $G_{sr}$ (kg/m$^2$s) | 120 | 20-120 |
| 2. Superficial gas velocity, $U_g$ (m/s) | 4 | 1-10 |
| 3. Spent catalyst flow rate , $G_{ss}$ (kg/m$^2$s) | 40 | 20-60 |
| 4. Carbon content on spent catalyst, $C_{Cs}$ (kg/kg catalyst) | 0.0125 | 0.010-0.035 |
| 5. Spent catalyst temperature, $T_s$ (K) | 763.15 | 703.15-803.15 |

## 5.3 Results and discussion

### 5.3.1 Effect of flow rate ratio of recycled to spent catalysts

The effect of the flow rate ratio of recycled to spent catalyst ($a = G_{sr}/G_{ss}$) on the regeneration performance is studied by varying the flow rate of the recycled catalyst while the spent catalyst flow rate is kept constant ($a$ = 0.5-3.0). Figure 5.3a shows that at each flow rate ratio, the void fraction increases along the downer length with high rate of increasing near the entrance of the first and second acceleration zone and then keeps constant in the constant velocity zone (Eq. (5.5)). When the flow rate ratio increases, the void fraction decreases due to the higher total flux of catalyst in the downer. It can be seen from Figure 5.3b that for each catalyst flow rate ratio, pressure drop occurs at the inlet and then rises along the length of the downer. This is because in the first acceleration zone, changing in gravitation energy and momentum cannot compensate the loss of energy due to the drag force and friction; therefore, the pressure decreases to balance those effects (Eq. (5.4)). After entering the second acceleration zone, the drag force becomes the resistance of particles acceleration where its value becomes positive. Therefore, the drag force together with the gravitational energy and momentum cause an increase in the pressure. The pressure drop and elevated pressure increase with the increased flow rate ratio of recycled to

(a)

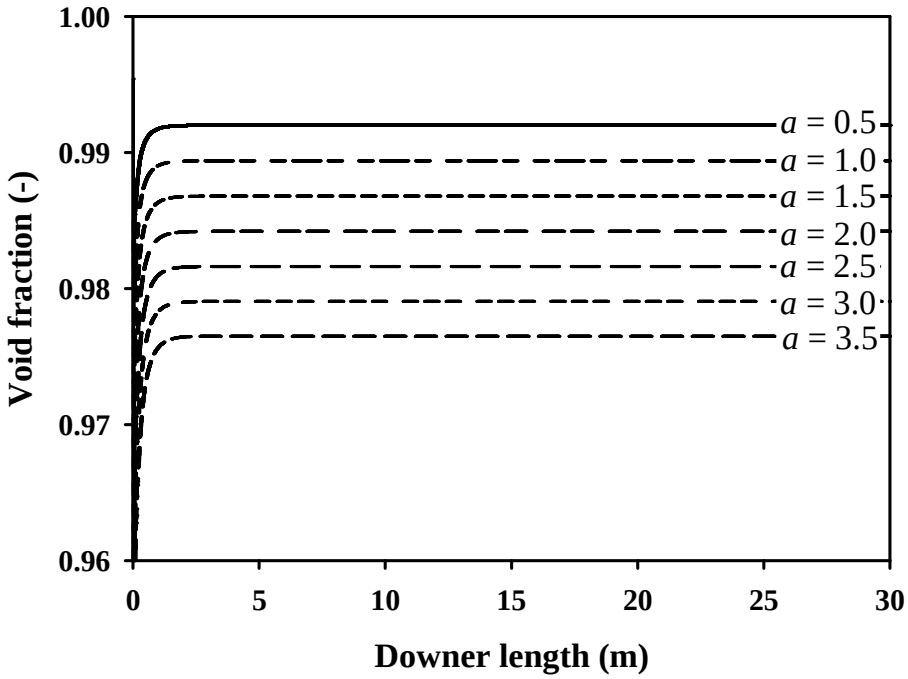


(b)

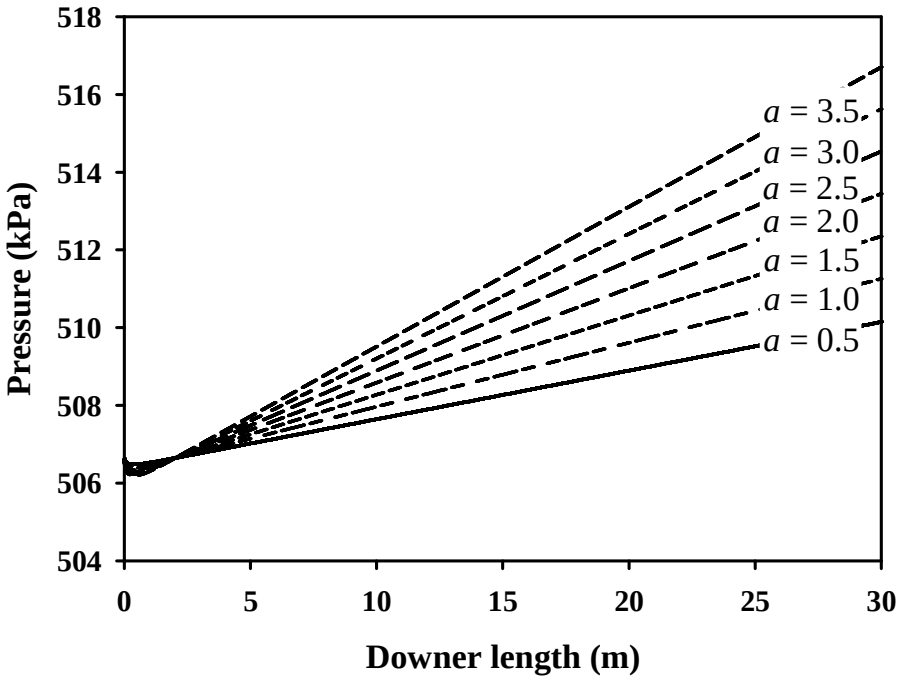


**Figure 5.3** Effect of flow rate ratio of recycled to spent catalysts on (a) void fraction and (b) pressure.

spent catalyst because a lower void fraction increases the drag force (Eq. (5.6)) that directly affects the pressure.

As burning reactions proceed, carbon, hydrogen and oxygen concentration decrease along the downer length while temperature increases due to the heat of reactions as shown in Figure 5.4a-Figure 5.4d. When the flow rate ratio of recycled to spent catalyst increases, the concentrations of carbon and hydrogen on the catalyst surface at the inlet decrease because of a higher fraction in the recycled flow rate of the catalyst, which has lower carbon and hydrogen contents. Actually, this would lead to a lower reaction rate and lower amount of oxygen consumed. However, since the increased flow rate of the recycled catalyst with high temperature causes a higher operating temperature (Figure 5.4d) and the decreased void fraction (Figure 5.3a) improves the amount of carbon and hydrogen to be burned, the burning reactions within the regenerator are more pronounced, resulting in high consumption of oxygen (Figure 5.4c). Moreover, it can be seen from Figure 5.4 that the burning reactions hardly occur at $a$ = 0.5 as a result of the insufficient heat needed for starting reaction. At the higher flow rate ratio (e.g., $a$ = 1.0), the concentrations of carbon and hydrogen on the catalyst surface and the amount of oxygen consumed near the inlet decrease gradually because the reactions proceed slowly, which is caused by low temperatures. After the temperature rises, the reactions proceed faster. At the high flow rate ratio, the recycled catalyst brings more heat to the reactor and therefore the burning reactions are more rapid as the flow rate ratio increases. The effect of temperature on the rate of reactions is indicated in Figure 5.5; the burning reactions start rapidly at temperature around 800 K. It is noted that an increase in the flow rate ratio would improve the regeneration performance. Operation of the downer regenerator at too low flow rate ratio (low recycled catalyst rate) would lead to a quenching effect of the reactions.

(a)

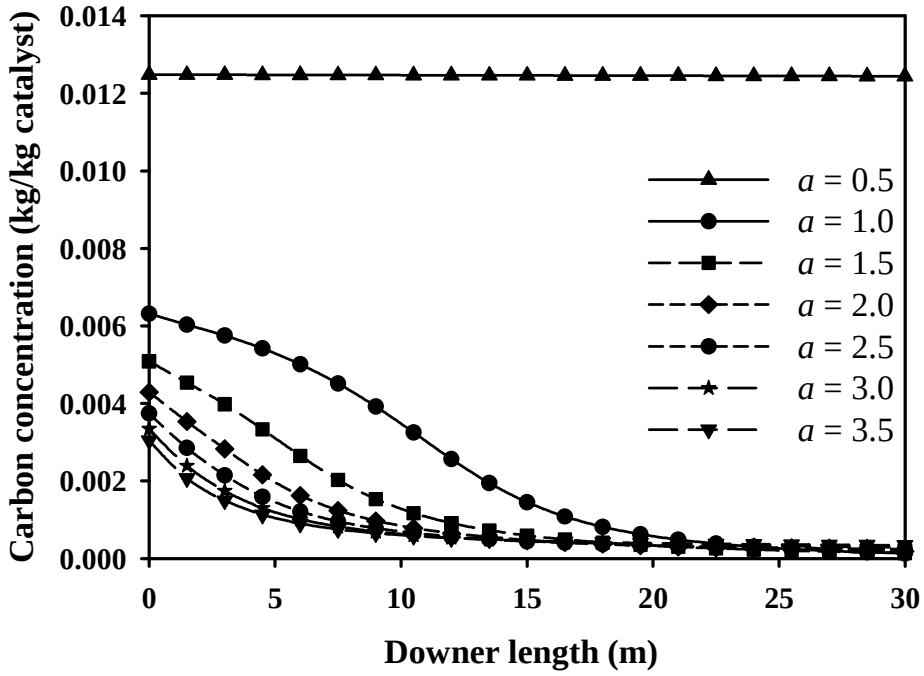
Carbon concentration (kg/kg catalyst)
0.014
0.012
0.010
0.008
0.006
0.004
0.002
0.000
0
5
10
15
20
25
30
Downer length (m)
a = 0.5
a = 1.0
a = 1.5
a = 2.0
a = 2.5
a = 3.0
a = 3.5

(b)

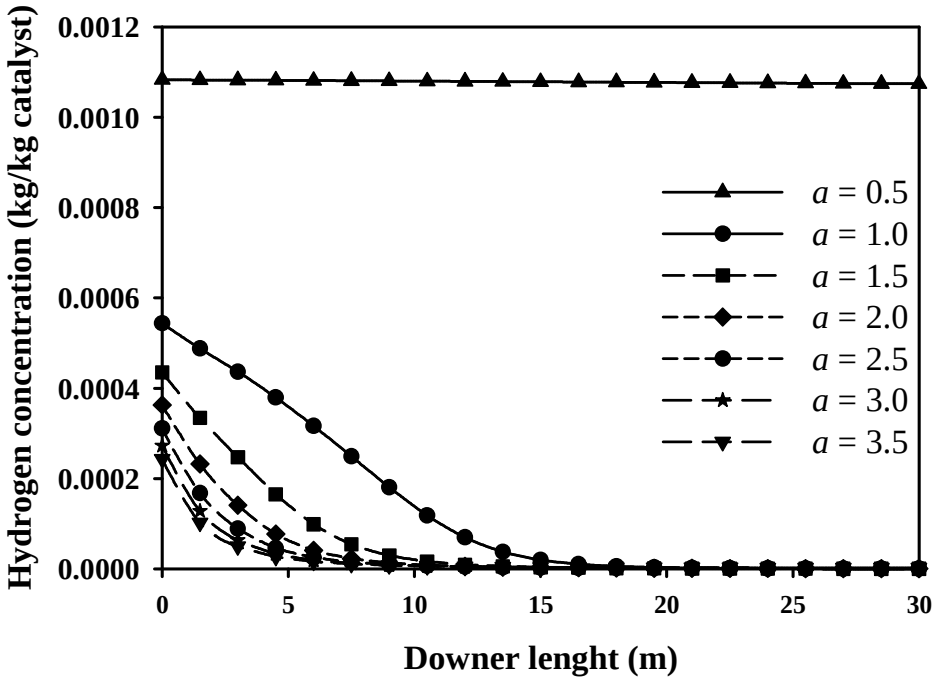
Hydrogen concentration (kg/kg catalyst)
0.0012
0.0010
0.0008
0.0006
0.0004
0.0002
0.0000
0
5
10
15
20
25
30
Downer lenght (m)
a = 0.5
a = 1.0
a = 1.5
a = 2.0
a = 2.5
a = 3.0
a = 3.5

(c)

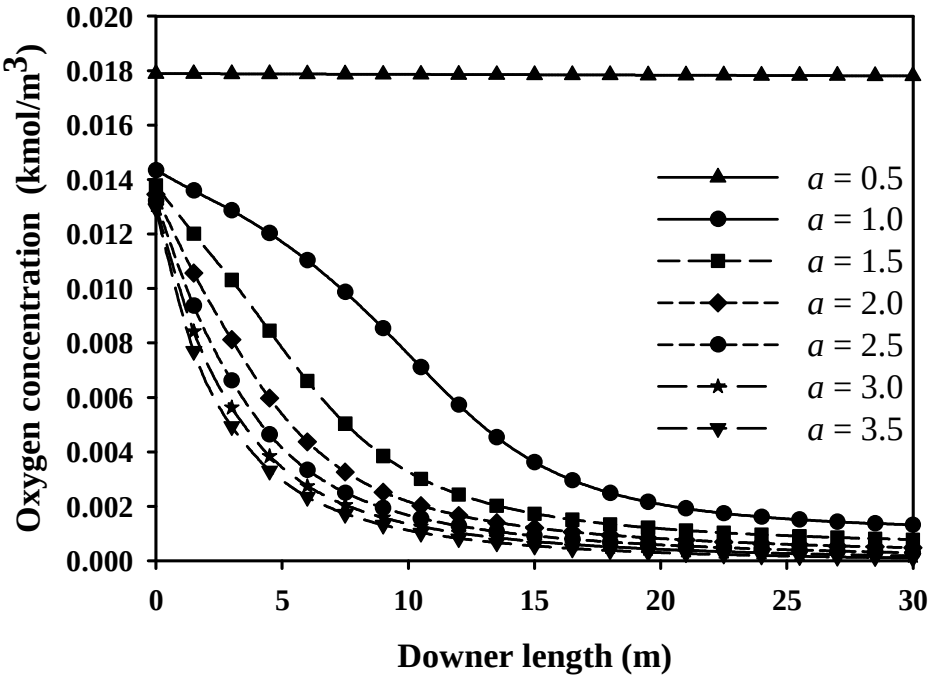


(d)

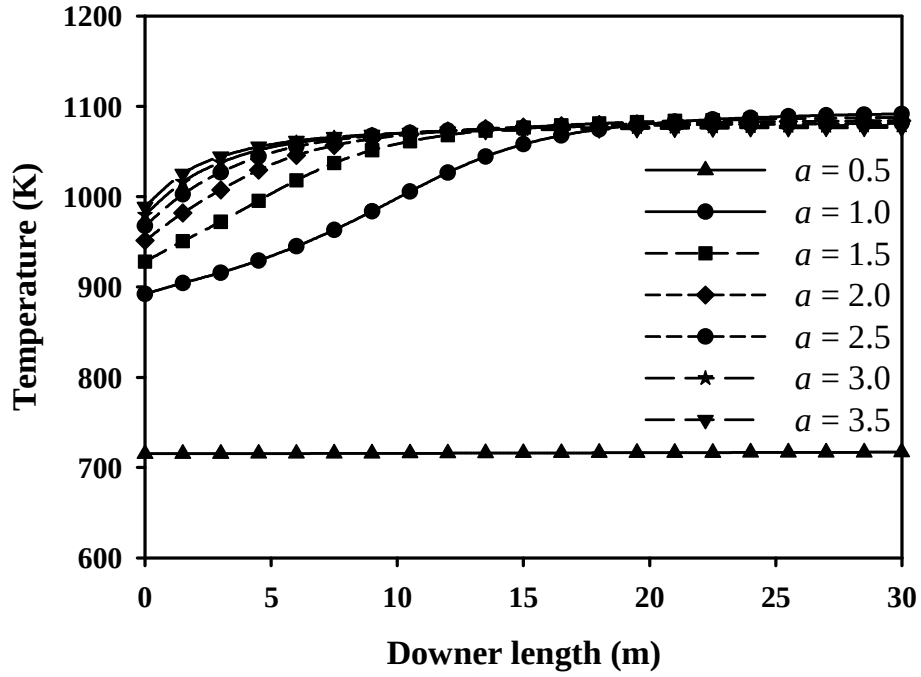


**Figure 5.4** Effect of flow rate ratio of recycled to spent catalysts on (a) carbon concentration, (b) hydrogen concentration, (c) oxygen concentration and (d) temperature.

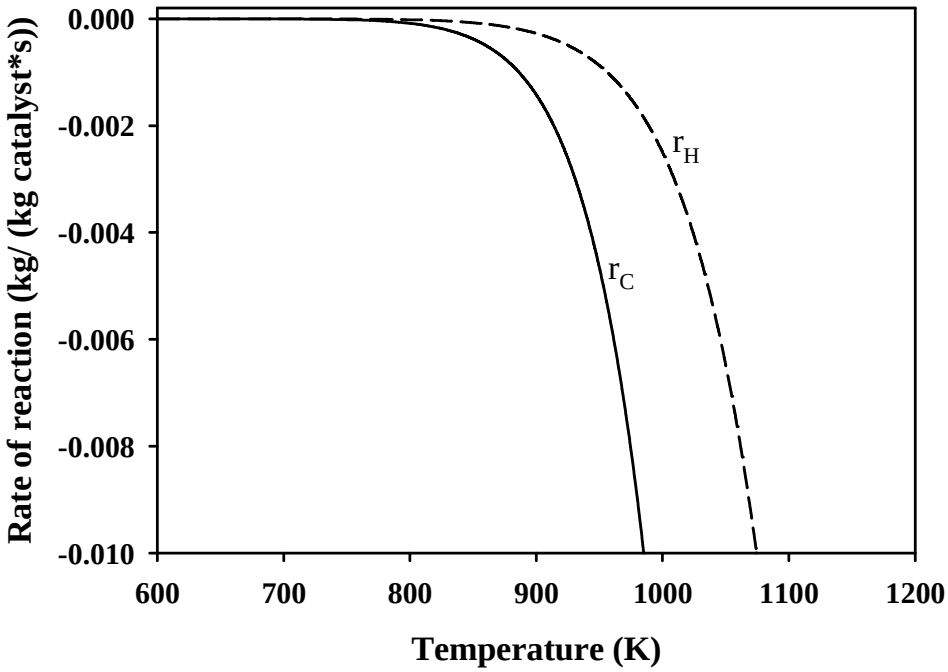


**Figure 5.5** Dependency of reaction rates on operating temperatures.

## 5.3.2 Effect of superficial gas velocity

The superficial gas velocity ($U_g$) is an important parameter that affects the operation of the downer regenerator. In this work, the effect of superficial gas velocity on the regeneration performance was studied in the range of 1-10 m $s^{-1}$. Figure 5.6 shows the simulation results at the downer exit. The increase of $U_g$ lowers the solid holdup in the downer and the pressure along the downer length. At the relatively low $U_g$ (1-3 m $s^{-1}$), the amount of oxygen supply is insufficient for complete burning reaction (Figure 5.6b) and thus high carbon and hydrogen contents on the regenerated catalyst at the regenerator outlet are observed. However, the amount of carbon and hydrogen burned is escalated when the amount of oxygen supply is higher as $U_g$ increases. This leads to an increase in the outlet temperature. Moreover, it can be seen that when $U_g$ is increased, more oxygen is supplied for the burning reactions and the completed regeneration can be achieved. However, for $U_g$ = 4-7 m $s^{-1}$, an increase in $U_g$ decreases the regeneration temperature because more heat is taken away from the downer, resulting in the reduced rate of the burning reaction. Additionally, at high $U_g$

(e.g., $U_g$ = 8-10 m $s^{-1}$), most of heat needed for the reaction is removed by gas flow and thus the reactions are less pronounced as a quenching effect.

The increasing $U_g$ mainly affects the regeneration performance caused by oxygen supply to and heat removal from the system. This simulation results clearly show that the suitable $U_g$ should be carefully determined since too low $U_g$ would lead to an insufficient oxygen condition but too high $U_g$ would lead to a quenching effect. From this simulation condition, the range of $U_g$ in which the downer regenerator can be operated successfully is 4-7 m $s^{-1}$.

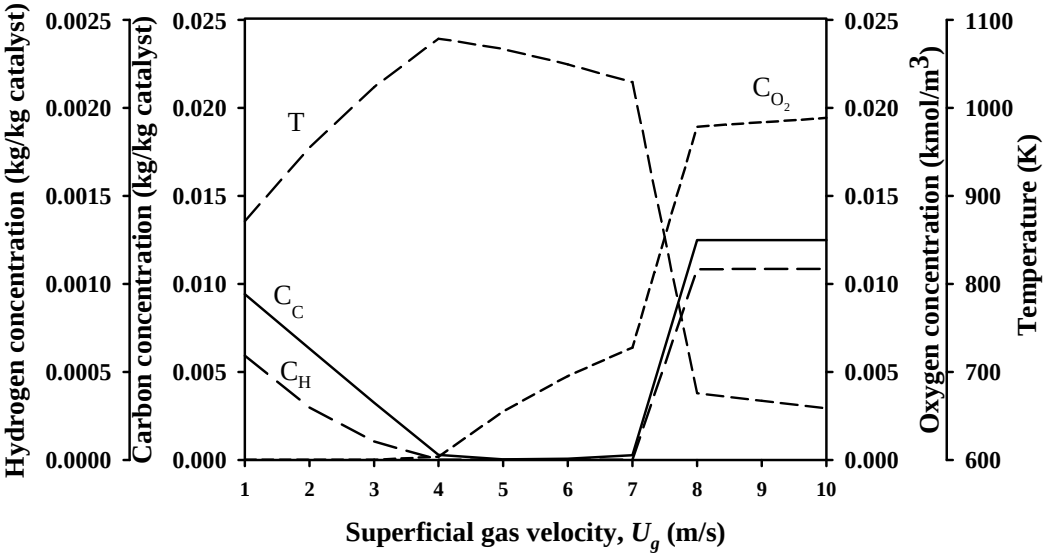


**Figure 5.6** Effect of superficial gas velocity on (a) void fraction and pressure and (b) carbon, hydrogen and oxygen concentrations and temperature at the downer exit.

## 5.3.3 Effect of spent catalyst flow rate

The spent catalyst flow rate ($G_{ss}$) is the parameter depending upon the operation of the FCC reactor. In this simulation, the effect of the spent catalyst flow rate is studied in the range of 20-60 kg $m^{-2}$ $s^{-1}$. It is found from the simulation results that the increased spent catalyst flow rate at constant recycled flow rate affects the void fraction and pressure in the same manner as in case of increasing the flow rate ratio of the recycled to spent catalyst. This is due to the raising of a total catalyst flux.

(a)

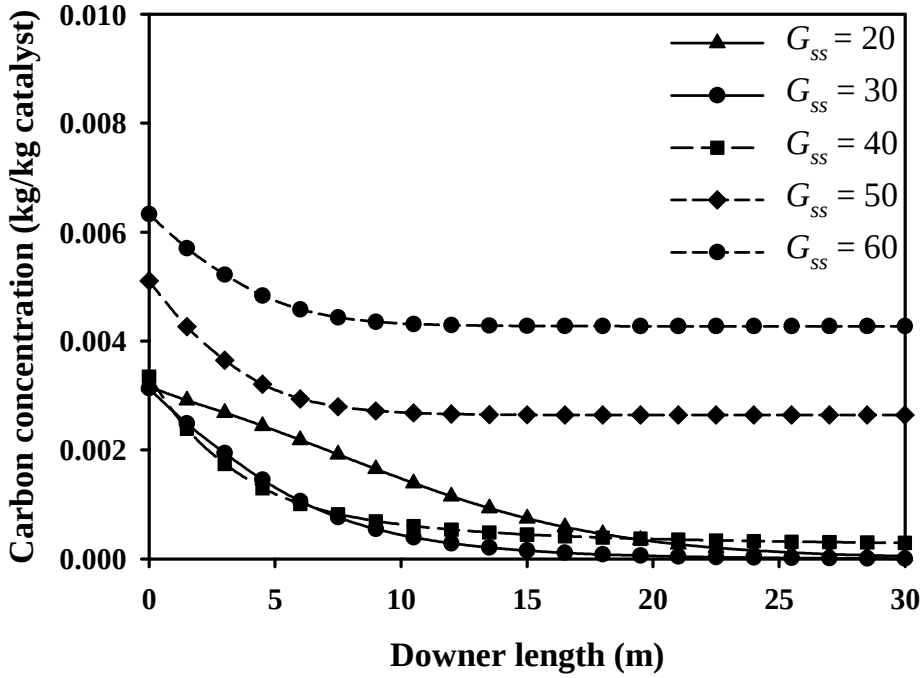
Carbon concentration (kg/kg catalyst)
0.010
0.008
0.006
0.004
0.002
0.000
0
5
10
15
20
25
30
Downer length (m)
$G_{ss}$ = 20
$G_{ss}$ = 30
$G_{ss}$ = 40
$G_{ss}$ = 50
$G_{ss}$ = 60

(b)

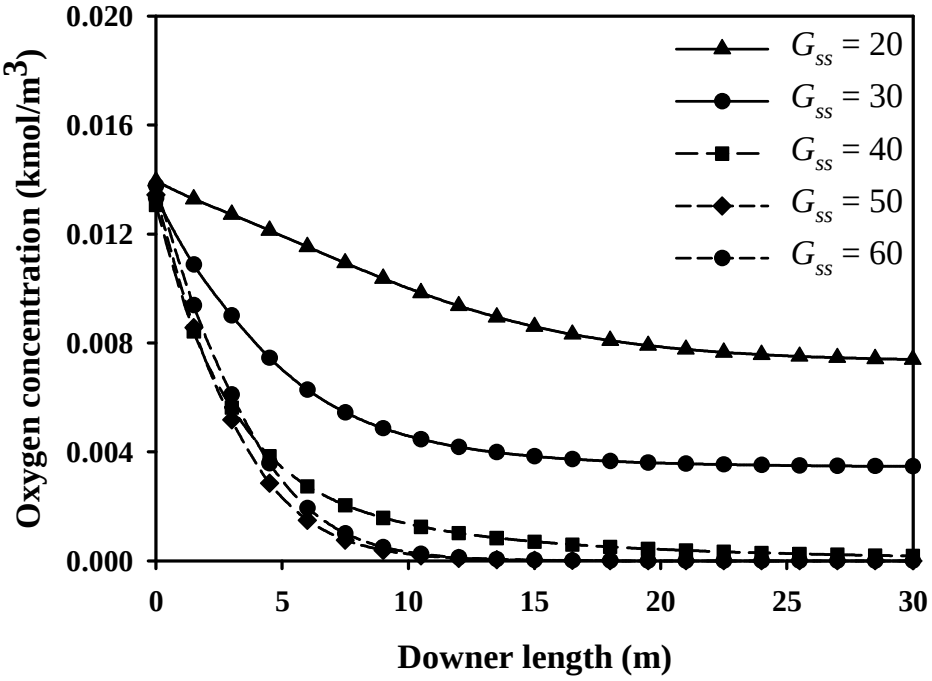
Oxygen concentration (kmol/m3)
0.020
0.016
0.012
0.008
0.004
0.000
0
5
10
15
20
25
30
Downer length (m)
$G_{ss}$ = 20
$G_{ss}$ = 30
$G_{ss}$ = 40
$G_{ss}$ = 50
$G_{ss}$ = 60

(c)

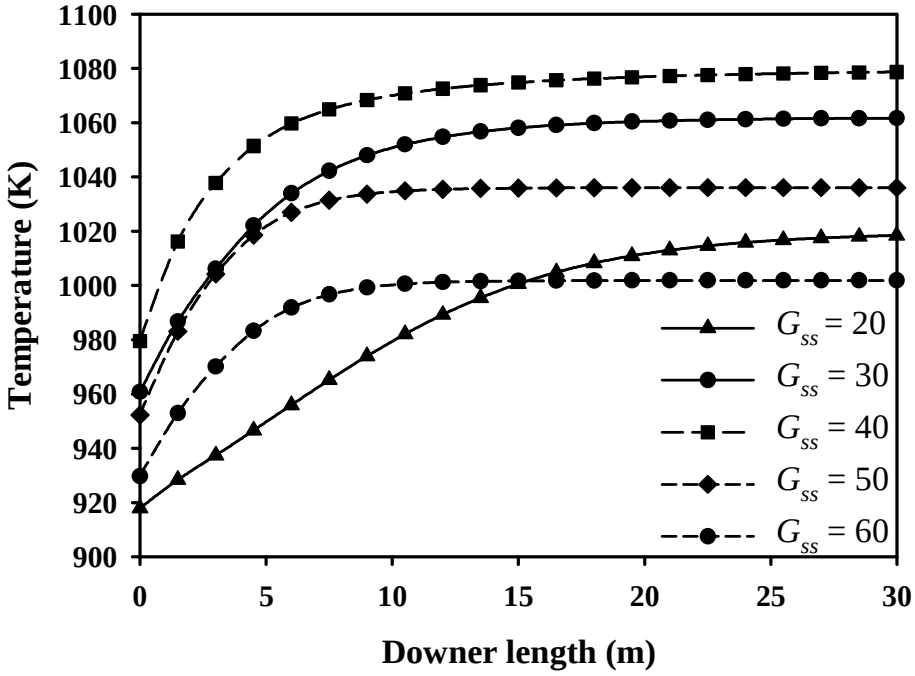


**Figure 5.7** Effect of spent catalyst flow rate on (a) carbon concentration, (b) oxygen concentration and (c) temperature.

Figure 5.7a-Figure 5.7c show that at low $G_{ss}$ (e.g., 20 kg $m^{-2}$ $s^{-1}$), the burning reactions are slow due to the low amount of carbon and hydrogen on the catalyst surface which results in the slow rate of burning reaction and oxygen consumption, and raising temperatures. Increasing the spent catalyst flow rate ($G_{ss}$) while keeping the recycled flow rate constant results in the increased carbon and hydrogen contents on the catalyst at the regenerator inlet. Further, a higher content of coke raises the temperature of the regenerator. These effects accelerate the rate of combustion reaction in the regenerator. Although the increased $G_{ss}$ enhances a regeneration process, too high $G_{ss}$ ($G_{ss}$ =50-60 kg $m^{-2}$ $s^{-1}$) would reduce the inlet temperature of the downer because more low-temperature catalyst are added (see Figure 5.7c). This effect lowers the regeneration performance. Moreover the spent catalyst flow rate is limited by the amount of oxygen supplied. It is found that at high $G_{ss}$ ($G_{ss}$ = 50-60 kg $m^{-2}$ $s^{-1}$), the supplied oxygen is insufficient for the burning reaction. As a result, there is the significant amount of carbon and hydrogen remaining on the regenerated catalyst. To handle with the high spent catalyst flow rate, the regenerator should be

operated with higher gas flow rate. However, it should be mentioned that the higher gas flow rate would also lower the temperature of the regenerated system. This effect together with the effect of high flow rate of low-temperature catalyst may cause the quenching effect. Considering the conditions used in this work, the optimal value of $G_{ss}$ for the downer regenerator that can regenerate the catalyst effectively is in the range of 20-40 kg m-$^{2}$ s$^{-1}$.

### 5.3.4 Effect of carbon content on spent catalyst

The amount of coke deposited on the surface of spent catalyst particles ($C_{Cs}$) affects the heat balance of the system because coke burning is the source of heat used for the endothermic cracking reactions and feed vaporization in the FCC reactor. The simulation result (Figure 5.8) shows that at $C_{Cs}$ = 0.010 kg kg catalyst$^{-1}$, the burning reactions proceed completely but at higher $C_{Cs}$, the oxygen depletes before the reactions are complete. Therefore, there is some carbon and hydrogen remaining on the spent catalyst at the exit of the downer. It is noted that to deal with a high amount of the carbon content on the spent catalyst, the downer regenerator could operate at a higher $U_g$ to supply more oxygen. However, increasing $C_{Cs}$ provides a higher burning intensity that consumes more oxygen and causes higher regenerator temperatures. The higher content of coke on the spent catalyst is useful for the burning reaction by supplying more heat; however, too high $C_{Cs}$ will cause the hydrothermal deactivation that deactivates the catalyst permanently. Therefore, this problem has to be considered in the operation of the downer regenerator. However, the operation with a higher $U_g$ is not only supply more oxygen, but also help remove the excess heat of regeneration.

### 5.3.5 Effect of spent catalyst temperature

The spent catalyst flowing to the regenerator contains useful heat, which can be employed for cracking reactions. Heat from the spent catalyst affects the inlet temperature of the downer regenerator. As shown in Figure 5.9, increasing the spent catalyst temperature causes a higher inlet temperature of the regenerator that can promote the combustion reactions. As a result, the contents of carbon and hydrogen on the catalyst surface as well as the amount of oxygen decrease rapidly. The

increased rates of the combustion reactions also raise the regeneration temperature. However, the increase of the inlet temperature leads to a lower oxygen concentration at the entrance of the downer. Therefore, in case of $T_s$ > 763.15 K the amount of oxygen is depleted before the reactions are carried out completely. As a consequence, the higher carbon content at the outlet is observed. The simulation results suggest that the spent catalyst temperatures in the range of 703.15-803.15 K do not much affect the overall performance of the regenerator since the carbon content on the regenerated catalyst at outlet is quite low for all cases. However, it should be noted that a high temperature of the spent catalyst may lead to the extreme regeneration temperature that would cause a catalyst deactivation.

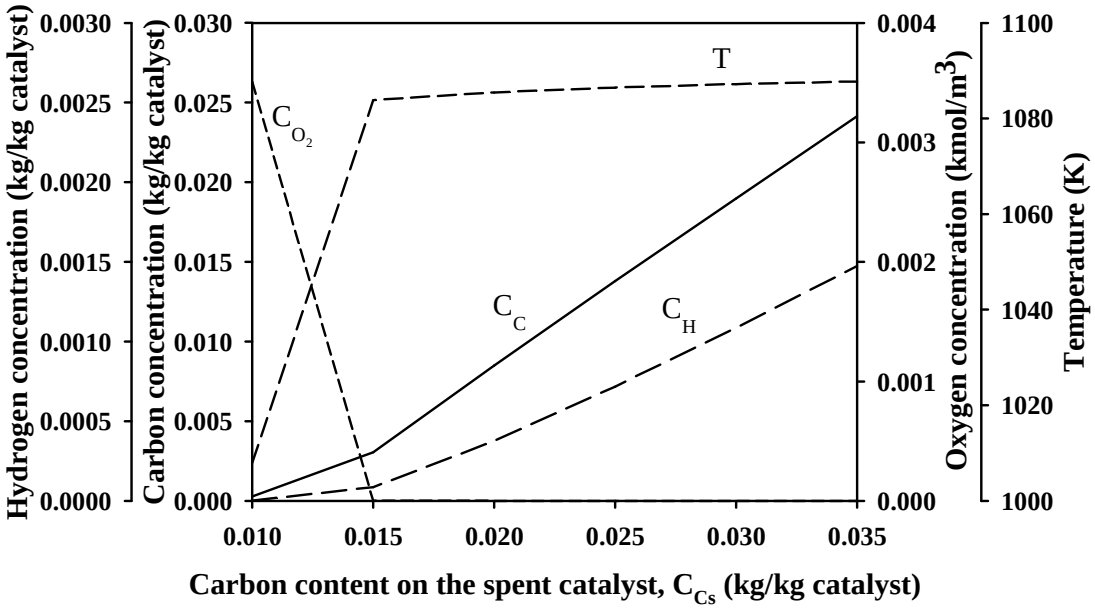


**Figure 5.8** Effect of carbon content on the spent catalyst on carbon, hydrogen and oxygen concentrations and temperature at the downer exit.

(a)

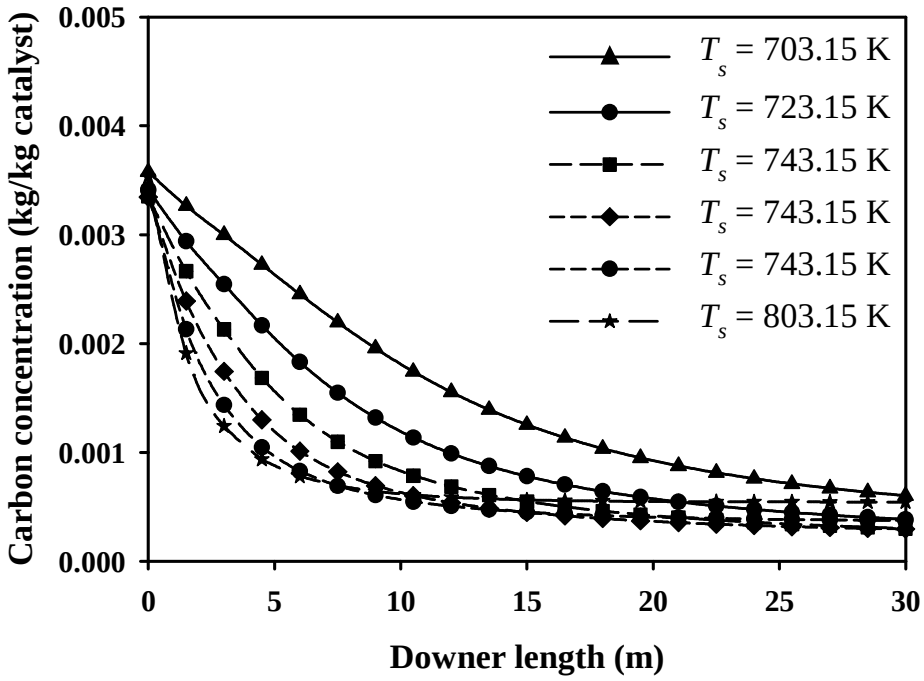
Carbon concentration (kg/kg catalyst)
0.005
0.004
0.003
0.002
0.001
0.000
0
5
10
15
20
25
30
Downer length (m)
$T_s$ = 703.15 K
$T_s$ = 723.15 K
$T_s$ = 743.15 K
$T_s$ = 743.15 K
$T_s$ = 743.15 K
$T_s$ = 803.15 K

(b)

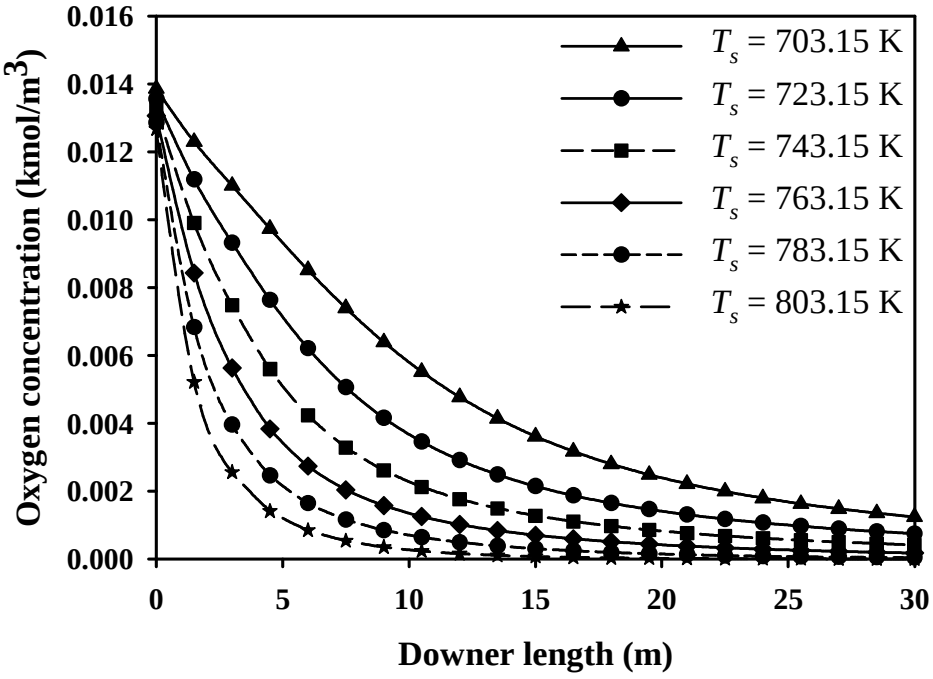
Oxygen concentration (kmol/m3)
0.016
0.014
0.012
0.010
0.008
0.006
0.004
0.002
0.000
0
5
10
15
20
25
30
Downer length (m)
$T_s$ = 703.15 K
$T_s$ = 723.15 K
$T_s$ = 743.15 K
$T_s$ = 763.15 K
$T_s$ = 783.15 K
$T_s$ = 803.15 K

(c)

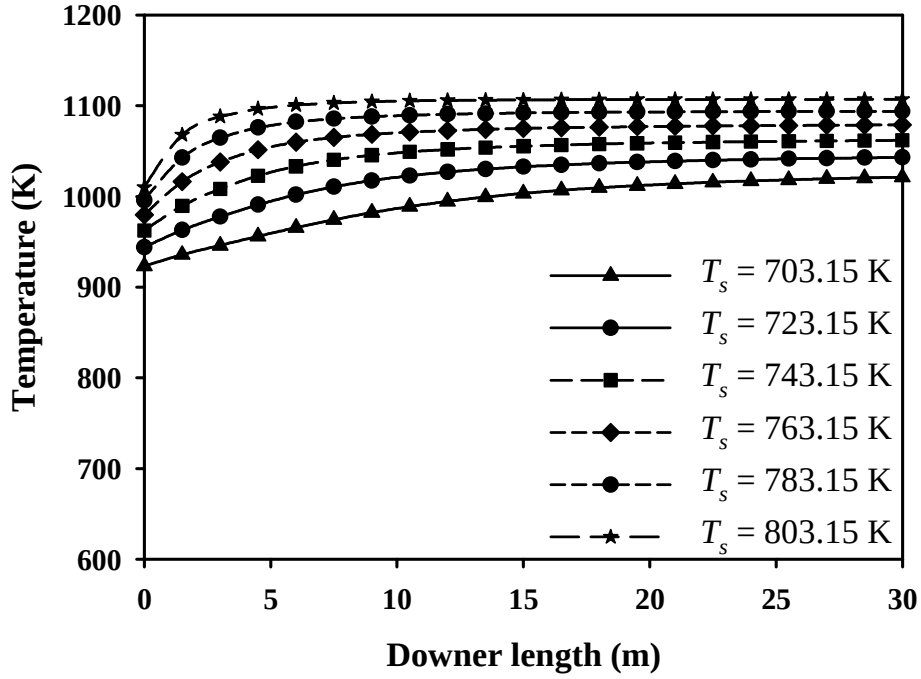


**Figure 5.9** Effect of spent catalyst temperature on (a) carbon concentration, (b) oxygen concentration and (c) temperature.

## 5.4 Conclusions

In this study, the performance of a novel downer regenerator was analyzed based on a systematic model-based approach using one-dimensional regenerator model taking into account mass and energy balances, hydrodynamic and kinetics of FCC catalyst regeneration. The simulation results showed that the efficient operation of the downer regenerator is influenced by various key parameters, e.g., recycled catalyst flow rate, carbon content on the spent catalyst and spent catalyst temperature. Parameters that affect the temperature of the downer regenerator should be carefully selected as they have the most significant effect on a regeneration process. High regeneration temperature could deactivate the catalyst permanently but low temperature operation lowers the regeneration performance. The results obtained from this model-based analysis are beneficial for an understanding of the downer regenerator, leading to an optimal design and efficient operation of the FCC process.

# CHAPTER VI

# NUMERICAL ANALYSIS OF THE FCC CATALYST REGENERATION VIA STEAM GASIFICATION AND BURNING REACTION IN A DOWNER-TYPE REGENERATOR

## 6.1 Introduction

The way to upgrade the regeneration performance can be done in two ways including the enhancement of regenerator configuration and the improvement of reactions. The studies on the improvement of regeneration configuration are discussed and shown in the previous chapter.

For improvement of reactions occuring in the regeneration, Corma et al. (2011) studied possibility of the coke steam gasification reaction for converting some part of coke into hydrogen in the regeneration environment while the another part is still eliminated by burning for maintaining the system heat balance. They found that FCC equilibrium catalyst (E-cat) has ability to catalyze the steam gasification of coke on the catalyst surface. In addition, they also developed the gasification catalyst for using in the FCC regeneration environment and proved that the new synthesized catalyst can enhance the gasification ability while it still gives the acceptable cracking activity.

Consideration of gasification reaction together with the burning reaction has the benefit of temperature reduction. Since the steam reforming reaction is the endothermic reactor, thereby, it can help reduce the high temperature caused by burning high amount of carbon deposited on spent catalyst from reactor.

However, the steam gasification can proceed at the limited condition. Therefore, this work aims to investigate the steam gasification together with

combustion for regeneration of the FCC catalyst in a downer-type regenerator via simulation study using one dimensional hydrodynamic model, material and energy balances and kinetics of reactions. The simulation results obtained suggest the possibility of the operation of the downer-type regenerator that processes high coke content on spent catalyst.

## 6.2 Process diagram

The schematic depiction of the FCC process that operate in downer mode both reactor and regenerator and the general process descriptions are shown in chapter V (Figure 5.1).

However, there is a possibility for other reactions to proceed in the regenerator i.e., steam gasification, boudouard, methanation, and water-gas shift reactions. These reactions also affects to the regeneration and heat balance of the FCC process. In this work, we considered that the endothermic gasification reaction of carbon atom with some amount of steam proceeds and forms carbon monoxide and hydrogen gas in the regeneration environment. After the regeneration, a part of regenerated catalyst is sent to the top of the downer reaction to continue the loop of operation and another part is recycled back to the regenerator.

## 6.3 Mathematical model

The mathematical models used in this work are consist of hydrodynamic model, kinetics of burning reactions, kinetics of gasification reactions and mass and energy balance. The details of each model are described in section 4.1, 4.3.1 and 4.4 of chapter IV.

**Table 6.1** The equations used in chapter VI.

| | |
|---|---|
| $\frac{d(\bar{\varepsilon}_g \rho_g \bar{V}_g)}{dz} = 0$ , where $G_g = \bar{\varepsilon}_g \rho_g \bar{V}_g = \text{constant}$ | (6.1) |
| $\frac{d(\bar{\varepsilon}_s \rho_s \bar{V}_s)}{dz} = 0$ , where $G_s = \bar{\varepsilon}_s \rho_s \bar{V}_s = \text{constant}$ | (6.2) |

**Table 6.1** The equations used in chapter VI (Continued).

$$\bar{\varepsilon}_g + \bar{\varepsilon}_s = 1 \tag{6.3}$$

$$\frac{d(\bar{\varepsilon}_g \rho_g \bar{V}_g^2)}{dz} = -\frac{dP}{dz} - F_D - F_{fg} + \bar{\varepsilon}_g \rho_g g \tag{6.4}$$

$$\frac{d(\bar{\varepsilon}_s \rho_s \bar{V}_s^2)}{dz} = F_D - F_{fs} + \bar{\varepsilon}_s (\rho_s - \rho_g) g \tag{6.5}$$

$$F_D = \frac{3}{4}\frac{C_D}{d_p}\bar{\varepsilon}_s \rho_g \left|\bar{V}_g - \bar{V}_s\right|\left(\bar{V}_g - \bar{V}_s\right) \tag{6.6}$$

$$\frac{C_D}{C_{Ds}} = \frac{14.1\left[1 + 2.78\left(G_g / G_s\right)\right]}{Fr} \tag{6.7}$$

$$Fr = \frac{U_g}{\sqrt{g d_p}} \tag{6.8}$$

$$C_{Ds} = \begin{cases} \dfrac{24}{\mathrm{Re}_r}\left(1 + 0.15\,\mathrm{Re}_r^{\,0.687}\right), & for\ \mathrm{Re} \le 1000 \\ 0.44, & for\ \mathrm{Re} > 1000 \end{cases} \tag{6.9}$$

$$\mathrm{Re}_r = \frac{\rho_g d_p \left|\bar{V}_g - \bar{V}_s\right|}{\mu_g} \tag{6.10}$$

$$F_{fg} = \frac{2 f_g \bar{\varepsilon}_g \rho_g \bar{V}_g^2}{D} \tag{6.11}$$

$$f_g = \begin{cases} \dfrac{16}{\mathrm{Re}_g}, & when\ \mathrm{Re}_g \le 2300 \\ \dfrac{0.079}{\mathrm{Re}_g^{\,0.313}}, & when\ \mathrm{Re}_g > 2300 \end{cases} \tag{6.12}$$

$$\mathrm{Re}_g = \frac{\rho_g U_g D}{\mu_g} \tag{6.13}$$

$$F_{fs} = \frac{2 f_s \bar{\varepsilon}_s \rho_s \bar{V}_s^2}{D} \tag{6.14}$$

$$f_s = \frac{0.0285\sqrt{gD}}{\left(G_s / \rho_s \bar{\varepsilon}_s\right)} \tag{6.15}$$

**Table 6.1** The equations used in chapter VI (Continued).

$$\bar{V}_g = \frac{U_g}{\bar{\varepsilon}_g} = \frac{G_g}{\rho_g \bar{\varepsilon}_g} \tag{6.16}$$

$$\bar{V}_s = \frac{G_s}{\rho_s \bar{\varepsilon}_s} \tag{6.17}$$

$$r_C = k_C \, p_{O_2} C_C \tag{6.18}$$

$$r_H = k_H \, p_{O_2} C_H \tag{6.19}$$

$$k_C = A_1 \exp\left(-\frac{E_{a1}}{RT}\right) \tag{6.20}$$

$$k_H = \begin{cases} A_2 \exp\left(-\dfrac{E_{a2}}{RT}\right), when\ T < 973K \\ A_2 \exp\left(-\dfrac{E_{a2}}{RT}\right) \times \\ \qquad \left[1 - 2.67 \times 10^{30} \exp(-7.34 \times 10^4 / T)\right], when\ T \geq 973K \end{cases} \tag{6.21}$$

$$r_{gf} = k_{gf} C_C \tag{6.22}$$

$$\frac{dC_C}{dz} = \frac{-(r_C + r_{gf})\rho_s (1 - \bar{\varepsilon}_g)}{G_s} \tag{6.23}$$

$$\frac{dC_H}{dz} = \frac{-r_H \rho_s (1 - \bar{\varepsilon}_g)}{G_s} \tag{6.24}$$

$$\frac{dC_{O_2}}{dz} = \frac{-(r_C / 12 + r_H / 4)\rho_s (1 - \bar{\varepsilon}_g)}{U_g} \tag{6.25}$$

$$\frac{dC_{CO_2}}{dz} = \frac{(r_C / 12)\rho_s (1 - \bar{\varepsilon}_g)}{U_g} \tag{6.26}$$

$$\frac{dC_{H_2O}}{dz} = \frac{((2r_H / 4) - r_{gf})\rho_s (1 - \bar{\varepsilon}_g)}{U_g} \tag{6.27}$$

$$\frac{dC_{CO}}{dz} = \frac{r_{gf} \rho_s (1 - \bar{\varepsilon})}{U_g} \tag{6.28}$$

$$\frac{dC_{H_2}}{dz} = \frac{r_{gf} \rho_s (1 - \bar{\varepsilon}_g)}{U_g} \tag{6.29}$$

**Table 6.1** The equations used in chapter VI (Continued).

| | |
|---|---|
| $\frac{dT}{dz} = \frac{\rho_s(1-\bar{\varepsilon}_g)(r_C\Delta H_C + r_H\Delta H_H + r_{gf}\Delta H_{gf})}{U_g\rho_g C_{p,g} + G_s C_{p,s}}$ | (6.30) |
| $C_{C,0} = \frac{G_{ss}C_{Cs} + G_{sr}C_{C,out}}{G_{ss} + G_{sr}}$ | (6.31) |
| $C_{H,0} = \frac{\alpha G_{ss}C_{Cs} + G_{sr}C_{H,out}}{G_{ss} + G_{sr}}$ | (6.32) |
| $T_0 = \frac{G_{ss}C_{p,s}T_s + G_{sr}C_{p,s}T_{g,out} + U_g\rho_g C_{p,g}T_a}{G_{ss}C_{p,s} + G_{sr}C_{p,s} + U_g\rho_g C_{p,g}}$ | (6.33) |

## 6.4 Results and discussions

### 6.4.1 The simulation results at standard condition

The simulation results obtained at standard condition (the same condition as in Chapter IV) are shown in the Figure 6.1. It can be seen that as the reactions proceed, the carbon and hydrogen on the catalyst and oxygen are reduced along the downer whereas carbon dioxide, carbon monoxide, water and gas hydrogen are produced. Carbon can be removed by two reactions, burning reaction and gasification reaction but hydrogen in coke is eliminated by burning reaction only. In burning reaction, carbon and hydrogen oxidize with oxygen to form carbon dioxide, water and heat. This causes the raising of temperature along the downer. However, gasification reaction which is the reaction of carbon in coke with water and produce carbon monoxide and gas hydrogen is endothermic. Therefore, this reaction will reduce the downer temperature. However, the gasification reaction rate is slower than burning reaction, therefore, the gasification can eliminate small amount of carbon. The total heat of both reactions is still exothermic which is necessary for the endothermic cracking reaction in the reactor. It is noted that because there is no steam at the inlet of the downer, the gasification reaction can proceed after the burning reaction producing steam as a product.

(a)

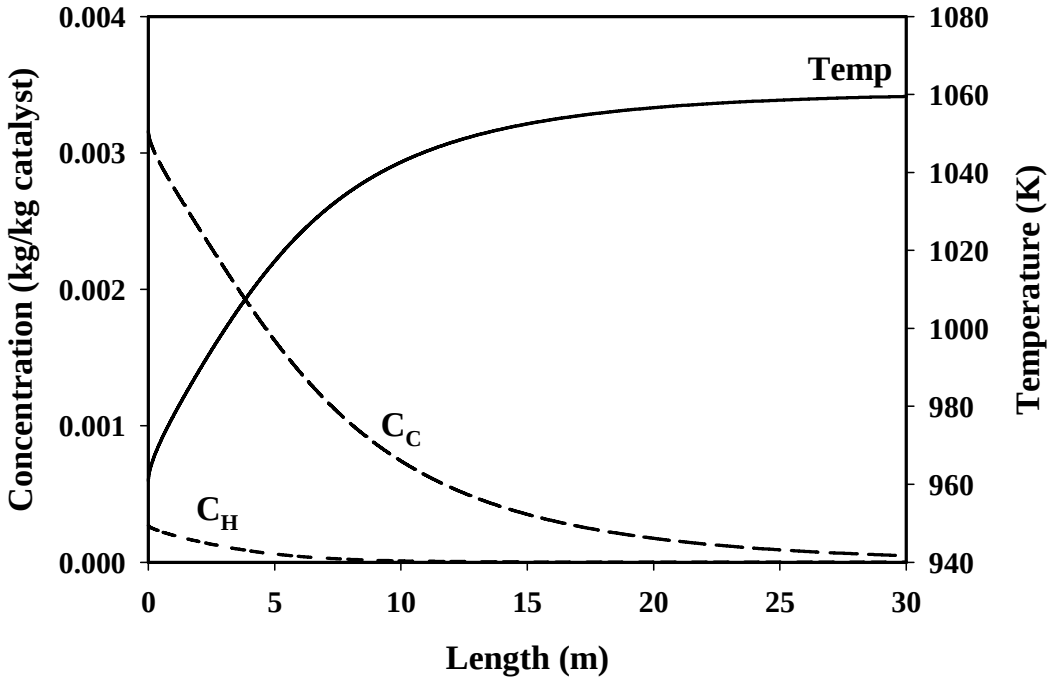


(b)

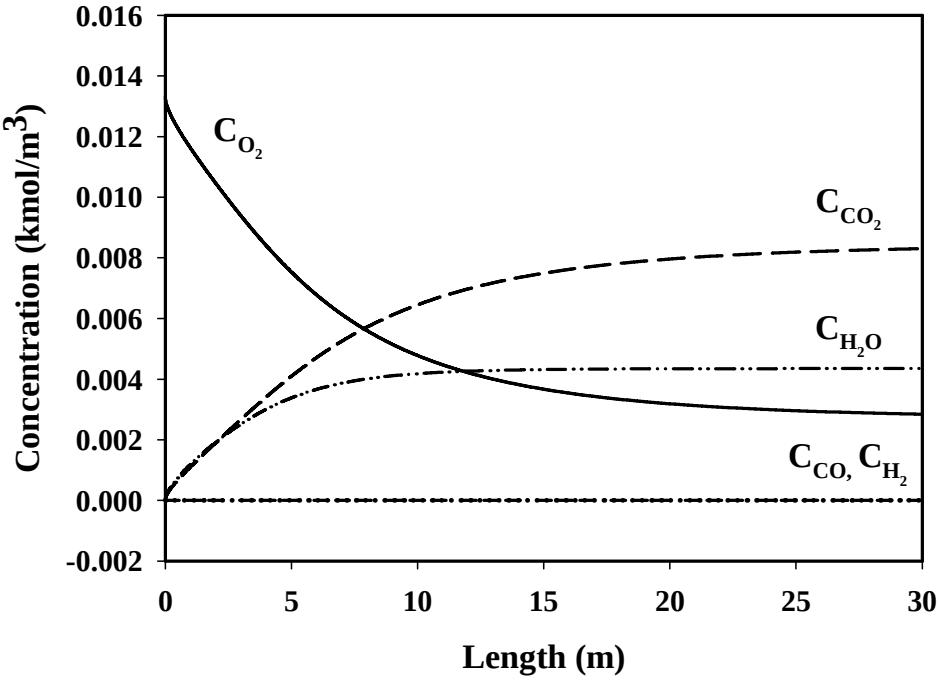


**Figure 6.1** Simulation results of downer regenerator at the standard condition.
For (a) carbon, hydrogen concentration and temperature, and
(b) oxygen, carbon dioxide, carbon monoxide, water, gas hydrogen concentration.

### 6.4.2 Burning reaction versus burning and gasification reactions

To confirm the advantage of gasification reaction, the comparison of regeneration with and without gasification reactions were studied.

Figure 6.2a and Figure 6.2b reveal that the carbon content on the catalyst and the amount of oxygen in the burning without gasification reaction case (B) reduces faster than the regeneration by burning with gasification reaction (BGF) case. This is because the temperature of the burning without gasification case is higher than another case (Figure 6.2c), therefore; the rate of carbon combustion is higher. However, both cases can eliminate the carbon from the catalyst efficiently. Another benefit of gasification reaction is the production of gas hydrogen as shown in Figure 6.4d.

Although, the currently used catalyst can produced only small amount of gas hydrogen, but if the new catalyst additive with higher activity of gasification reaction has been synthesized and implemented to the FCC process, the hydrogen production rate would be higher as shown in Figure 6.3c and the steam gasification reaction in the regenerator will play the important role as the reaction for reducing the temperature from burning of high coke content and produce gas hydrogen as byproduct. However, it can be from Figure 6.3a that at this simulation condition (carbon content on spent catalyst of 0.0125 kg kg catalyst$^{-1}$) the higher rate of gasification reaction would reduce the regeneration performance since higher carbon content is left at higher rate of gasification reaction. This is because the temperature is lower in case of higher rate of gasification reaction catalyst additive is used (Figure 6.3b).

### 6.4.3 Regeneration characteristics at higher carbon content on spent catalyst

The steam gasification reaction of carbon to carbon monoxide and hydrogen is expected to be useful for reducing regeneration temperature in case of high coke

(a)

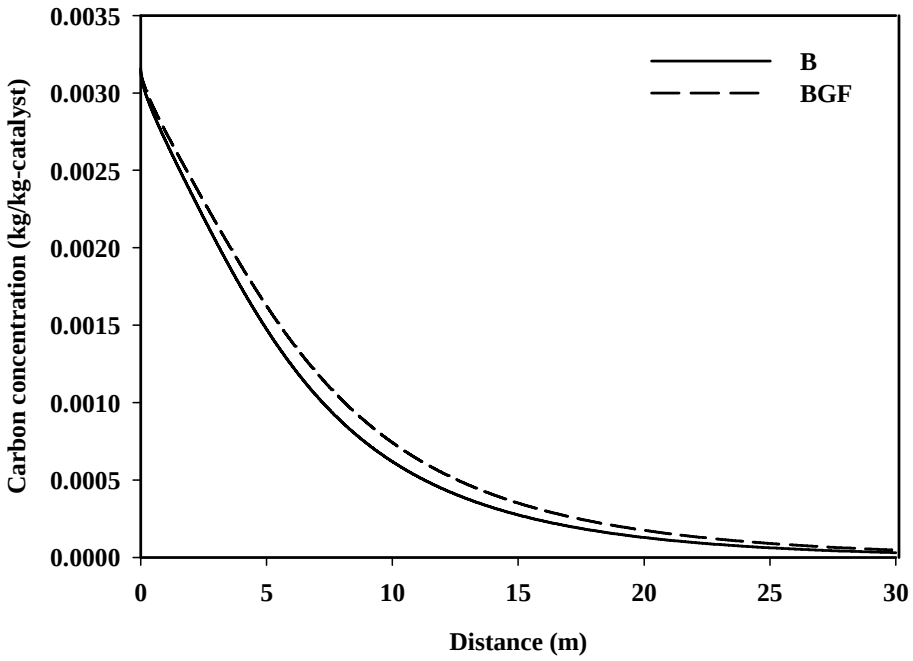
0.0035
0.0030
0.0025
0.0020
0.0015
0.0010
0.0005
0.0000
Carbon concentration (kg/kg-catalyst)
0
5
10
15
20
25
30
Distance (m)
B
BGF

(b)

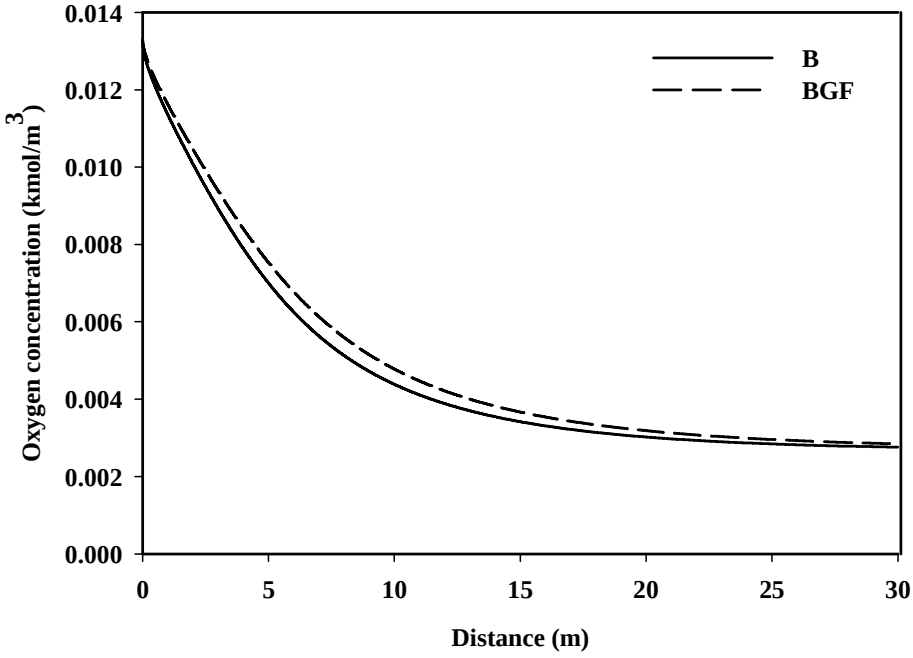
0.014
0.012
0.010
0.008
0.006
0.004
0.002
0.000
Oxygen concentration (kmol/m3)
0
5
10
15
20
25
30
Distance (m)
B
BGF

(c)

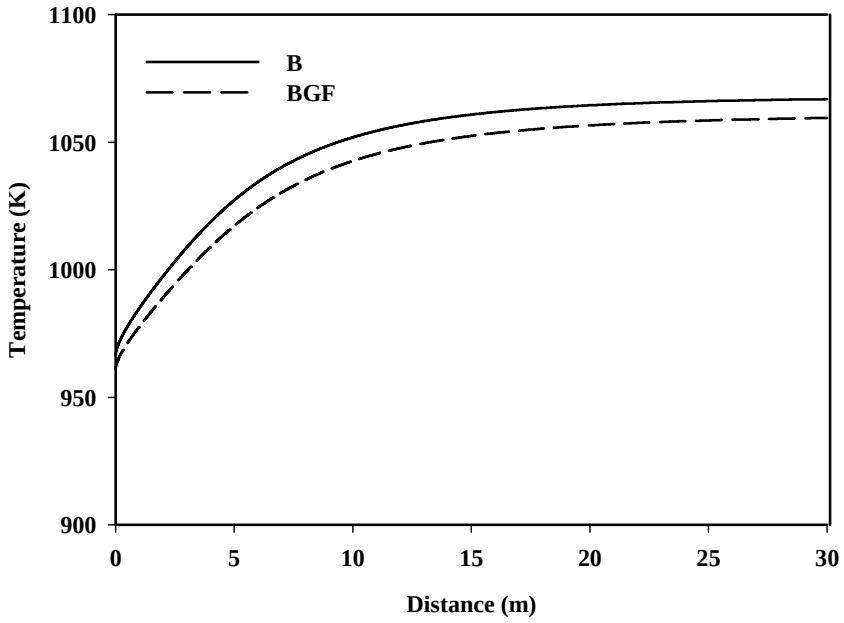


(d)

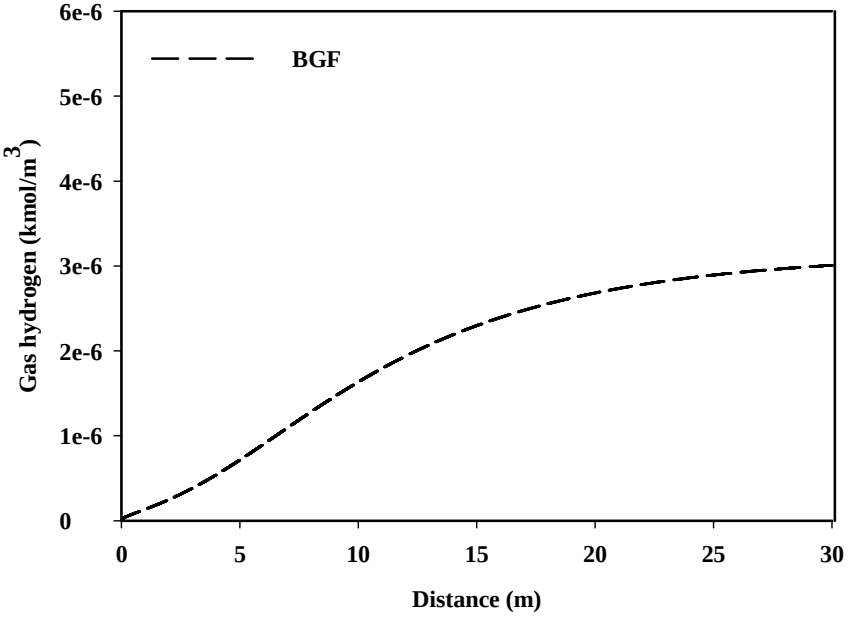


**Figure 6.2** Comparison of regeneration with gasification and without gasification reactions of (a) carbon concentration, (b) oxygen concentration, (c) temperature and (d) gas hydrogen concentration.

content on spent catalyst. The regeneration characteristics at different carbon content, e.g., 0.01, 0.02, and 0.03 kg kg catalyst$^{-1}$ are studied. Figure 6.4a reveals that at $C_{Cs}$=0.01 kg kg catalyst$^{-1}$ the carbon is regenerated efficiently but at higher $C_{Cs}$, carbon cannot be regenerated efficiently with significant amount of carbon is remained at the downer exit. This is because all oxygen is consumed before reactions are accomplished (Figure 6.4b).

When the burning reaction is dominant in case of $C_{Cs}$=0.01 kg kg catalyst$^{-1}$, the temperature of the regenerator is raised. However, when oxygen is totally consumed in case of $C_{Cs}$=0.02 and 0.03 kg kg catalyst$^{-1}$, the endothermic steam gasification is the only reaction in the regenerator, therefore; the temperatures of the regenerator begin to be reduced after entire oxygen are consumed (Figure 6.4c). Thus, higher amount of hydrogen are obtained (Figure 6.4d).

Interestingly, Corma et al. (2011) was successfully improved the steam reforming activity of the FCC catalyst. Their new catalyst has the rate of gasification reaction higher than the conventional e-cat about seven times and still has a good cracking activity.

(a)

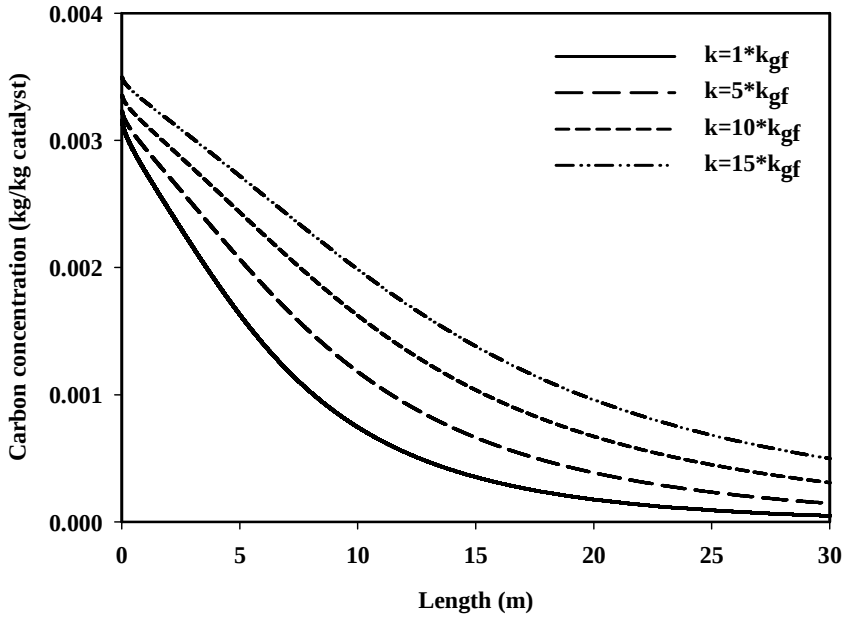

(b)

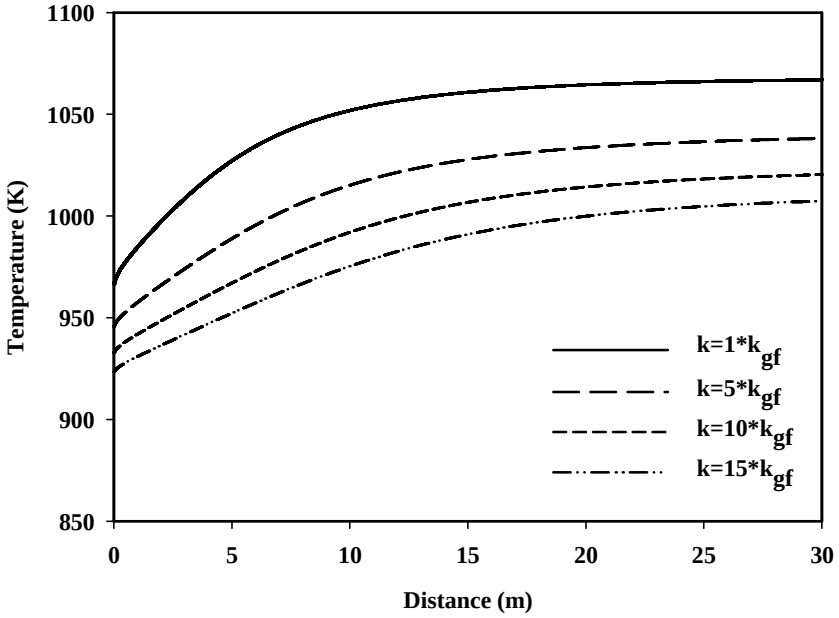


(c)

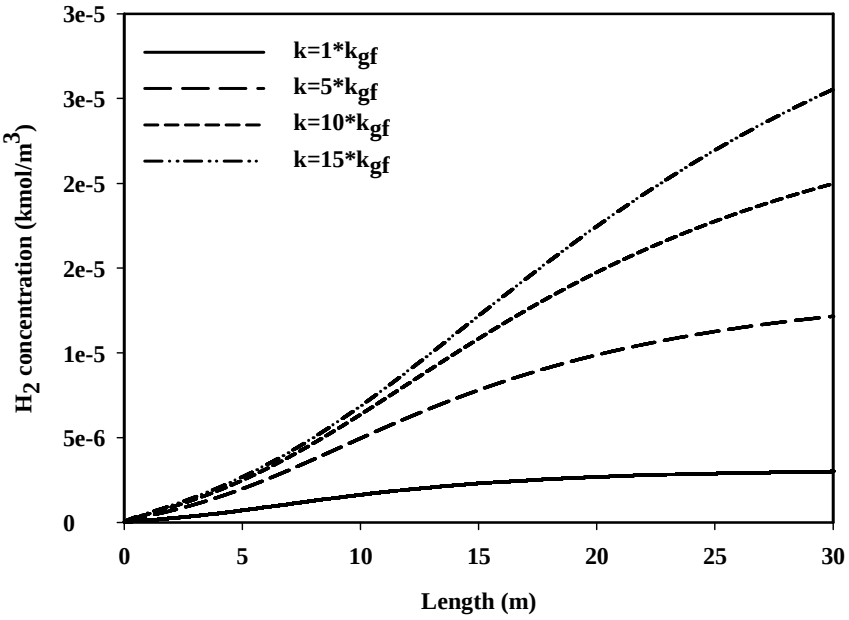


**Figure 6.3** The variations of (a) carbon concentration, (b) temperature, and (c) hydrogen production at different rates of gasification reaction.

(a)

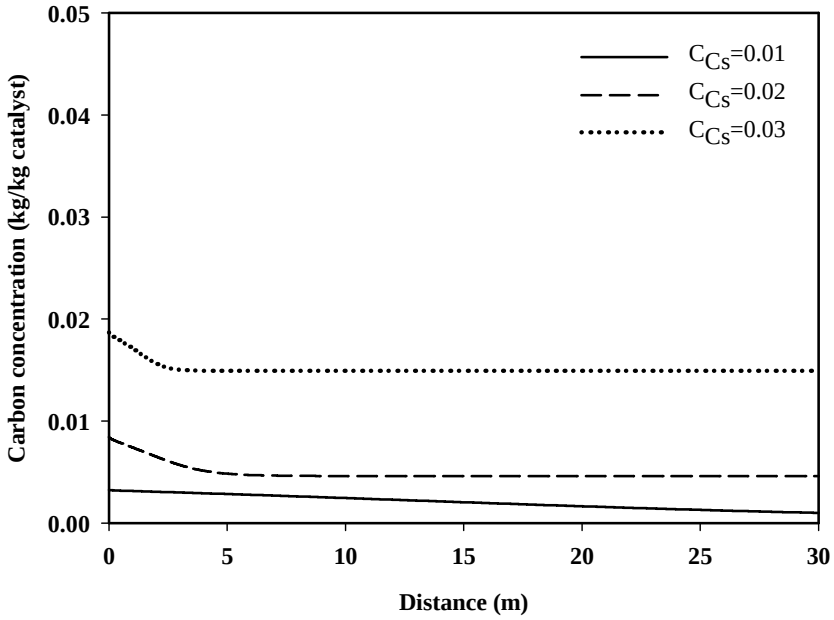
0.05
0.04
0.03
0.02
0.01
0.00
Carbon concentration (kg/kg catalyst)
0
5
10
15
20
25
30
Distance (m)
$C_{Cs}$=0.01
$C_{Cs}$=0.02
$C_{Cs}$=0.03

(b)

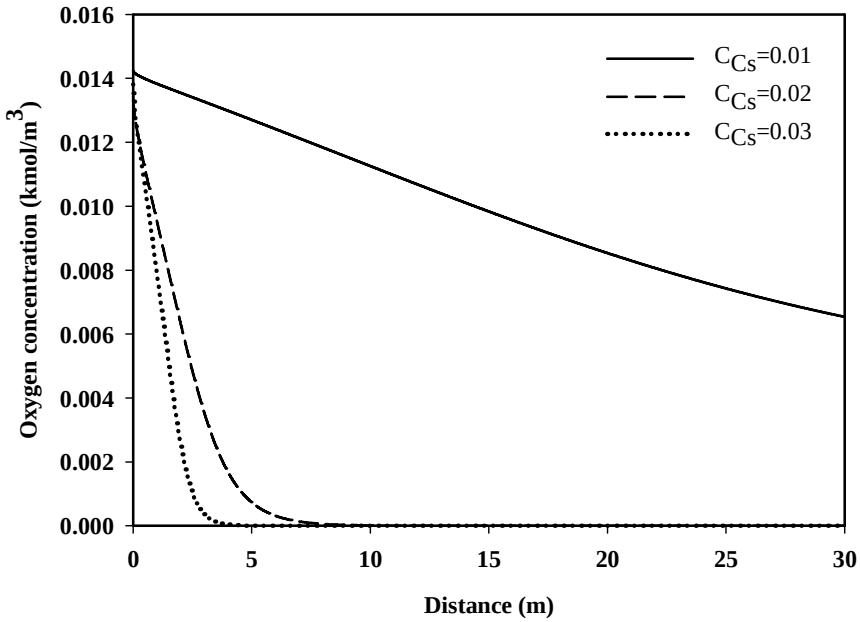
0.016
0.014
0.012
0.010
0.008
0.006
0.004
0.002
0.000
Oxygen concentration (kmol/m3)
0
5
10
15
20
25
30
Distance (m)
$C_{Cs}$=0.01
$C_{Cs}$=0.02
$C_{Cs}$=0.03

(c)

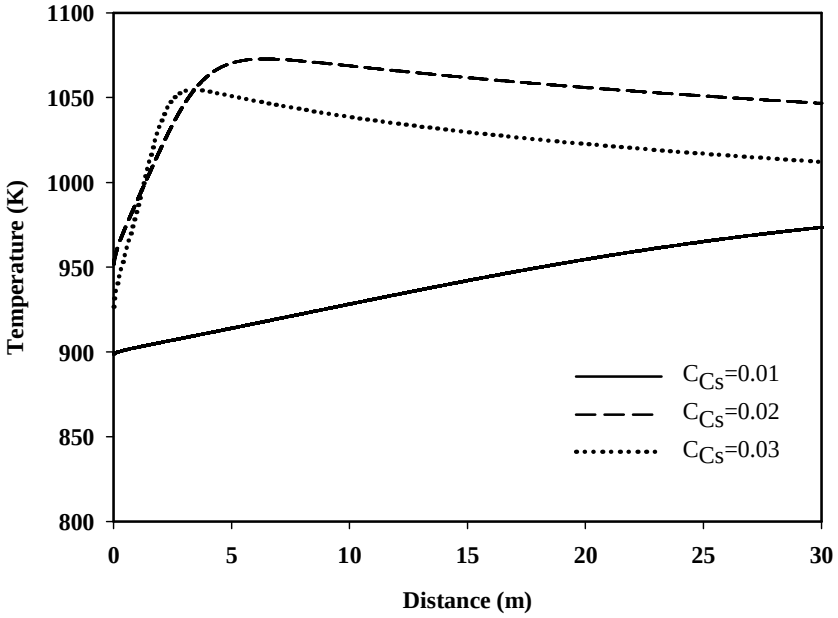


(d)

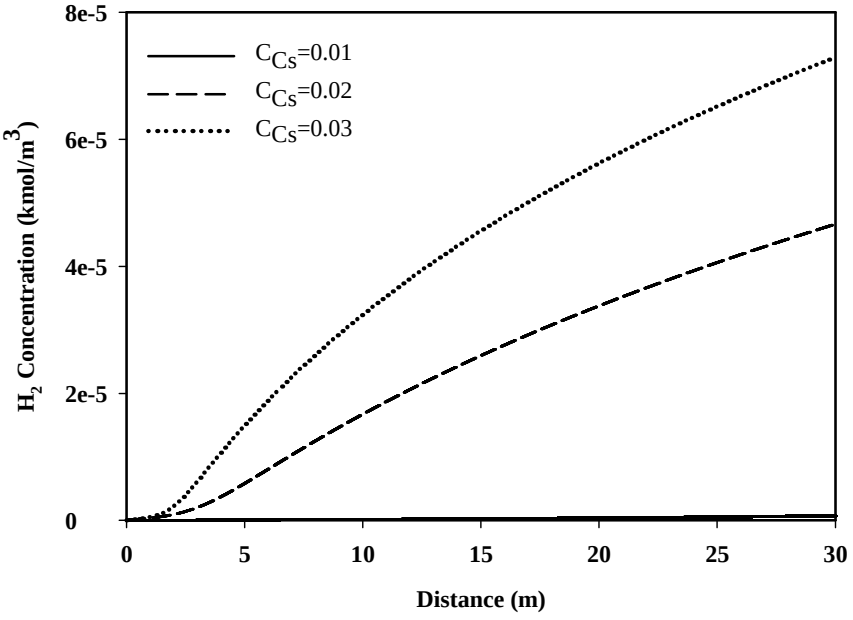


**Figure 6.4** The variations of (a) carbon concentrarion, (b) oxygen concentraion, (c) temperature, and (d) hydrogen concentarion at different carbon content on spent catalyst.

## 6.5 Conclusions

This work investigated the steam gasification with combustion for regeneration of the FCC catalyst in a downer-type regenerator by simulation study using one dimensional hydrodynamic model, material and energy balances and kinetics of reactions. The simulation results show that steam gasification and burning reaction can well reduce the amount of coke deposited on the catalyst surface. Although the rate of gasification reaction of E-cat catalyst currently used in FCC process is quite slow, the gasification reaction is the supplementary reaction helping to reduce the coke on catalyst and the regenerator temperature and gives the valuable hydrogen as a byproduct.

# CHAPTER VII

# THEORETICAL ANALYSIS OF A DOWNER REACTOR AND RISER REGENERATOR INTEGRATED SYSTEM IN FCC PROCESS

## 7.1 Introduction

A fluid catalytic cracking (FCC) unit plays an increasing role in the petroleum and petrochemical industries. This unit had been used a commercial operation in 1942 (Letzsch, 2008). It is used for modification of the hydrocarbon molecules by cracking of long chain molecules into smaller molecules which have higher demand and value. In general, FCC unit in the current generation is composed of two main units, i.e., riser reactor and turbulent bed regenerator. The profit margin obtained from this unit in combination with facing new constraints, such as more residual feedstock, higher product quality, and environmental concern, stimulates the improvement of its operation and performance.

From the hydrodynamic point of view, it is found that the concurrent up-flow reactor (riser) provides several drawbacks compared to the concurrent down-flow reactor (downer). Flow direction of gas and solids in downer reactor is in the same direction of the gravitational force; therefore, the disadvantage of gas and solids back-mixing of the riser reactor have been reduced. This enables more uniform flow structure and narrower solids residence time distribution (Zhu et al, 1995; Jin et al., 2002). In addition, both experimental and simulated results suggest that using the downer as a reactor in a fluid catalytic cracking process can improve both yield and selectivity of the desired products (Abul-Hamayel, 2004; Wu et al., 2009). However, the knowledge of the downer reactor in the literature usually considers only the downer itself, with a few studies that provides details about the accompanying regenerator. Shortcomings of the conventional regenerator, such as high solids inventory and long residence time, enable the development of the regenerator. The

high efficiency regenerator with turbulent fluidized bed at bottom part and the entrained fast fluidized is the effective design that allows the invention of a concurrent up-flow regenerator (the riser) that operates in fast fluidization regime having advantages of high heat and mass transfer, low catalyst inventory and high throughput (Bai et al., 1997, 1998).

In the Chapter V and VI, the downer is used as a regenerator of the FCC process but in this Chapter, the downer is used as a reactor. The main reason behind this selection is that the reducing in back-mixing is more useful for the reactor than that of the regenerator. The back-mixing occurred in the reactor would lead to the over cracking of the desired products and lower their yields affecting to the profit margin of the process while the back-mixing in the regenerator only affects to the regeneration performance which is not the main objective of the process. Moreover, from the concept of circulating fluidized bed, the integrated system should be composed of one up-flow column and one down-flow column. Therefore, if the down-flow operation is used as a reactor, the up-flow operation will be used as a regenerator. The integrated system is the system of a downer reactor and a riser regenerator.

This work carries out a theoretical analysis of an integrated system between downer reactor and riser regenerator in the FCC process. Simulation of the FCC process is performed using a one-dimensional model of hydrodynamic and kinetics of cracking and burning reactions. Obtained results provide useful information about the operation of a downer reactor with a riser regenerator, which can be used for optimal design of the reactor and regenerator system in the FCC process.

## 7.2 Process description

The process diagram of the integrated system of downer reactor and riser regenerator and its ancillary unit in fluid catalytic cracking process are shown in Figure 7.1. It consists of a downer reactor, a riser regenerator, a storage tank for regenerated catalyst, a quick separator, a stripper and a set of cyclones installed in a cyclone housing. The routine operation begins with the injection of the feedstock

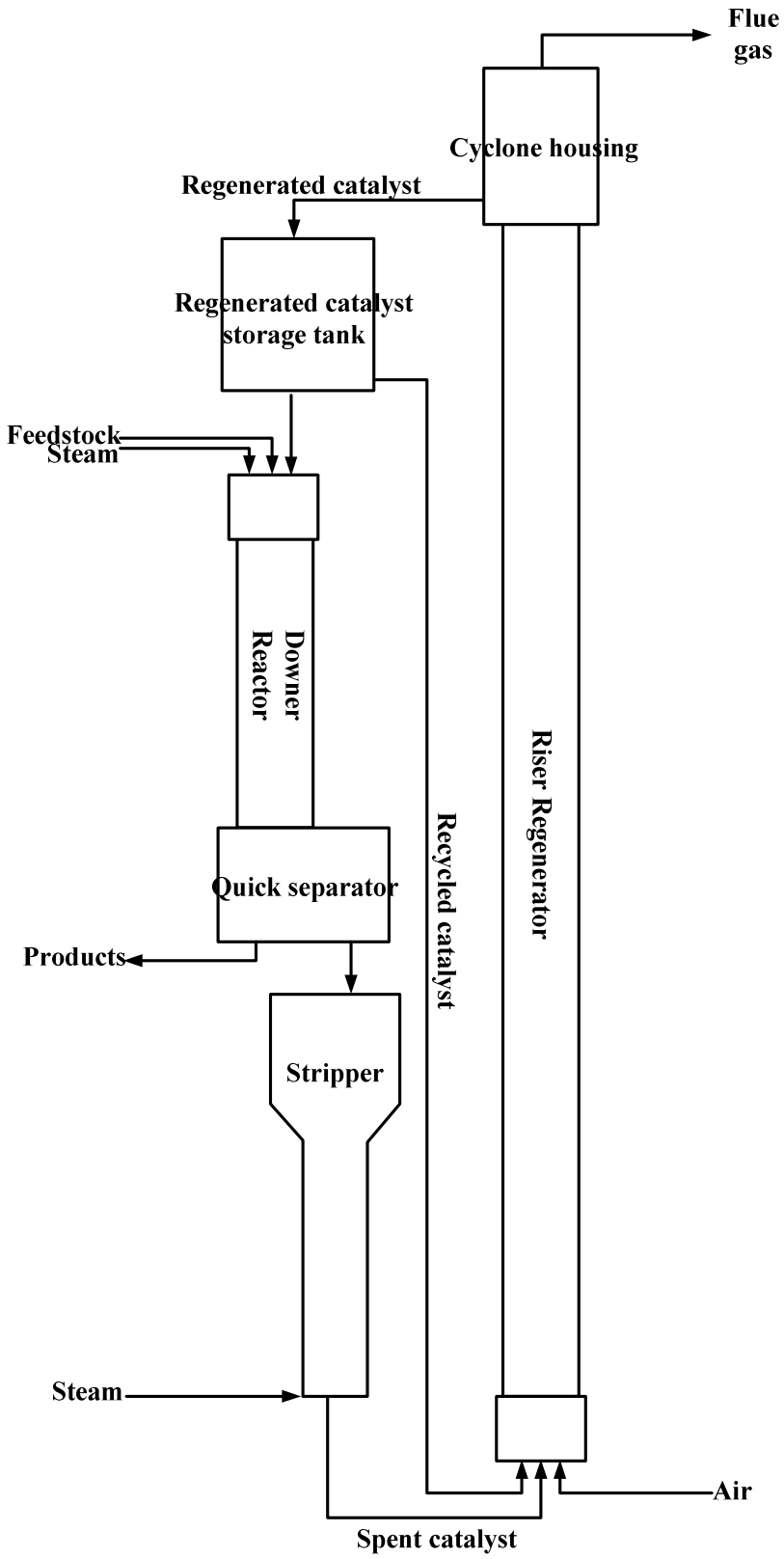


**Figure 7.1** Schematic diagram of integrated system of downer reactor and riser regenerator.

together with steam for atomization. After contacting with high-temperature regenerated catalyst flowing from the storage tank, feedstock vaporizes and moves downward with catalyst. The endothermic cracking reactions proceed while feedstock vapour is contacted with the catalyst. As a by-product of the reactions, the carbonaceous material (coke) forms on the catalyst surface causing the reduction of the catalytic activity. Therefore, a regeneration process is needed for restoring the catalyst activity. Moreover, this process provides heat for vaporization of the feedstock and endothermic cracking reactions that occur in the reactor.

At the exit of downer reactor, spent catalyst and gaseous products including cracked and un-cracked feedstock are separated using a quick separator. Due to the fact that the desired product of the cracking reactions is gasoline which is an intermediate substance, the fast separation is required. A quick separator is used for separation of the gaseous products and spent catalyst because the separation resident time is less than that of cyclones. The products are sent to a main fractionator for separation (not shown here) and the spent catalyst falls into the stripper where steam is used to remove the entrained products. Then, spent catalyst and air are fed together at the bottom of the riser for starting the regeneration process. Coke is oxidized with oxygen in air to form CO, $CO_2$ and $H_2O$ inside the regenerator. Flue gas and regenerated catalyst are separated by a set of cyclones installed in the cyclone housing. A portion of regenerated catalyst are recycled back to the bottom of the riser regenerator to maintain heat balance of the regeneration process and the rest is stored in the storage tank before feeding to the downer reactor.

## 7.3 Mathematical model

The models are derived based on the following assumption.

1. The main objective of this study is to analyse the performance of the integrated system of downer reactor and riser regenerator, therefore, we assume that there is no effect of ancillary units such as the cyclones, quick separator, storage tank and stripper, on the performance of the integrated system.

2. It was assumed that the cracking reactions only take place in a downer reactor and coke burning reactions proceed in the riser regenerator.

3. The model of a downer reactor used in this work is one-dimensional model. Although, two- and three-dimensional model may be better predicted the performance of the downer reactor, a report on three-dimension model of riser reactor indicates that one-dimension model can be well used to predict the overall performance of the mass and energy in riser. (Theologos and Markatos, 1993).

4. The model of a riser regenerator was also modeled in one-dimensional model since there is limited data on this type of reactor. Only data available in the literature are proposed by Bai et al., 1997.

5. Reactor and Regenerator are operated in an adiabatic condition.

6. Gas and catalyst phases in the riser regenerator are in thermal equilibrium, therefore; temperatures of gas and catalyst phase are the same.

7. Dispersion and adsorption inside the catalyst particles are neglected.

8. Coke does not affect to the flow characteristic.

9. All Conradson Carbon Residue is converted to the coke depositing on the catalyst.

The mathematical models used in this study including the model of downer reactor, and the model of riser regenerator. The equations are shown in Table 7.1 and Table 7.2.

**Table 7.1** The mathematical for downer reactor model used in chapter VII.

$$\frac{d(\bar{\varepsilon}_{g,rxt}\rho_{g,rxt}\bar{V}_{g,rxt})}{dz_{rxt}} = 0 \text{ , where } G_{g,rxt} = \bar{\varepsilon}_{g,rxt}\rho_{g,rxt}\bar{V}_{g,rxt} = \text{constant} \tag{7.1}$$

$$\frac{d(\bar{\varepsilon}_{s,rxt}\rho_{s}\bar{V}_{s,rxt})}{dz_{rxt}} = 0 \text{ , where } G_{s,rxt} = \bar{\varepsilon}_{s,rxt}\rho_{s}\bar{V}_{s,rxt} = \text{constant} \tag{7.2}$$

$$\bar{\varepsilon}_{g,rxt} + \bar{\varepsilon}_{s,rxt} = 1 \tag{7.3}$$

$$\frac{d(\bar{\varepsilon}_{g,rxt}\rho_{g,rxt}\bar{V}^{2}_{g,rxt})}{dz_{rxt}} = -\frac{dP_{rxt}}{dz_{rxt}} - F_{D,rxt} - F_{fg,rxt} + \bar{\varepsilon}_{g,rxt}\rho_{g,rxt}g \tag{7.4}$$

$$\frac{d(\bar{\varepsilon}_{s,rxt}\rho_{s}\bar{V}^{2}_{s,rxt})}{dz_{rxt}} = F_{D,rxt} - F_{fs,rxt} + \bar{\varepsilon}_{s,rxt}(\rho_{s} - \rho_{g,rxt})g \tag{7.5}$$

$$F_{D,rxt} = \frac{3}{4}\frac{C_{D,rxt}}{d_{p}}\bar{\varepsilon}_{s,rxt}\rho_{g,rxt}\left|\bar{V}_{g,rxt} - \bar{V}_{s,rxt}\right|\left(\bar{V}_{g,rxt} - \bar{V}_{s,rxt}\right) \tag{7.6}$$

$$\frac{C_{D,rxt}}{C_{Ds,rxt}} = \frac{14.1\left[1 + 2.78\left(G_{g,rxt}/G_{s,rxt}\right)\right]}{Fr_{rxt}} \tag{7.7}$$

$$Fr_{rxt} = \frac{U_{g,rxt}}{\sqrt{gd_{p}}} \tag{7.8}$$

$$C_{Ds,rxt} = \frac{24}{\mathrm{Re}_{r,rxt}}\left(1 + 0.15\,\mathrm{Re}_{r,rxt}^{\ 0.687}\right) \text{ for } \mathrm{Re}_{r,rxt} \le 1000 \tag{7.9}$$

$$C_{Ds,rxt} = 0.44 \text{ for } \mathrm{Re}_{r,rxt} > 1000$$

$$\mathrm{Re}_{r,rxt} = \frac{\rho_{g,rxt}d_{p}\left|\bar{V}_{g,rxt} - \bar{V}_{s,rxt}\right|}{\mu_{g,rxt}} \tag{7.10}$$

$$F_{fg,rxt} = \frac{2f_{g,rxt}\bar{\varepsilon}_{g,rxt}\rho_{g,rxt}\bar{V}^{2}_{g,rxt}}{D_{rxt}} \tag{7.11}$$

$$f_{g,rxt} = \frac{16}{\mathrm{Re}_{g,rxt}}, \text{ when } \mathrm{Re}_{g,rxt} \le 2300$$

$$f_{g,rxt} = \frac{0.079}{\mathrm{Re}_{g,rxt}^{\ 0.313}}, \text{ when } \mathrm{Re}_{g,rxt} > 2300 \tag{7.12}$$

$$\mathrm{Re}_{g,rxt} = \frac{\rho_{g,rxt}U_{g,rxt}D_{rxt}}{\mu_{g,rxt}} \tag{7.13}$$

**Table 7.1** The mathematical for downer reactor model used in chapter VII. (Continued).

$$F_{fs,rxt} = \frac{2 f_{s,rxt} \bar{\varepsilon}_{s,rxt} \rho_{s,rxt} \bar{V}^2_{s,rxt}}{D_{rxt}} \tag{7.14}$$

$$f_{s,rxt} = \frac{0.0285\sqrt{gD_{rxt}}}{\left(G_{s,rxt} / \rho_s \bar{\varepsilon}_{s,rxt}\right)} \tag{7.15}$$

$$\bar{V}_{g,rxt} = \frac{U_{g,rxt}}{\bar{\varepsilon}_{g,rxt}} = \frac{G_{g,rxt}}{\rho_{g,rxt} \bar{\varepsilon}_{g,rxt}} \tag{7.16}$$

$$\bar{V}_{s,rxt} = \frac{G_{s,rxt}}{\rho_s \bar{\varepsilon}_{s,rxt}} \tag{7.17}$$

$$U_{g,rxt} = \frac{n_{t,rxt} R T_{g,rxt}}{P_{rxt} A_{rxt}} \tag{7.18}$$

$$\frac{dy_{i,rxt}}{dz_{rxt}} = \frac{\rho_s \bar{\varepsilon}_{s,rxt} A_{rxt} \phi_s}{F_{g,rxt}} r_{i,rxt}\ ,\ i = go, gl, gs, \text{and } ck \tag{7.19}$$

$$\phi_c = \exp\left(-\alpha_c C_{ck,rxt}\right), \text{where } \alpha_c = \alpha_{c0} \exp\left(\frac{-E_c}{R T_{g,rxt}}\right) R_{AN}^{\alpha_c^*} \tag{7.20}$$

$$k_{i,rxt} = k_{i,rxt,0} \exp\left(\frac{-E_{i,rxt}}{R T_{g,rxt}}\right) \text{ for } i = 1,...,5 \tag{7.21}$$

$$r_{go,rxt} = -\left(k_{1,rxt} + k_{2,rxt} + k_{3,rxt}\right) y^2_{go,rxt} \tag{7.22}$$

$$r_{gl,rxt} = k_{1,rxt} y^2_{go,rxt} - k_{4,rxt} y_{gl,rxt} - k_{5,rxt} y_{gl,rxt} \tag{7.23}$$

$$r_{gs,rxt} = k_{2,rxt} y^2_{go,rxt} + k_{4,rxt} y_{gl,rxt} \tag{7.24}$$

$$r_{ck,rxt} = k_{3,rxt} y^2_{go,rxt} + k_{5,rxt} y_{gl,rxt} \tag{7.25}$$

$$r_{wv,rxt} = 0 \tag{7.26}$$

$$T_{g,FS} = \frac{B_{\text{lg}}}{A_{\text{lg}} - \log\left(P_{FS} y_{go,FS}\right)} - C_{\text{lg}} \tag{7.27}$$

$$T_{s,FS} = T_{s,reg,out} - \frac{1}{F_{s,CL} C_{p,s}} \Big[ F_{\text{lg}} C_{p,\text{lg}} \left(T_{g,FS} - T_{\text{lg}}\right) + F_{ds} C_{p,ds} \left(T_{g,FS} - T_{ds}\right) + F_{\text{lg}} \Delta H_{v\text{lg}} \tag{7.28}$$

**Table 7.1** The mathematical for downer reactor model used in chapter VII. (Continued).

$$\frac{dT_{g,rxt}}{dz} = \frac{A_{rxt}}{F_{g.rxt}C_{pg,rxt}}\left[h_{p,rxt}A_{p,rxt}\left(T_{s,rxt} - T_{g,rxt}\right) + \rho_s \bar{\varepsilon}_{s,rxt} Q_{react,rxt}\right] \tag{7.29}$$

$$\frac{dT_{s,rxt}}{dz} = \frac{A_{rxt}h_{p,rxt}A_{p,rxt}}{F_{s,rxt}C_{p,s}}\left(T_{g,rxt} - T_{s,rxt}\right) \tag{7.30}$$

$$Q_{react,rxt} = -\left(\Delta H_{1,rxt}k_{1,rxt}y_{go,rxt}^2 + \Delta H_{2,rxt}k_{2,rxt}y_{go,rxt}^2 + \Delta H_{3,rxt}k_{3,rxt}y_{go,rxt}^2 + \Delta H_{4,rxt}k_{4,rxt}y_{gl,rxt} + \Delta H_{5,rxt}k_{5,rxt}y_{gl,rxt}\right)\phi_c \tag{7.31}$$

$$h_{p,rxt} = 0.03\frac{k_{g,rxt}}{d_p^{2/3}}\left[\frac{\left|\bar{V}_{g,rxt} - \bar{V}_{s.rxt}\right|\rho_{g,rxt}\bar{\varepsilon}_{g,rxt}}{\mu_{g,rxt}}\right]^{1/3} \tag{7.32}$$

$$k_{g,rxt} = 10^{-6}\times\left(1.9469 - 0.374M_{wm,rxt} + 1.4815\times10^{-3}M_{wm,rxt}^2 + ... 0.1028T_{g,rxt}\right) \tag{7.33}$$

**Table 7.2** The mathematical for riser regenerator model used in chapter VII.

$$\frac{d(\bar{\varepsilon}_{g,reg}\rho_{g,reg}\bar{V}_{g,reg})}{dz_{reg}} = 0 \text{, where } G_{g,reg} = \bar{\varepsilon}_{g,reg}\rho_{g,reg}\bar{V}_{g,reg} = \text{constant} \tag{7.34}$$

$$\frac{d(\bar{\varepsilon}_{s,reg}\rho_{s,reg}\bar{V}_{s,reg})}{dz_{reg}} = 0 \text{, where } G_{s,reg} = \bar{\varepsilon}_{s,reg}\rho_s\bar{V}_{s,reg} = \text{constant} \tag{7.35}$$

$$\frac{d(\bar{\varepsilon}_{g,reg}\rho_{g,reg}\bar{V}_{g,reg}^2)}{dz_{reg}} = -\frac{dP_{reg}}{dz_{reg}} - F_{D,reg} - F_{fg,reg} - \bar{\varepsilon}_{g,reg}\rho_{g,reg}g \tag{7.36}$$

$$\frac{d(\bar{\varepsilon}_{s,reg}\rho_s\bar{V}_{s,reg}^2)}{dz_{reg}} = F_{D,reg} - F_{fs,reg} - \bar{\varepsilon}_{s,reg}(\rho_s - \rho_{g,reg})g \tag{7.37}$$

$$F_{D,reg} = \frac{3}{4}\frac{C_{D,reg}}{d_p}\bar{\varepsilon}_{s,reg}\rho_{g,reg}\left(\bar{V}_{g,reg} - \bar{V}_{s,reg}\right)^2 \tag{7.38}$$

$$\frac{C_{D,reg}}{C_{Ds,reg}} = 1.405\left(\bar{\varepsilon}_{g,reg}\right)^{2.322}\left(\frac{\mathrm{Re}_{r,reg}}{\mathrm{Re}_{t,reg}}\right)^{-0.932}\left(\frac{d_p}{D_{reg}}\right)^{0.105}\eta_{reg} \tag{7.39}$$

**Table 7.2** The mathematical for riser regenerator model used in chapter VII. (Continued).

$$\eta_{reg} = 1 - \frac{0.5e^{8(D_{reg}-0.8)}}{1+e^{8(D_{reg}-0.8)}} \tag{7.40}$$

$$C_{Ds,reg} = \frac{24}{\mathrm{Re}_{r,reg}}\left(1+0.15\,\mathrm{Re}_{r,reg}^{\ 0.687}\right) \quad \text{for } \mathrm{Re}_{r,reg} \le 1000 \tag{7.41}$$

$$C_{Ds,reg} = 0.44 \quad \text{for } \mathrm{Re}_{r,reg} > 1000 \tag{7.42}$$

$$\mathrm{Re}_{r,reg} = \frac{\rho_{g,reg} d_p \left|\bar{V}_{g,reg} - \bar{V}_{s,reg}\right|}{\mu_{g,reg}} \tag{7.43}$$

$$F_{fg,reg} = \frac{2 f_{g,reg} \bar{\varepsilon}_{g,reg} \rho_{g,reg} \bar{V}^2_{g,reg}}{D_{reg}} \tag{7.44}$$

$$f_{g,reg} = \frac{16}{\mathrm{Re}_{g,reg}}, \quad \text{when } \mathrm{Re}_{g,reg} \le 2300 \tag{7.45}$$

$$f_{g,reg} = \frac{0.079}{\mathrm{Re}_{g,reg}^{\ 0.313}}, \quad \text{when } \mathrm{Re}_{g,reg} > 2300 \tag{7.46}$$

$$\mathrm{Re}_{g,reg} = \frac{\rho_{g,reg} U_{g,reg} D_{reg}}{\mu_{g,reg}} \tag{7.47}$$

$$F_{fs,reg} = \frac{2 f_{s,reg} \bar{\varepsilon}_{s,reg} \rho_s \bar{V}^2_{s,reg}}{D_{reg}} \tag{7.48}$$

$$f_{s,reg} = \frac{0.0285\sqrt{gD_{reg}}}{\left(G_{s,reg} / \rho_s \bar{\varepsilon}_{s,reg}\right)} \tag{7.49}$$

$$\bar{V}_{g,reg} = \frac{U_{g,reg}}{\bar{\varepsilon}_{g,reg}} = \frac{G_{g,reg}}{\rho_{g,reg} \bar{\varepsilon}_{g,reg}} \tag{7.50}$$

$$\bar{V}_{s,reg} = \frac{G_{s,reg}}{\rho_s \bar{\varepsilon}_{s,reg}} \tag{7.51}$$

$$U_{g,reg} = \frac{n_{t,reg} R T_{g,reg}}{P_{reg} A_{reg}} \tag{7.52}$$

$$\beta_{C,reg} = \beta_{C,reg,0} \exp(-E_{\beta,reg} / R T_{reg}) \tag{7.53}$$

**Table 7.2** The mathematical for riser regenerator model used in chapter VII. (Continued).

$$k_{1,reg} = \frac{\beta_{C,reg} k_{C,reg}}{\beta_{C,reg} + 1} \tag{7.54}$$

$$k_{2,reg} = \frac{k_{C,reg}}{\beta_{C,reg} + 1} \tag{7.55}$$

$$k_{C,reg} = k_{1,reg} + k_{2,reg} = k_{C,reg,0} \exp(-E_{c,reg} / RT_{reg}) \tag{7.56}$$

$$k_{3c,reg} = k_{3c,reg,0} \exp(-E_{3c,reg} / RT_{reg}) \tag{7.57}$$

$$k_{3h,reg} = k_{3h,reg,0} \exp(-E_{3c,reg} / RT_{reg}) \tag{7.58}$$

$$k_{4,reg} = \begin{cases} k_{4,reg,0} \exp\left(-E_{4,reg} / (RT_{reg})\right), \; T_{reg} < 973\,\mathrm{K} \\ k_{4,reg,0} \exp\left(-E_{4,reg} / (RT_{reg})\right)\left[1 - 2.67 \times 10^{30}\right. \\ \quad \left. \times \exp(-7.34 \times 10^{4} / T_{reg})\right], \; T_{reg} \geq 973\,\mathrm{K} \end{cases} \tag{7.59}$$

$$r_{1,reg} = k_{1,reg} P_{O_{2,reg}} C_{C,reg} \tag{7.60}$$

$$r_{2,reg} = k_{2,reg} P_{O_{2,reg}} C_{C,reg} \tag{7.61}$$

$$r_{3c,reg} = \bar{\varepsilon}_{s,reg} \rho_s k_{3c,reg} P_{O_{2,reg}} P_{CO,reg} \tag{7.62}$$

$$r_{3h,reg} = \bar{\varepsilon}_{g,reg} k_{3h,reg} P_{O_{2,reg}} P_{CO,reg} \tag{7.63}$$

$$r_{4,reg} = k_{4,reg} P_{O_{2,reg}} C_{H,reg} \tag{7.64}$$

$$\frac{dC_{C,reg}}{dz_{reg}} = \frac{-\left(r_{1,reg} + r_{2,reg}\right) \rho_s \bar{\varepsilon}_{s,reg}}{G_{s,reg}} \tag{7.65}$$

$$\frac{dC_{H,reg}}{dz_{reg}} = \frac{-r_{H,reg} \rho_s \bar{\varepsilon}_{s,reg}}{G_{s,reg}} \tag{7.66}$$

$$\frac{dC_{O_2,reg}}{dz_{reg}} = \frac{1}{U_{g,reg}} \left[ \left( -\frac{1}{2} \frac{r_{1,reg}}{12} - \frac{r_{2,reg}}{12} - \frac{r_{4,reg}}{4} \right) \rho_s \bar{\varepsilon}_{s,reg} + \left( -\frac{1}{2} r_{3c,reg} - \frac{1}{2} r_{3h,reg} \right) \right] \tag{7.67}$$

$$\frac{dC_{CO,reg}}{dz_{reg}} = \frac{1}{U_{g,reg}} \left[ \left( \frac{r_{1,reg}}{12} \right) \rho_s \bar{\varepsilon}_{s,reg} + \left( -r_{3c,reg} - r_{3h,reg} \right) \right] \tag{7.68}$$

**Table 7.2** The mathematical for riser regenerator model used in chapter VII. (Continued).

$$\frac{dC_{CO_2,reg}}{dz_{reg}} = \frac{1}{U_{g,reg}}\left[\left(\frac{r_{2,reg}}{12}\right)\rho_s\bar{\varepsilon}_{s,reg} + \left(r_{3c,reg} + r_{3h,reg}\right)\right] \tag{7.69}$$

$$\frac{dC_{H_2O,reg}}{dz_{reg}} = \frac{1}{U_{g,reg}}\left[r_{4,reg}\rho_s\bar{\varepsilon}_{s,reg}\right] \tag{7.70}$$

$$C_{\mathrm{C,reg},0} = \frac{G_{s,rxt}C_{C,rxt,out} + G_{sr,reg}C_{\mathrm{C,reg,out}}}{G_{s,rxt} + G_{sr,reg}} \tag{7.71}$$

$$C_{\mathrm{H,reg},0} = \frac{\alpha G_{s,rxt}C_{C,rxt,out} + G_{sr,reg}C_{H,reg,out}}{G_{s,rxt} + G_{sr,reg}} \tag{7.72}$$

$$T_{reg,0} = \frac{G_{s,rxt}C_{p,s}T_{s,rxt,out} + G_{sr,reg}C_{p,s}T_{g,reg,\mathrm{out}} + U_{g,reg,0}\rho_{g,reg,0}C_{p,g,reg,0}T_{a,reg}}{G_{s,rxt}C_{p,s} + G_{sr,reg}C_{p,s} + U_{g,reg,0}\rho_{g,reg,0}C_{p.g,reg,0}} \tag{7.73}$$

$$\frac{dT_{reg}}{dz_{reg}} = \frac{1}{U_{g,reg}\rho_{g,reg}C_{p,g,reg} + G_{s,reg}C_{p,s}}\left[\left(\frac{\rho_s\bar{\varepsilon}_{s,reg}}{12}(r_{1,\mathrm{reg}}\Delta H_{1,reg} + r_{2,\mathrm{reg}}\Delta H_{2,\mathrm{reg}})\right) + r_{3c,\mathrm{reg}}\Delta H_{3,\mathrm{reg}} + r_{3h,\mathrm{reg}}\Delta H_{3,\mathrm{reg}} + \left(\rho_s\bar{\varepsilon}_{s,reg}r_{4,\mathrm{reg}}\Delta H_{4,reg}\right)\right] \tag{7.74}$$

## 7.4 Simulation results and discussion

### 7.4.1 Model validation

Predicted data of the downer reactor is compared with the available experimental data in the literature. The comparison of product yields and outlet temperature obtained from pilot plant (Abul-hamayel, 2004) and model of downer reactor using the same feed properties at the catalyst/oil ratio of 20 and 80% conversion are shown in Table 7.3 It can be seen that the simulation data obtained by the model prediction is very close to the experimental data obtained from pilot plant. Hence, the model predictions are likewise reasonable.

**Table 7.3** Product yields of downer reactor from experimental and predicted data.

| Parameters | Pilot plant (Abul-hamayel, 2004) | Model | Deviation (%) |
|---|---|---|---|
| Conversion (%) | 80 | 80 | - |
| Catalyst to oil ratio (CTO) | 20 | 20 | - |
| Downer outlet temperature (K) | 873.15 | 882.07 | 1.02 |
| Yield (wt.%) | | | |
| $C_1$-$C_4$ Gases | 29.50 | 30.66 | 3.93 |
| Gasoline | 48.50 | 47.86 | -1.32 |
| Coke | 2.00 | 1.55 | -22.5 |

Due to the limited availability of the data in the literature, the hydrodynamic model of riser is validated against the experimental data (Zhang et al., 1999) as shown in Figure 4.2 of Chapter IV. The results reveal that the model prediction and the experimental data of solid holdup in riser reactor are in a good agreement. The kinetic model of the regeneration used in this work is obtained from the literature. This model was used to predict the regeneration characteristics in several works (Arbel et al., 1995; Affum et al., 2011).

## 7.4.2 Equation solving scheme

In order to obtain the profile of temperatures and yields in the reactor and regenerator, the set of differential algebraic equations (DAE) together with the parameters and initial conditions of both reactor and regenerator were solved by Euler's method to obtain the variations of the species concentration and temperature profile along the length of the reactor and the regenerator.

The solving scheme initiates with calculations of the yields and temperatures profiles in downer regenerator (Figure 7.2). To obtain these, the operating conditions for the downer reactor and the feedstock properties are needed to be specified and unknown inlet variables from riser regenerator i.e., $T_{s,reg,out}$ , $C_{c,reg,out}$ , needed to be guessed. Then the temperature of gas and catalyst will be calculated from Antoine

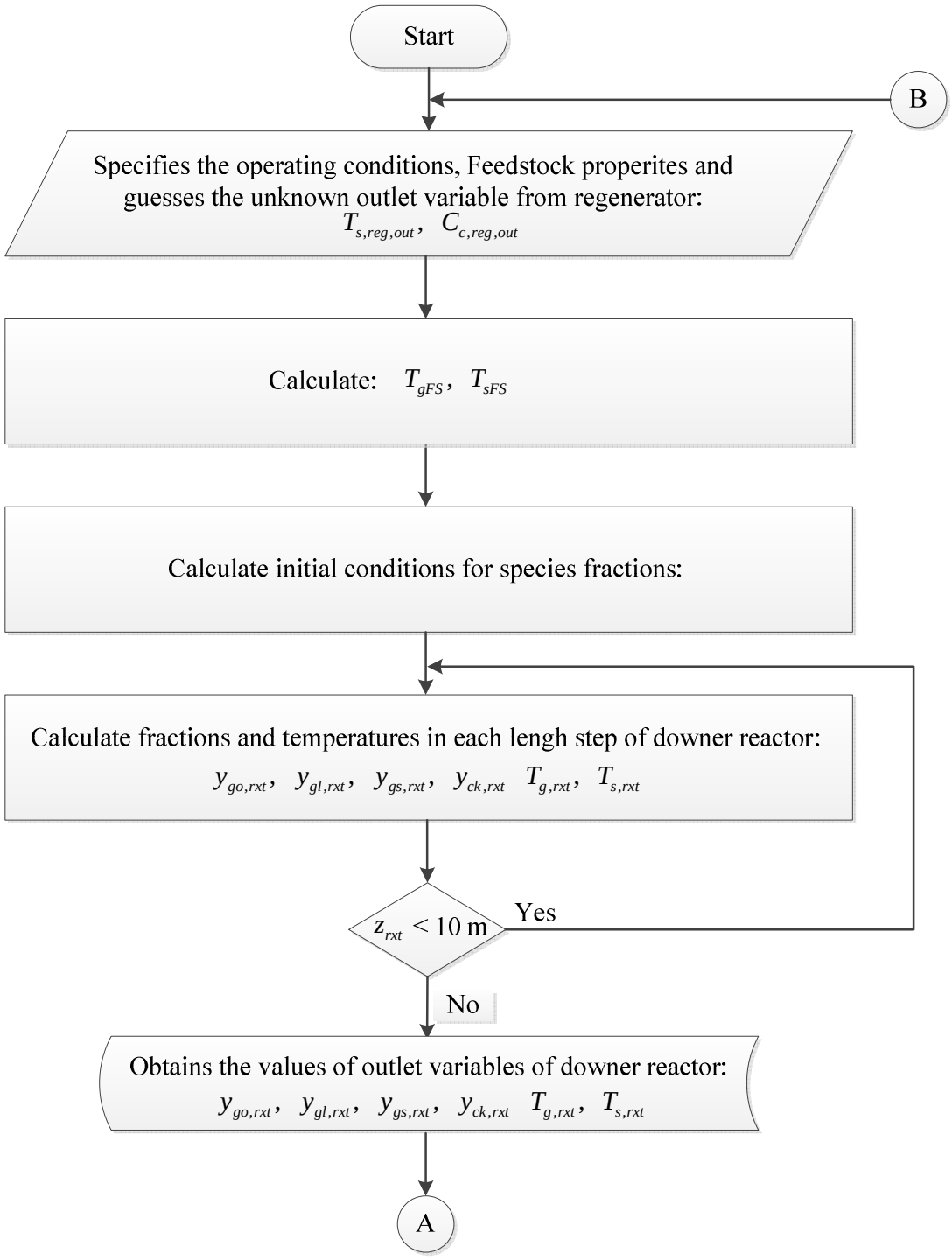


**Figure 7.2** Calculation diagram for downer reactor.

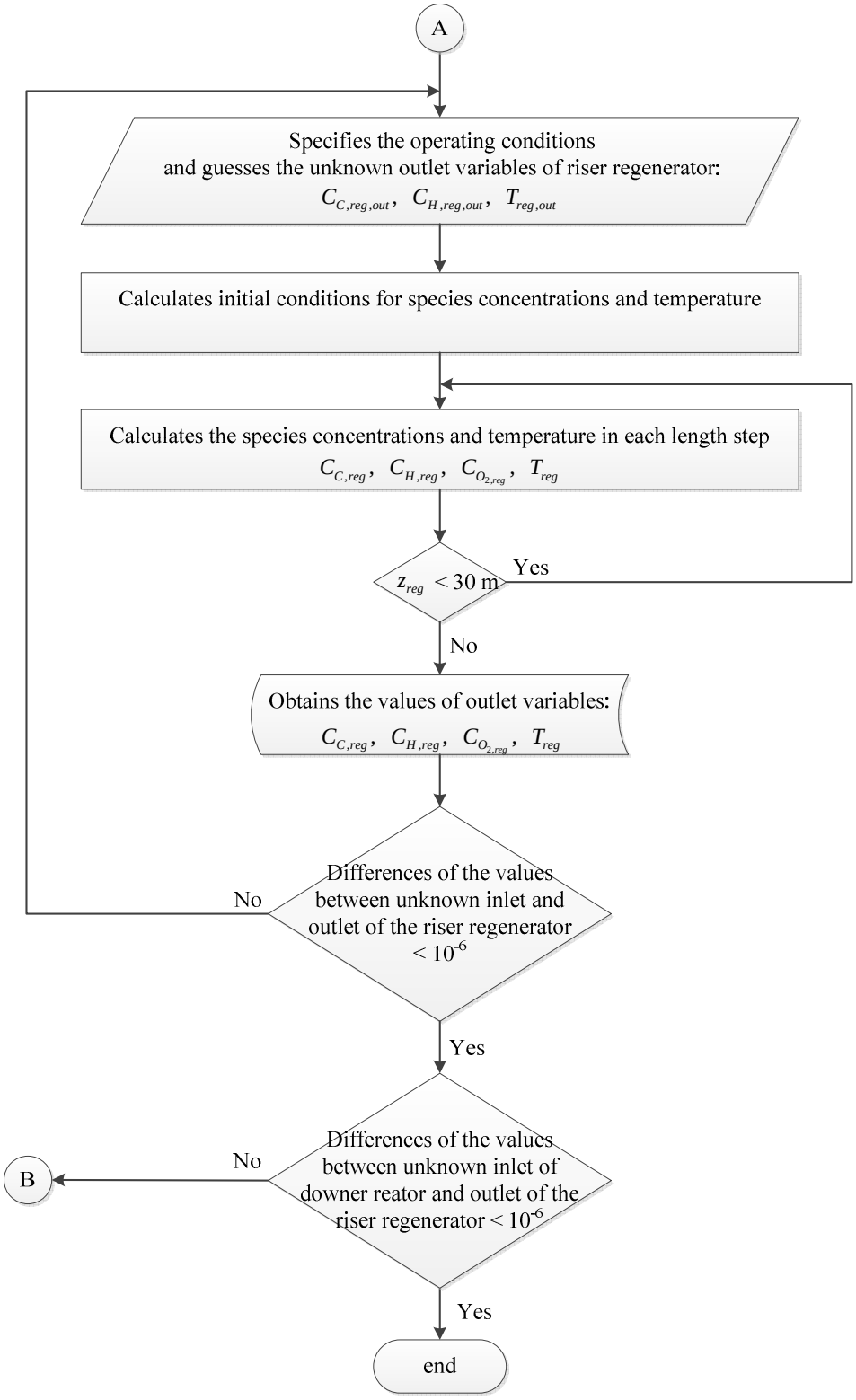


**Figure 7.3** Calculation diagram for riser regenerator.

Equation and energy balances, respectively. The species fractions and temperature profiles along the length of the downer reactor were calculated in each infinitestimal length step until reach the final step. Then, outlet variables of the downer regenerator are obtained. (The point A in Figure 7.2 indicates the link between point A in Figure 7.2 and point A in Figure 7.3.) The next step of the calculation is for riser regenerator (Figure 7.3). It was started from specifying the operating condition for the riser regenerator and guessed the unknown outlet variables of riser regenerator the occurred from the recycled stream. Then the species concentrations and temperature of the riser regenerator will be calculated. After calculation of the final step in riser regenerator, the unknown outlet variables that we guessed before calculation will be compared. The calculation will be finished if the guessed and the calculated value is less than tolerance ($10^{-6}$). (The point B in Figure 7.3 links with point B in Figure 7.2)

## 7.5 Results and discussions

### 7.5.1 The product yields and coke burning at standard condition

The product yields variation along the downer reactor length according to the reactor and regenerator dimensions and catalyst properties, operating condition and feedstock properties in Table 7.4 to Table 7.6 are shown in Figure 7.4

The simulation results reveal the fact according to the nature of the cracking reactions that the reactant of the reaction i.e., gasoil reduces along the length while the products containing C1-C4 gases, gasoline and coke increase. The temperature of gas phase increases while the temperature of catalyst reduces due to the transfer of heat from the catalyst to gas. The temperatures of gas and catalyst phases at inlet condition in Figure 7.5 are the temperatures after vaporization of the feedstock. The entrance feedstock ($T_{lg}$) at temperature of 535 K is heated to the vaporized temperature (around 675 K) which depends on the properties of feedstock and the operating pressure. Then the feedstock is vaporized at the aforementioned temperature. Temperature of catalyst flowing from the regenerator drops from 1040 to 1015 K due to the vaporization of the feedstock.

**Table 7.4** Reactor and regenerator dimensions and catalyst properties.

| | |
|---|---|
| **Dimensions** | |
| Downer reactor height, $L_{rxt}$ (m) | 3 |
| Downer reactor diameter, $D_{rxt}$ (m) | 0.3 |
| Riser regenerator height, $L_{reg}$ (m) | 30 |
| Riser regenerator diameter, $D_{reg}$ (m) | 0.3 |
| **Catalyst properties** | |
| Averaged diameter, $d_p$ ($\mu$m) | 70 |
| Density, $\rho_s$ (kg/m$^3$) | 1500 |
| Heat capacity $C_{p,s}$ (kJ/(kg K)) | 1.15 |

**Table 7.5** Operating condition at standard condition.

| **Downer reactor operating condition at standard condition** | |
|---|---|
| Mass flow rate of liquid feed, $F_{lg}$ (kg/s) | 0.5 |
| Entrance temperature of liquid feedstock, $T_{lg}$ (K) | 535 |
| Temperature of steam, $T_{ds}$ (K) | 773 |
| Reactor pressure, $P_{rxt}$ (kPa) | 250 |
| Catalyst-to-Oil Ratio, CTO (-) | 20 |
| Catalyst flux, $G_{s,rxt}$ (kg/m$^2$s) | 141.47 |
| **Riser regenerator operating condition at standard condition** | |
| Ratio of regenerated to spent catalyst, $G_{sr,reg}/G_{ss,reg}$ (-) | 3.0 |
| Catalyst flux, $G_{s,reg}$ (kg/m$^2$s) | 565.88 |
| Regenerator pressure, $P_{reg}$ (kPa) | 250 |
| Air inlet temperature, $T_a$ (K) | 573.15 |

The operation of the accompanying riser regenerator is shown in Figure 7.6. It is clearly seen that most of coke on the catalyst surface is removed with this operating condition. It is reduced from 0.00083 kg/kg catalyst at inlet of the riser regenerator to approximately 0.0002 kg/kg catalyst. Actually, coke content on spent catalyst flowing from the reactor is 0.0030 kg/kg catalyst (see Table 7.7). With this amount of coke, the regenerated catalyst shows the satisfying cracking activity (Figure 7.6). The heat obtained from coke burning raises the temperature of the regenerator up and this

amount of heat is adequate for providing to the downer reactor and thus, the heat balance of the system is maintained.

**Table 7.6** Feedstock properties.

| **Parameters** | **Value** |
|---|---|
| Weight fraction of Conradson Carbon Residue (CCR) in feedstock, $Y_{cc}$ (wt.%) | 0.5 |
| Aromatics to naphthenes weight ratio in feedstock, $R_{AN}$ (-) | 2.1 |
| Specific gravity of liquid feedstock, $S_g$ (-) | 0.894 (API=26.8) |
| Alpha, $\alpha$ (-) | 0.067 |
| H/C atomic ratio in coke | 0.8 |
| **Distilled volume (%)** | **TBP distillation temperatures (K)** |
| 10 | 554.3 |
| 30 | 605.4 |
| 50 | 647.0 |
| 70 | 688.2 |
| 90 | 744.8 |

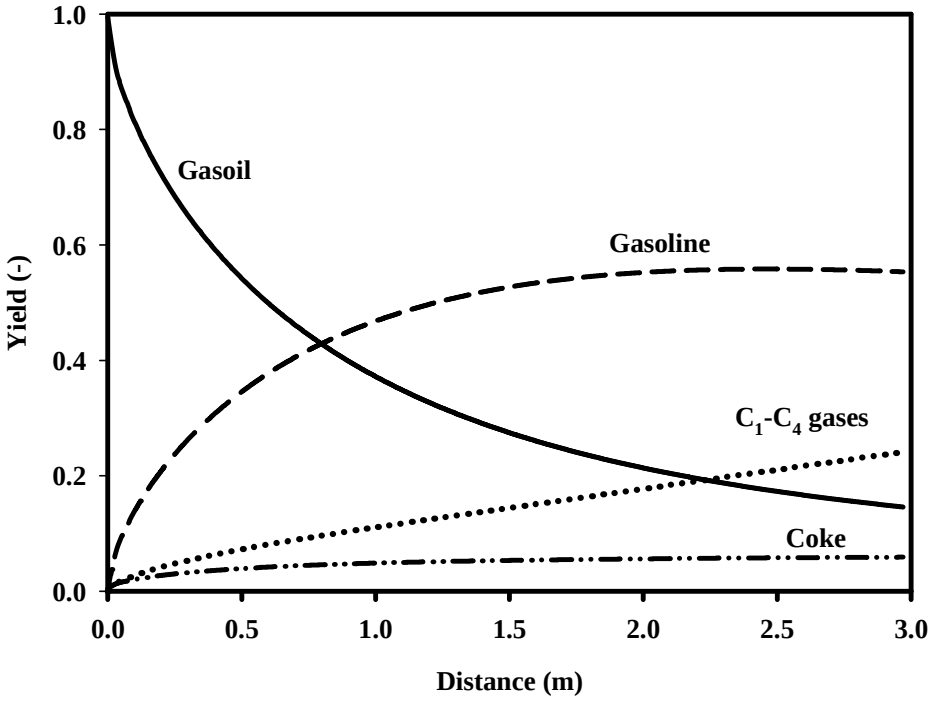


**Figure 7.4** Product yields along the downer regenerator.

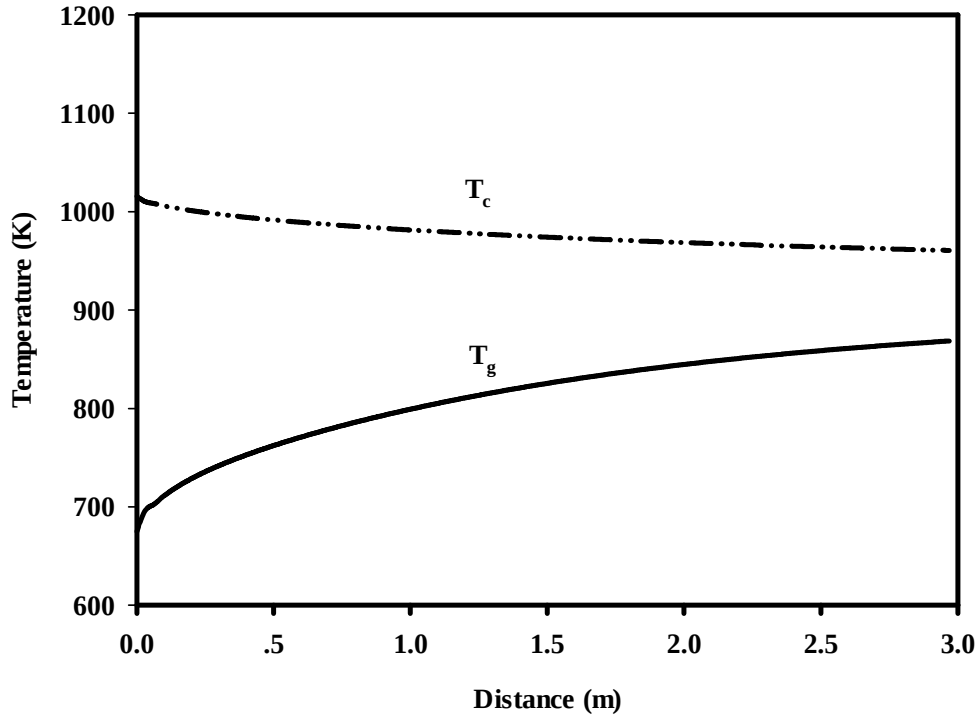


**Figure 7.5** Temperature of gas and catalyst phases along the downer reactor.

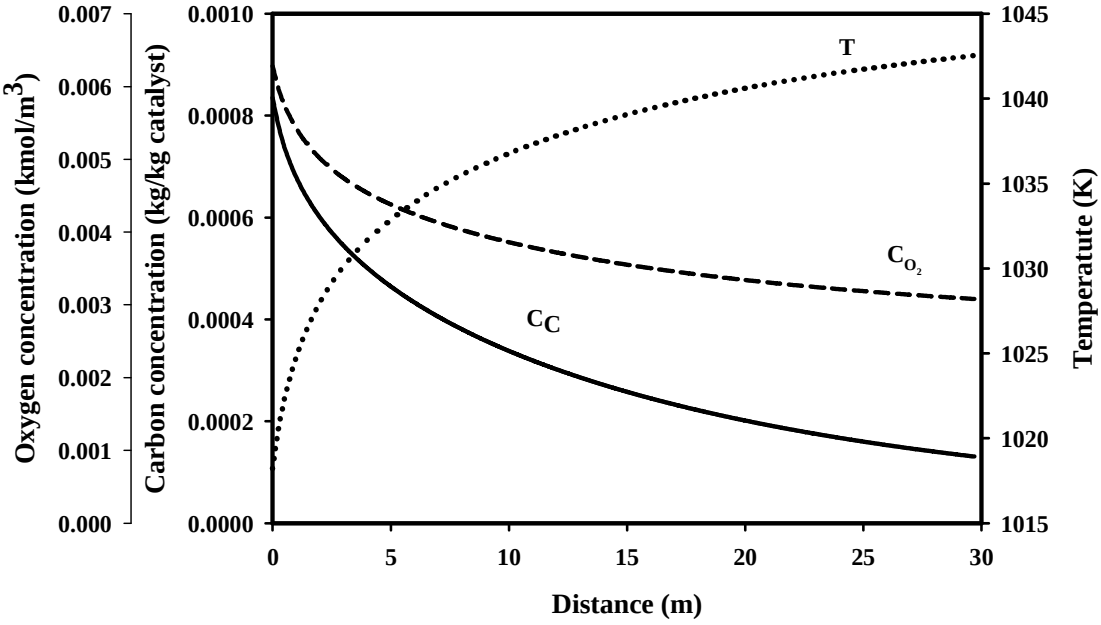


**Figure 7.6** Carbon concentration, oxygen concentration, and temperature along the riser regenerator.

In the operation of the FCC process, the main parameter that has a major effect on the performance and operation is the catalyst-to-oil (CTO) ratio. This ratio indicates the amount of catalyst used at the constant feedstock and affects to the intense of reactions as well as the heat balance of the system.

## 7.5.2 The effect of catalyst-to-oil ratio (CTO)

In this work, the value of CTO ratio that keeps this system run stably ranges from 10 to 20. The simulation results indicate that the increasing of CTO ratio enables the higher conversion resulting in higher yields of the three products (Figure 7.7 to Figure 7.10). Although the yield of gasoline is increased as increasing of CTO ratio, this trend occurs at near inlet of downer only. At the outlet of downer, the yields of gasoline are almost the same. Moreover, they are likely to be reduced beyond 3 m. of the downer reactor. This is different from the yields of $C_1$-$C_4$ gases and coke that increase as CTO ratio increases but their trends always increase. This is because the higher CTO ratio, the higher gasoline would be cracked to be $C_1$-$C_4$ gases and coke.

**Table 7.7** Some important variables at different CTO.

| | **CTO=10** | **CTO=15** | **CTO=20** |
|---|---|---|---|
| $G_{s,rxt}$ (kg/m$^2$s) | 70.73 | 106.10 | 141.47 |
| $G_{s,reg}$ (kg/m$^2$s) | 282.94 | 424.41 | 565.88 |
| $C_{C,rxt,out}$ (kg/kg catalyst) | 0.0051 | 0.0037 | 0.0030 |
| $C_{C,reg,0}$ (kg/kg catalyst) | 0.00130 | 0.00094 | 0.00083 |

The effects of the increased CTO ratio on temperature of both phases are shown in Figure 7.11. It can be seen that increasing of the CTO ratio affects to the heat balance of the system. Though yield of coke is higher at high CTO ratio, the higher amount of catalyst causes the lower amount of carbon content on spent catalyst flowing to the riser regenerator (Table 7.7). Therefore, the temperature of regeneration in the case of high CTO ratio, i.e., CTO = 20 is lower than that of lower CTO ratio. However, the high catalyst flow rate also affects to the temperature of the reaction. As it is indicated in Figure 7.13 that at CTO=10, catalyst accommodate the

highest temperature than other cases but the temperature of gas is the lowest. This is because the lower catalyst flow rate carries lower heat for providing to the gas phase.

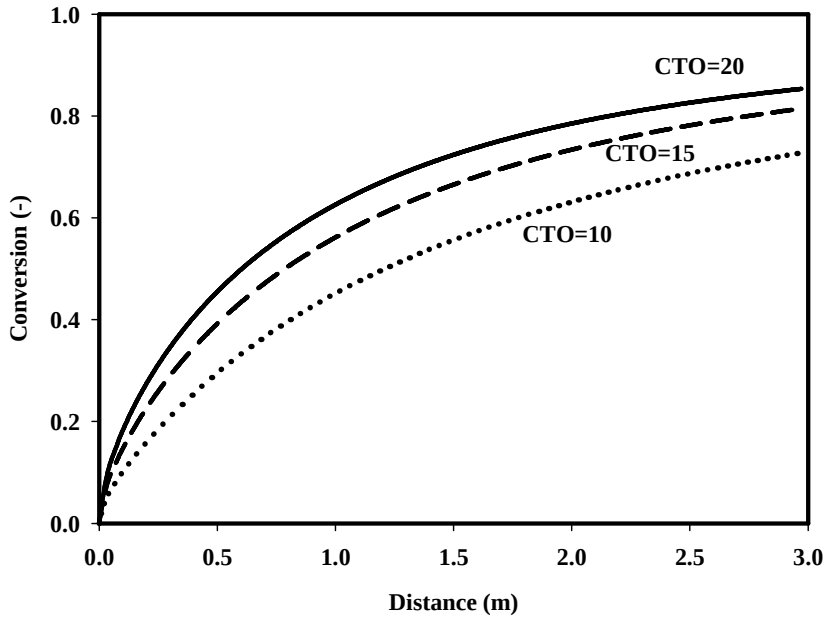


**Figure 7.7** Conversion of gas oil along the length of the downer reactor at different CTO ratio.

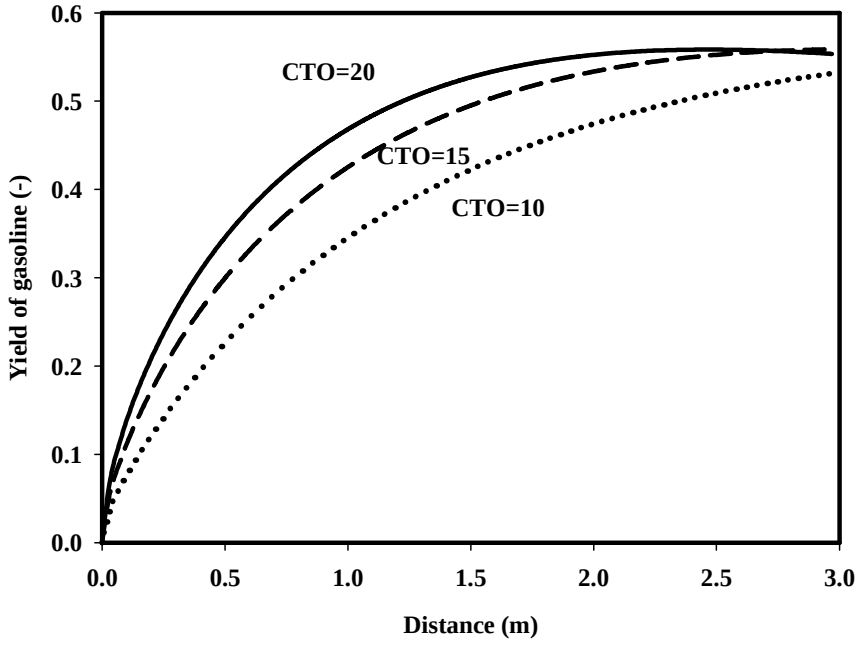


**Figure 7.8** Yield of gasoline along the length of the downer reactor at different CTO ratio.

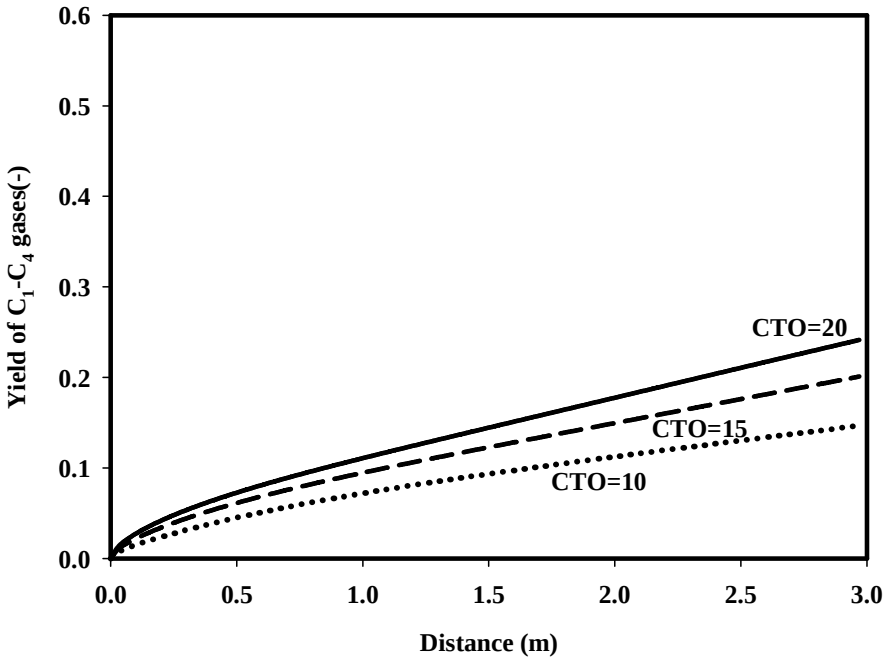


**Figure 7.9** Yield of $C_1$-$C_4$ gases along the length of the downer reactor at different CTO ratio.

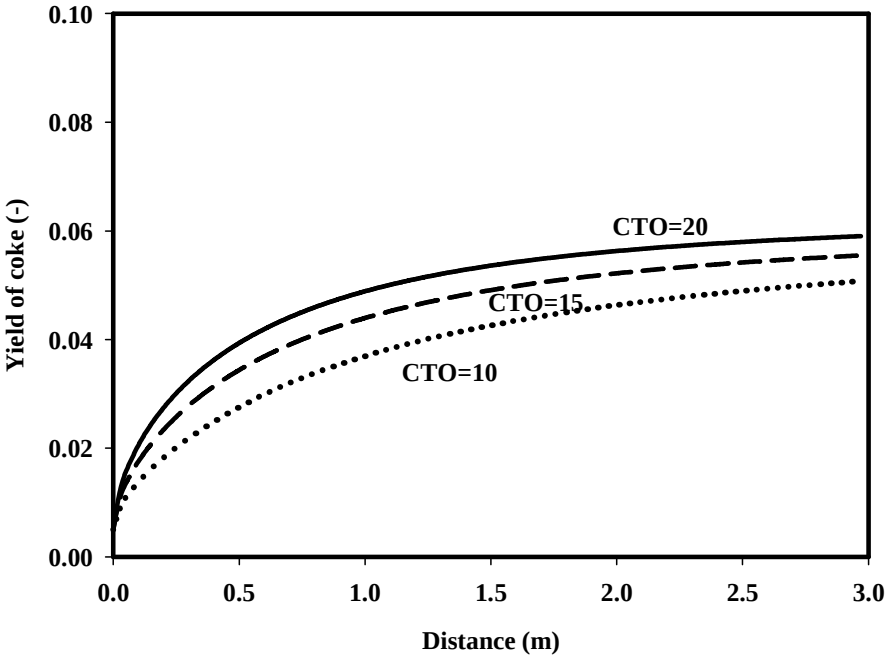


**Figure 7.10** Yield of coke along the length of the downer reactor at different CTO ratio.

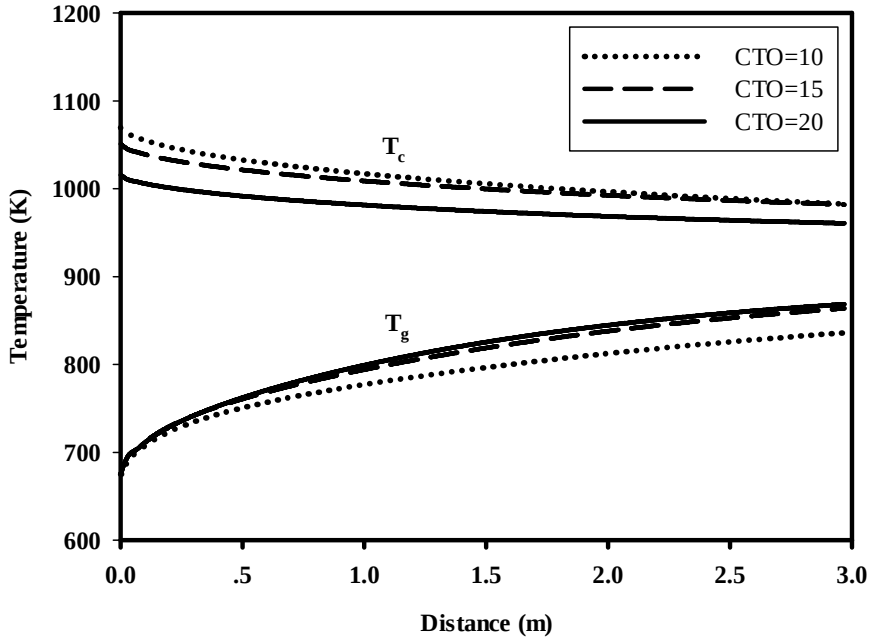


**Figure 7.11** Temperatures of gas and catalyst along the length of downer reactor at different CTO ratio.

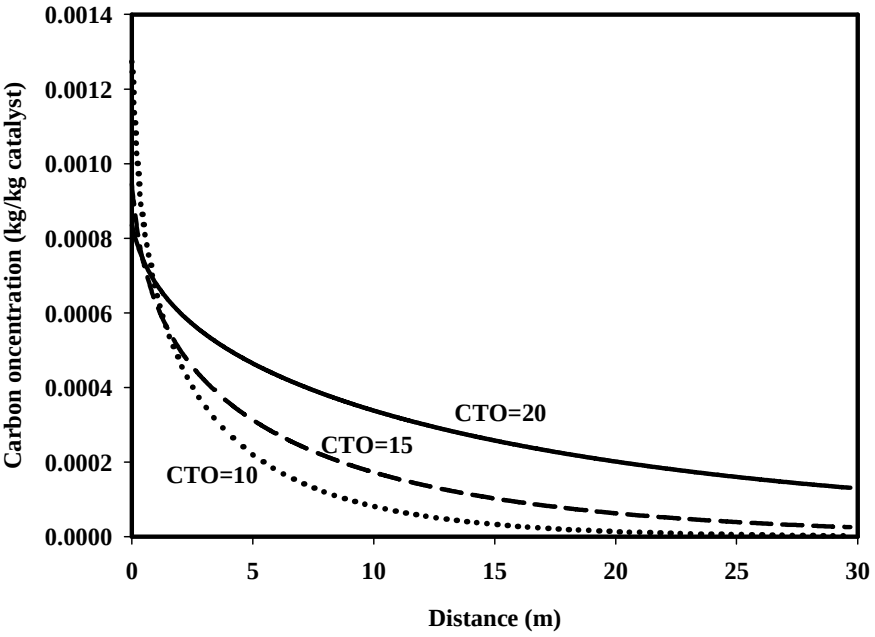


**Figure 7.12** Carbon concentration along the length of riser regenerator at different CTO ratio.

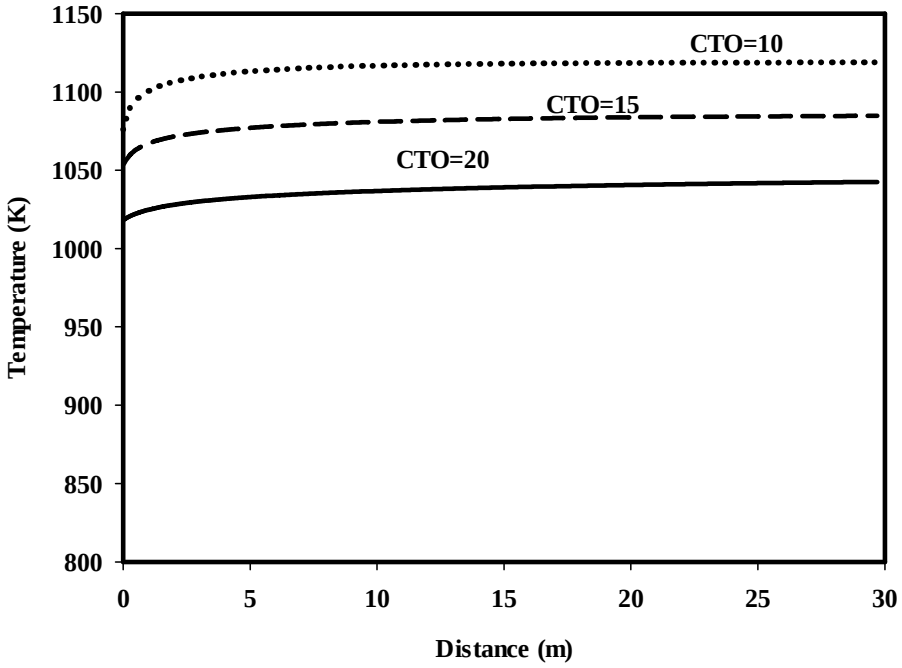


**Figure 7.13** Temperature along the length of riser regenerator at different CTO ratio.

## 7.6 Conclusions

This work presents the theoretical analysis of an integrated system between a downer reactor and riser regenerator. The model used for simulation consists of the hydrodynamic model and reaction kinetics of both the downer reactor and riser regenerator. From simulation studied, the ranges of catalyst to oil (CTO) ratio that can maintain heat balance of the system are 10 to 20. However, the catalyst to oil (CTO) ratio equal to 20 is the most suitable for operating for this integrated system as this ratio provides the satisfying gasoline yield and keep the regeneration temperature in the acceptable range (should not over 1100 K). The results obtained from this study enable the better understanding on the complex integrated process of the downer reactor and the riser regenerator and can be used for optimal design the FCC process with this type of reactor and regenerator.

# CHAPTER VIII

# CONCLUSIONS AND RECOMMENDATIONS

## 8.1 Conclusions

The aim of this study is to design and analyze the performance of a fluid catalytic cracking process for gasoline production. Generally, the fluid catalytic cracking process includes two main units; a reactor and a regenerator. Therefore, this work accommodates the investigation on both units. In order to design and evaluation of the performance, the mathematical models of each unit were used and validated against the experimental data that are available in the literature. In this work, the issue of the work is separated into three parts; an analysis of a downer-type regenerator using a systematic model-based approach, a numerical analysis of FCC catalyst regeneration via steam gasification and burning reaction in a downer-type regenerator, and the theoretical analysis of a downer reactor and a riser regenerator integrated system. The conclusions in each part are listed in the following section.

### 8.1.1 A systematic model-based analysis of a downer-type regenerator in fluid catalytic cracking processes

In this part, a systematic model-based analysis approach was adapted to evaluate the performance of a novel downer regenerator. The one-dimensional model for a downer regenerator taking into account the hydrodynamic characteristics, and kinetics of the FCC catalyst regeneration as well as mass and energy balances were used in the approach. Five scenarios were selected to perform a sensitivity analysis including effect of flow rate ratio of recycled to spent catalysts, effect of superficial gas velocity, effect of spent catalyst flow rate, effect of carbon content on the spent catalyst and effect of spent catalyst temperature. The simulation results showed that the efficient operation of the downer regenerator is mainly influenced by parameters that affect to the temperature of the downer regenerator e.g., recycled catalyst flow

rate, carbon content on the spent catalyst and spent catalyst temperature. These parameters should be carefully selected as they have the most significant effect on a regeneration process. High regeneration temperature could deactivate the catalyst permanently but low temperature operation lowers the regeneration performance. The results obtained from this model-based analysis are beneficial for an understanding of the downer regenerator, leading to an optimal design and efficient operation of the FCC process.

### 8.1.2 Numerical analysis of the FCC catalyst regeneration via steam gasification and burning reaction in a downer-type regenerator

This work performed an investigation of an approach for reducing the high temperature of regeneration caused by burning of high coke content. The steam gasification reaction was selected as the approach due to an endothermic nature. In this work, the steam gasification reaction was considered together with the burning reaction. The investigation was done by simulation study using one dimensional hydrodynamic model, material and energy balances and kinetics of reactions. The simulation results show that steam gasification and burning reaction can well reduce the amount of coke deposited on the catalyst surface but the rate of gasification reaction is quite slow compared to the rate of burning reaction. Although the rate of gasification reaction of E-cat catalyst currently used in FCC process is quite slow, the gasification promotion additive was successfully developed. Therefore, the gasification reaction is the promising approach for reduction of the coke on catalyst and the regenerator temperature. Moreover, this reaction gives the valuable hydrogen as a by-product.

### 8.1.3 Theoretical analysis of a downer reactor and riser regenerator integrated system in FCC process

This work presents the theoretical analysis of an integrated system between a downer reactor and a riser regenerator. In order to design and evaluate the

performance, the one-dimensional model of both units were used for simulation studies. The models consist of the hydrodynamic model and reaction kinetics of both the downer reactor and riser regenerator. The results from the simulation reveal that catalyst-to-oil (CTO) ratio that can maintain heat balance of the system and keep the system running efficiently are in the ranges of 10 to 20. However, the CTO ratio equal to 20 is the most suitable for operating for this integrated system as this ratio provides the satisfying gasoline yield and control the regeneration temperature in the acceptable range (should not over 1100 K). The results obtained from this study enable the better understanding on the complex integrated process of the downer reactor and the riser regenerator and can be used for optimal design the FCC process with this type of reactor and regenerator.

## 8.2 Recommendations

The recommendations related to this work are list below:

1. In the operation of the downer regenerator, there is a recycled stream that brings the regenerated catalyst back to the inlet of downer regenerator again. In practical, air is used for transportation of the regenerated catalyst. This would enable the recycled pipe to be another regenerator as burning reactions would proceed. Therefore, if air is used for transportation of catalyst, this point should be aware of. However, in this work we assumed that the transportation media is the flue gas derived from burning of the coke in the downer regenerator which contains low oxygen. Therefore, no burning reactions proceed in the recycled pipe.

2. In the operation of the downer regenerator and the integrated system, the effect of the ancillary unit such as the cyclones, the stripper, and the separators should be included since they might have some effects on the operation of the system.

# REFERENCES


Abul-Hamayel, M.A. Comparison of downer and riser based fluid catalytic cracking process at high severity condition : A pilot plant study. Petroleum science and technology 22 (2004) : 475-490.

Abul-Hamayel, M.A., Aitani, A.M., and Saeed, M.R. Enhancement of propylene production in a downer FCC operation using a ZSM-5 additive. Chemical Engineering & Technology 28 (2005) : 923-929.

Affum et al. Modeling Conversion in a fluid catalytic cracking regenerator in petroleum refining. Research Journal of Applied Sciences, Engineering and Technology 3 (2011) : 533-539.

Ahari, J.S., Farshi, A., and Forsat, K. A mathematical modeling of the riser reactor in industrial FCC unit. Petroleum & Coal 50 (2008) : 15-24.

Ahsan, M. Computational fluid dynamics (CFD) prediction of mass fraction profiles of gas oil and gasoline in fluid catalytic cracking (FCC) riser. Ain Shams Engineering Journal 3 (2012) : 403-409.

Alaradi, A.A., and Rohani, S. Identification and control of a riser-type FCC unit using neural networks. Computers and Chemical Engineering 26 (2002) : 401-421.

Ali, H., Rohani, S., and Corriou, J.P. Modeling and control of a riser-type fluid catalytic cracking (FCC) unit. Transactions of the Institution of Chemical Engineers 75 (1997) : 401-412.

Ancheyta-Juarez, J., Lopez-Isunza, F., and Aguilar-Rodriguez, E. 5-lump kinetic model for gas oil catalytic cracking. Applied Catalysis A : General 177 (1999) : 227-235.

Arbel, A., Huang, Z., Rinard, I.H., and Shinnar, R. Dynamic and control of fluidized catalytic crackers 1. Modeling of the current generation of FCC's. Industrial & Engineering Chemistry Research 34 (1995) : 1288-1243.

Araujo-Monroy, C., and Lopez-Isunza, F. Modeling and Simulation of an Industrial Fluid Catalytic Cracking Riser Reactor Using a Lump-Kinetic Model for a Distinct Feedstock. Industrial & Engineering Chemistry Research 45 (2005) : 120-128.

Avidan, A.A., and Shinnar, R.. Development of catalytic cracking technology. A lesson in chemical reactor design. Industrial & Engineering Chemistry Research 29 (1990) : 931-942.

Bai, D., Zhu, J.X., Jin, Y., and Yu, Z. Novel designs and simulations of FCC riser regeneration. Industrial & Engineering Chemistry Research 36 (1997) : 4543-4548.

Bai, D., Zhu, J.X., Jin, Y., and Yu, Z. Simulation of FCC catalyst regeneration in a riser regenerator. Chemical Engineering Journal 71 (1998) : 97-109.

Bolkan-Kenny, Y.G., Pugsley, T.S., and Berruti, F. Computer simulation of the performance of fluid catalytic cracking risers and downers. Industrial & Engineering Chemistry Research 33 (1994): 3043-3052.

Bollas, G.M., Lappas, A.A., Iatridis, D.K., and Vasalos, I.A. Five-lump kinetic model with selective catalyst deactivation for the prediction of the product selectivity in the fluid catalytic cracking process. Catalysis Today 127 (2007) : 31-43.

Bollas, G.M., Vasalos, I.A., Lappas, A.A., Latridis, D.K., Voutetakis, S.S., and Papadopoulou , S.A. Integrated FCC riser-regenerator dynamics studied in a fluid catalytic cracking pilot plant. Chemical Engineering Science 62 (2007) : 1887-1904.

Cerqueira, H.S., Biscaia, E.C.Jr., and Souza-Aguiar, E.F. Mathematical Modeling of Deactivation by Coke Formation in the Cracking of Gasoil Catalyst Deactivation 111 (1997) : 303-310.

Chen, H., Li, H., and Kwauk, M. Two-phase structure in a high-density downer. Powder Technology 158 (2005) : 115-123.

Corma, A., Sauvanaud, A., Doskocil, E., and Yaluris, G. Coke steam reforming in FCC regenerator: A new mastery over high coking feeds. Journal of Catalysis 279 (2011) : 183-195.

Coxson, P.G., and Bischoff, K.B. Lumping Strategy. 1. Introductory Techniques and Applications of Cluster Analysis. Industrial & Engineering Chemistry Research 26 (1987) : 1239-1248.

Cristea, M.V., Agachi, S.P., and Marinoiu, V. Simulation and model predictive control of a UOP fluid catalytic cracking unit. Chemical Engineering and Processing 42 (2003) : 67-91.

Das, A.K., Baudrez, E., Marin, G.B., and Heyderickx, G.J. Three-Dimensional Simulation of a Fluid Catalytic Cracking Riser Reactor. Industrial & Engineering Chemistry Research 42 (2003) : 2602-2617.

Deng, R., Liu, H., Gao, L., Wang, L., Wei, F., and Jin, Y. Study on the FCC process in a novel riser−downer−coupling reactor (II): Simulation and hot experiments. Industrial & Engineering Chemistry Research 44 (2005): 1446-1453.

Deng R., Liu H., Wei F., and Jin Y. Axial flow structure at the varying superficial gas velocity in a downer reactor. Chemical Engineering Journal 99 (2004) : 5-14.

Deng, R., Wei, F., Jin, Y., Zhang, Q., and Jin, Y. Experimental study of the deep catalytic cracking process in a downer reactor. Industrial & Engineering Chemistry Research 41 (2002): 6015-6019.

Derouin, C., Nevicato, D., Forissier, M., Wild, G., and Bernard, J.R. Hydrodynamics of riser units and their impact on FCC operation. Industrial & Engineering Chemistry Research 36 (1997) : 4504-4515.

Dupain, X., Gamas, E.D., Madon, R., Kelkar, C.P., Makkee, M., and Moulijn, J.A. Aromatic gas oil cracking under realistic FCC conditions in a microriser reactor. Fuel 82 (2003) : 1559-1569.

Gauthier, T., Bayle, J., and Leroy, P. FCC: Fluidization phenomena and technologies. Oil & Gas Science and Technology - Rev. IFP 55 (2000) : 187–207.

Fernandes, J.L., Pinheiro, C.I.C., Oliveira, N.M.C., Neto, A.I., and Ramoa, R.F. Steady state multiplicity in an UOP FCC unit with high-efficiency regenerator. Chemical Engineering Science 62 (2007) : 6308-6322.

Fernandes, J. L., Verstraete, J. J., Pinheiro, C.I.C., and Oliveira N.M.C. Dynamic modelling of an industrial R2R FCC unit. Chemical Engineering Science 62 (4) (2007) : 1184-1198.

Fujiyama, Y., Redhwi, H.H., Aitani, A.M., Saeed, M.R., and Dean, C.F, Demonstration plant for new FCC technology yields increased propylene. Oil & Gas Journal 103 (2005) : 54-58.

Gupta, R.K., Kumar, V., and Srivastava, V.K. A new generic approach for the modeling of fluid catalytic cracking (FCC) riser reactor. Chemical Engineering Science 62 (2007) : 4510-4528.

Han, I.S., Chung, C.B., and Riggs, J.B. Modeling of a fluidized catalytic cracking process. Computers and Chemical Engineering 24 (2000) :1681-1687.

Han, I.-S. and Chung, C.-B. Dynamic modeling and simulation of a fluidized catalytic cracking process. Part I: Process modeling. Chemical Engineering Science 56 (2001) : 1951-1971.

Han, I.-S. and Chung, C.-B. Dynamic modeling and simulation of a fluidized catalytic cracking process. Part II: Properties estimation and simulation. Chemical Engineering Science 56 (2001) : 1973-1990.

Han, I.-S., Riggs, J. B., and Chung, C.-B. Modeling and optimization of a fluidized catalytic cracking process under full and partial combustion modes. Chemical Engineering and Processing: Process Intensification 43 (2004) : 1063-1084.

Hernandez-Barajas, J.R., Vazquez-Roman, R., and Salazar-Sotelo, D. Multiplicity of steady states in FCC units: effect of operating conditions. Fuel 85 (2006) : 849-859.

Heydari, M., Ebrahim, H.A., and Dabir, B. Modeling of an Industrial Riser in the Fluid Catalytic Cracking Unit. American Journal of Applied Sciences 7 (2010) : 221-226.

Hongjun, Y., Chunming, X., Jinsen, G., Zhichang, L., and Pinxiang, Y. Nine lumped kinetic models of FCC gasoline under the aromatization reaction conditions. Catalysis Communications 7 (2006) : 554-448.

Hsing, H., and Mudra IV, J. Fluid catalytic cracking process yielding hydrogen. United States Patent 5362380, 1994.

Jacob, S.M., Gross, B., Voltz, S.E., and Weekman, V.W. A lumping and Reaction Scheme for Catalytic Cracking AIChE Journal 22 (1976) : 701-713.

Jia, C., Rohani, S., and Jutan, A. FCC unit modeling, identification and model predictive control, a simulation study. Chemical Engineering and Processing: Process Intensification 42 (2003) : 311-325.

Jin, Y., Zheng, Y., and Wei, F. In J. Grace, J. Zhu, H. de Lasa (ed.), Circulating Fluidized Bed Technology VII, pp.40. Niagara Falls : Canadian Society for Chemical Engineers, 2002.

Juarez, J.A., Isunza, F.L., and Rodriguez, E.A. 5-Lump kinetic model for gas oil catalytic cracking. Applied Catalysis A: General 177 (1999) : 227-235.

Kim, S.W., Namkung, W., and Kim, S.D. Solid behavior in freeboard of FCC regenerator. Journal of Chemical Engineering of Japan 33 (2000) : 78-85.

Lan, X., Xu, C., Wang, G., Wu, L., and Gao, J. CFD modeling of gas-solid flow and cracking reaction in two-stage riser FCC reactors. Chemical Engineering Science 64 (2009) : 3847-3858.

Larocca, M., Ng, S., and de Lasa, H. Fast catalytic cracking of heavy gas oils: modeling coke deactivation Industrial & Engineering Chemistry Research 29 (1990) : 171-180.

Lee, L., Chen, Y., Huang, T. and Pan, W. Four lump kinetic model for fluid catalytic cracking process. The Canadian Journal of Chemical Engineering 67 (1989) : 615-619.

Letzsch, W. Fluid catalytic cracking. In Jones, D.S.J., and Pujado, P.R., Handbook of Petroleum Processing, pp.239-286. Dordrecht, Netherlands : Springer, 2008.

Liu, H., Deng, R., Gao, L., Wei, F., and Jin, Y. Study on the FCC process in a novel riser-downer-coupling reactor (I): hydrodynamics and mixing behaviors. Industrial & Engineering Chemistry Research 44 (2005) : 733-741.

Liu et al. Study on the FCC process of a novel riser-downer coupling reactor (III): Industrial trial and CFD modeling. Industrial & Engineering Chemistry Research 47 (2008): 8582-8587.

Lopes, G.C., Rosa, L.M., Mori, M., Nunhez, J.R., and Martignoni, W.P. Three-dimensional modeling of fluid catalytic cracking industrial riser flow and reactions. Computers & Chemical Engineering 35 (2011) : 2159-2168.

Lui, F., Wei, F., Zheng, Y., and Jin, Y. CFD simulation of fluid catalytic cracking in downer reactors China Particuology 4 (2006) : 160-166.

Luo, L., Rainer, D., and Gonzalez, J.A. Laboratory deactivation testing for the stability of FCC CO combustion promoters. Applied Catalysis B: Environmental 72 (2007) : 212-217.

Namkung, W., Kim, S.W., and Kim, S.D. Hydrodynamic characteristics of a FCC regenerator. Korean Journal of Chemical Engineering 20 (2003) : 110-115.

Ou-guan, X., Hong-ye, S., Sheng-jing., M., and Jian, C. 7-lump kinetic model for residual oil catalytic cracking. Journal of Zhejiang University SCIENCE A 7 (2006) : 1932-1941.

Pitault, I., Nevicato, D., Forissier, M., and Bernard, J.R. (1994). Kinetic model on a molecular description for catalytic cracking of vacuum gas oil. Chemical Engineering Science 49 (1994) : 4249-4262.

Qi, X.B., Zhang, H., and Zhu, J. Solids concentration in the fully developed region of circulating fluidized bed downers. Powder Technology 183 (2008) : 417–425.

Ramachandran, R., Rangaiah, G.P., and Lakshminarayanan, S. Data analysis, modeling and control performance enhancement of an industrial fluid catalytic cracking unit. Chemical Engineering Science 62 (2007) : 1958-1973.

Roman, R., Nagy, Z.K., Cristea, M.V. and Agachi, S.P. Dynamic modelling and nonlinear model predictive control of a Fluid Catalytic Cracking Unit. Computers & Chemical Engineering 33 (2009) : 605-617.

Sadeghbeigi, R. Fluid catalytic cracking handbook. Houston, Texas : Gulf Publishing Company, 2000.

Shaikh, A.A., Al-Mutairi, E.M., and Ino T. Modeling and simulation of a downer-type HS-FCC unit. Industrial & Engineering Chemistry Research 47 (2008) : 9018-9024.

Takatsuka, T., Sato, S., Morimoto, Y., and Hashimoto, H. A reaction model for fluidized-bed catalytic cracking of residual oil. International Chemical Engineering 27 (1987) : 107-116.

Talman, J.A., and Reh, L. An experimental study of fluid catalytic cracking in a downer reactor. Chemical Engineering Journal 84 (2001) : 517-523.

Theologos, K.N., and Markatos, N.C. Advanced modeling of fluid catalytic cracking riser-type reactors. AIChE Journal 39 (1993) : 1007-1017.

Theologos, K.N., Nikou, I.D., Lygeros, A.I., and Markotos, N.C. Simulation and design of Fluid-Catalytic Cracking riser-type reactors. Computers & Chemical Engineering 20 (1996) : S757-S762.

Wang, Z., Bai, D., and Jin, Y. Hydrodynamics of cocurrent downflow circulating fluidized bed (CDCFB). Powder Technology 70 (1992) : 271-275.

Wang, G.X., Lin, S.X., Mo, W.J., Peng, C.L., and Yang G.H. Kinetics of combustion of carbon and hydrogen in carbonaceous deposits on zeolite-type cracking catalysts. Industrial & Engineering Chemistry Process Design and Development 25 (1986) : 626-630.

Weekman, V.W. A model of catalytic cracking conversion in fixed, moving, and fluid-bed reactors. Industrial & Engineering Chemistry Process Design and Development 7 (1968) : 90-95.

Weekman, V.W., and Nace, D.M. Kinetics of catalytic cracking selectivity in fixed, moving, and fluid bed reactors. AIChE Journal 16 (1970) : 397-404.

Weisz, P.B. Combustion of carbonaceous deposits within porous catalyst particles III. The $CO_2$/CO product ratio. Journal of Catalysis 6 (1966) : 425-430.

Wu, C., Cheng, Y., Ding, Y., and Jin, Y. CFD-DEM simulation of gas-solid reacting flows in fluid catalytic cracking (FCC) process. Chemical Engineering Science 64 (2010) : 542-549.

Wu, C., Cheng, Y., and Jin Y. Modeling the hydrodynamics in a coupled high-density downer to riser reactor. Powder Technology 181 (2008) : 255-265.

Wu, C., Cheng, Y., and Jin, Y. Downer-to-riser coupling technique for petroleum refining. Chemical Engineering & Technology 32 (2009) : 482-491.

Wu, C., Cheng, Y., and Jin, Y. Understanding Riser and Downer Based Fluid Catalytic Cracking Processes by a Comprehensive Two-Dimensional Reactor Model. Industrial & Engineering Chemistry Research 48 (2009) : 12–26.

Yaw, C.L. Chemical properties handbook. New York, NY : McGraw-Hill companies, 1999.

Zhang, H. Hydrodynamics of gas-solids downflow fluidized bed (downer) reactor. Doctoral dissertation, Faculty of Graduate Studies, The University of Western Ontario, 1999.

Zheng, Y., Cheng, Y., Wei, F., and Jin, Y. (2002). CFD simulation of hydrodynamics in downer reactors. Chemical Engineering Communications 189 (2002) : 1598-1610.

Zhu, J.-X., Yu, Z.-Q., Jin, Y., Grace, J.R., and Issangya, A. Cocurrent downflow circulating fluidized bed (downer) reactors — A state of the art review. The Canadian Journal of Chemical Engineering 73 (1995) : 662-677.

Zimmermann, S., and Taghipour, F. CFD modeling of the hydrodynamics and reaction kinetics of FCC fluidized-bed reactors. Industrial & Engineering Chemistry Research 44 (2005) : 9818-9827.

# APPENDICES

# APPENDIX A

# PROPERTIES ESTIMATION

## A.1 Hydrocarbon properties

All equations for hydrocarbon properties estimation used in this work obtain from Han and Chung, 2001.

### A.1.1 Volume average boiling temperature (K)

$$T_{\mathrm{VABP}} = 0.2\left(T_{10} + T_{30} + T_{50} + T_{70} + T_{90}\right) \tag{A.1.1}$$

### A.1.2 Molal average boiling temperature (K)

$$T_{\mathrm{MABP}} = T_{\mathrm{VABP}} - 0.5556\exp\left[-0.5638 - ... \right. \\ \left. 0.0080\left(1.8T_{\mathrm{VABP}} - 491.67\right)^{0.6667} + 3.0473\left(Sl\right)^{0.3333}\right] \tag{A.1.2}$$

### A.1.3 Mean average boiling point temperature (K)

$$T_{\mathrm{MeABP}} = T_{\mathrm{VABP}} - 0.5556\exp\left[-0.9440 - ... \right. \\ \left. 0.0087\left(1.8T_{\mathrm{VABP}} - 491.67\right)^{0.6667} + 2.9972\left(Sl\right)^{0.3333}\right] \tag{A.1.3}$$

where $\left(Sl\right) = 0.0125\left(T_{90} - T_{10}\right)$

### A.1.4 Specific gravity

$$S_g = \frac{141.5}{\left(\mathrm{API}\right) + 131.5} \tag{A.1.4}$$

### A.1.5 Watson characterization factor

$$K_f = \frac{\left(1.8T_{\text{MeABP}}\right)^{1/3}}{S_g} \tag{A.1.5}$$

### A.1.6 Molecular weight of gas oil and gasoline lump

$$M_w = 42.965\Big[\exp\left(2.097\times10^{-4}T_{\text{MeABP}} - 7.787S_g + \ldots\right.$$
$$\left.2.085\times10^{3}T_{\text{MeABP}}S_g\right)\Big]\times T_{\text{MeABP}}^{1.26007}S_g^{4.98308} \tag{A.1.6}$$

### A.1.7 Average molecular weight

$$M_{wm} = 1/\sum_{i=1}^{n}\left(\frac{y_i}{M_{wi}}\right) \tag{A.1.7}$$

### A.1.8 Gas phase heat capacity of $C_1$-$C_4$ gases lump

$$C_{p,gs} = 0.2457 + 5.3\times10^{-3}T - 2.1527\times10^{-6}T^2 \tag{A.1.8}$$

### A.1.9 Liquid phase heat capacity of gas oil lump

$$C_{p,lg} = \alpha_1 + \alpha_2 T + \alpha_3 T^2 \tag{A.1.9}$$

where

$$\alpha_1 = -4.90383 + \left(0.099319 + 0.104281S_g\right)K_f + \frac{\left(4.814066 - 0.194833K_f\right)}{S_g}$$

$$\alpha_2 = \left(7.53624\times10^{-4}\right)\left(1.0 + 0.82463K_f\right)\times\left(1.12172 - \frac{0.27634}{S_g}\right)$$

$$\alpha_3 = \left(-1.356523\times10^{-7}\right)\left(1.0 + 0.82463K_f\right)\times\left(2.9027 - \frac{0.70958}{S_g}\right)$$

## A.1.10 Gas phase heat capacity of gas oil and gasoline lump

$$C_p = \beta_1 + \beta_2 T + \beta_3 T^2 \tag{A.1.10}$$

where

$$\beta_1 = -1.492343 + 0.124432 K_f + \beta_4 \times \left(1.23519 - \frac{1.04025}{S_g}\right)$$

$$\beta_2 = \left(-7.53624 \times 10^{-4}\right)\left[2.9247 - \left(1.5524 - 0.05543 K_f\right) K_f + \beta_4 \left\{\left(6.0283 - \frac{5.0694}{S_g}\right)\right\}\right]$$

$$\beta_3 = \left(1.356523 \times 10^{-6}\right)\left(1.6946 + 0.0884 \beta_4\right)$$

$$\beta_4 = \left[\left(\frac{12.8}{K_f} - 1.0\right)\left(1.0 - \frac{10.0}{K_f}\right) \times \left(S_g - 0.885\right)\left(S_g - 0.70\right)\left(10^4\right)\right]^2 ,$$

for $10.0 < K_f < 12.8$

Otherwise;

$\beta_4 = 0$

## A.1.11 Mean heat capacity of *n* component mixture

$$C_{pm} = \frac{\int_{T_{ref}}^{T} \sum_{i=1}^{n} y_i C_{pi}(T)\, dT}{T - T_{\text{ref}}} \tag{A.1.11}$$

## A.1.12 Mean viscosity of gas phase hydrocarbon lumps

$$\mu_g = \mu_{pr} \mu_{pc} = 3.515 \times 10^{-8} \mu_{pr} \frac{\sqrt{M_{wm} P_{pc}^{2/3}}}{T_{pc}^{1/6}} \tag{A.1.12}$$

The availability ranges are:

$0.75 < T_{pr} = \frac{T}{T_{pc}} < 0.3$ , and $0.01 < P_{pr} = \frac{P}{P_{pc}} < 0.2$

where

$$\mu_{pr} = 0.435 \exp\left[\left(1.3316 - T_{pr}^{0.6921}\right) P_{pr}\right] T_{pr} + 0.0155$$

### A.1.13 Critical properties of hydrocarbon

$$T_{pc} = 17.1419\left[\exp\left(-9.3145\times10^{-4} T_{\text{MeABP}} - 0.5444 S_g + \ldots \right.\right. \quad \text{(A.1.13)}$$
$$\left.\left. 6.4791\times10^{-4} T_{\text{MeABP}} S_g\right)\right] \times T_{\text{MeABP}}^{0.81067} S_g^{0.53691}$$

$$P_{pc} = 4.6352\times10^{6}\left[\exp\left(-8.505\times10^{-3} T_{\text{MeABP}} - 4.8014 S_g + \ldots \right.\right. \quad \text{(A.1.14)}$$
$$\left.\left. 5.749\times10^{-3} T_{\text{MeABP}} S_g\right)\right] \times T_{\text{MeABP}}^{-0.4844} S_g^{4.0846}$$

### A.1.14 Heat of vaporization of gasoil (available in the ranges of molecular weight from 200 to 400)

$$\Delta H_{vlg} = 0.3843 T_{\text{MABP}} + 1.0878\times10^{3} \exp\left(\frac{-M_{wm}}{100}\right) - 98.153 \quad \text{(A.1.15)}$$

### A.1.15 Vapor pressure of gas oil

$$P_g = 0.133322\times10^{(3000.538\omega - 6.761560)/(43\omega - 0.987672)} \quad \text{(A.1.16)}$$

for $\omega > 0.0022$

$$P_g = 0.133322\times10^{(2663.129\omega - 5.994296)/(95.76\omega - 0.972546)} \quad \text{(A.1.17)}$$

for $0.0013 \le \omega \le 0.0022$

$$P_g = 0.133322\times10^{(2770.085\omega - 6.412631)/(36\omega - 0.989679)} \quad \text{(A.1.18)}$$

for $\omega < 0.0013$

where

$$\omega = \frac{T_{\text{MeABP}}^{*} / T_v - 0.00051606 T_{\text{MeABP}}^{*}}{748.1 - 0.3861 T_{\text{MeABP}}^{*}}$$

$$T_{\text{MeABP}}^{*} = T_{\text{MeABP}} - 1.3889\alpha \times \left(K_f - 12\right) \log\left(0.0098684 P_g\right)$$

$\alpha = 1$ for $\text{T}_{\text{MeABP}} > 477.8\ \text{K}$

$\alpha = 0$ for $\text{T}_{\text{MeABP}} > 333.3\ \text{K}$

$$\alpha = \left(1.8\mathrm{T}_{\mathrm{MeABP}} - 659.7\right)/200 \text{ for } 366.7\,\mathrm{K} \le \mathrm{T}_{\mathrm{MeABP}} \le 477.8\,\mathrm{K}$$

### A.1.16 Three coefficients in Antoine equation for gas oil vapor pressure

In order to evaluate the three coefficients in Antoine equation, the vapor pressures are estimated using the equations A.1.15.1 to A.1.15.3 at three temperatures i.e., $\mathrm{T}_{\mathrm{MeABP}}$, $\mathrm{T}_{\mathrm{MeABP}} - 15$, $\mathrm{T}_{\mathrm{MeABP}} + 15$.

$$F_i\left(A_{lg}, B_{lg}, C_{lg}\right) = \left(T_{vi} + C_{lg}\right)\left[A_{lg} - \log\left(P_{gi}\right)\right] - B_{lg} = 0,\ \ i = 1,2,3 \tag{A.1.19}$$

### A.1.17 Thermal conductivity of hydrocarbons

$$k_g = 1\times10^{-6}\left(1.9469 - 0.374M_{wm} + 1.4815\times10^{-3}M_{wm}^2 + 0.1028T\right) \tag{A.1.20}$$

### A.1.18 Interface heat transfer coefficient between solids and hydrocarbon gases

$$h_p = 0.03\frac{k_g}{d_c^{2/3}}\left[\frac{\left|\bar{\mathrm{V}}_g - \bar{\mathrm{V}}_\mathrm{s}\right|\rho_g\bar{\varepsilon}_g}{\mu_g}\right]^{1/3} \tag{A.1.21}$$

## A.2 Gas properties

### A.2.1 Viscosity of gas (kg/m s)

The mean viscosity of gases can be estimated from the following equation (Han and Chung, 2001):

$$\mu_m = \sum_{i=1}^{n}\mu_i\left\{1 + \sum_{\substack{j=1\\ j\neq1}}^{n}\frac{\left[1+\left(\mu_i/\mu_j\right)^{1/2}\left(M_{wj}/M_{wi}\right)^{1/4}\right]^2}{\sqrt{8}\left[1+M_{wi}/M_{wj}\right]^{1/2}}\frac{f_i}{f_j}\right\}^{-1} \tag{A.2.1}$$

where the viscosities of each species are (Yaw, 1999):

Oxygen : $\mu_{O_2} = 44.224 + 5.6200\times10^{-1}T - 1.1300\times10^{-4}T^2$

Carbon dioxide : $\mu_{CO} = 35.086 + 5.0651\times10^{-1}T - 1.3314\times10^{-4}T^2$

Carbon monoxide : $\mu_{CO_2} = 11.336 + 4.9918\times10^{-1}T - 1.0876\times10^{-4}T^2$

Nitrogen : $\mu_{N_2} = 42.606 + 4.7500\times10^{-1}T - 9.8800\times10^{-5}T^2$

Hydrogen : $\mu_{H_2} = 27.758 + 2.1200\times10^{-1}T - 3.2800\times10^{-5}T^2$

Water : $\mu_{H_2O} = -36.826 + 4.2900\times10^{-1}T - 1.6200\times10^{-5}T^2$

### A.2.2 Enthalpy of formation (kJ/kg mol)

In order to calculate the heat of reaction, the enthalpy of formation is needed. The enthalpies of formation listed below obtain from Han and Chung, 2001.

$$\Delta H_r = \sum\left(n\Delta H_f\right)_{products} - \sum\left(n\Delta H_f\right)_{reactants} \quad \text{(A.2.2)}$$

Coke : $\Delta H_{f,ck} = -4800.22 + 16.1T$

Oxygen : $\Delta H_{f,O_2} = -10364.88 + 34.60T + 0.00055T^2$

Carbon dioxide : $\Delta H_{f,CO_2} = -406909.11 + 43.26T + 0.00575T^2$

Carbon monoxide : $\Delta H_{f,CO} = -118975.04 + 27.61T + 0.00251T^2$

Water : $\Delta H_{f,H_2O} = -252111.38 + 34.39T + 0.000315T^2$

### A.2.3 Heat capacity of gas (J/mol K) (Yaw, 1999)

Oxygen:

$C_{p,O_2} = 29.526 - 8.8999\times10^{-3}T + 3.8083\times10^{-5}T^2 - 3.2629\times10^{-8}T^3 + 8.8607\times10^{-12}T^4$

Carbon dioxide:

$C_{p,CO} = 29.556 - 6.5807\times10^{-3}T + 2.0130\times10^{-5}T^2 - 1.2227\times10^{-8}T^3 + 2.2617\times10^{-12}T^4$

Carbon monoxide:

$C_{p,CO_2} = 27.437 + 4.2315\times10^{-2}T - 1.9555\times10^{-5}T^2 + 3.9968\times10^{-9}T^3 - 2.9872\times10^{-13}T^4$

Nitrogen:

$$C_{p,N_2} = 29.342 - 3.5395\times10^{-3}T + 1.0076\times10^{-5}T^2 - 4.3116\times10^{-9}T^3 + 2.5935\times10^{-13}T^4$$

Hydrogen:

$$C_{p,H_2} = 25.399 + 2.0178\times10^{-2}T - 3.8549\times10^{-5}T^2 + 3.1880\times10^{-8}T^3 - 8.7585\times10^{-12}T^4$$

Water:

$$C_{p,H_2O} = 33.933 - 8.4186\times10^{-3}T + 2.9906\times10^{-5}T^2 - 1.7825\times10^{-8}T^3 + 3.6934\times10^{-12}T^4$$

# APPENDIX B

# LIST OF PUBLICATIONS

## International publications

1. **Chuachuensuk, A.**, Paengjuntuek, W., Kheawhom, S. and Arpornwichanop, A. (2010). Performance of a Downer-Type Regenerator of Fluid Catalytic Cracking Process. Computer Aided Chemical Engineering, 28, page 1369-1374.
2. **Chuachuensuk, A.**, Paengjuntuek, W., Kheawhom, S. and Arpornwichanop, A. (2013). A systematic model-based analysis of a downer regenerator in fluid catalytic cracking processes. Computers & Chemical Engineering, Volume 49, February 2013, page 136-145.
3. **Chuachuensuk, A.**, Paengjuntuek, W., Kheawhom, S. and Arpornwichanop, A. Numerical analysis of the FCC catalyst regeneration via steam gasification and burning reactions in a downer-type regenerator. (in preparation)
4. **Chuachuensuk, A.**, Zhu, J., and Arpornwichanop, A. Theoretical analysis of a downer reactor and riser regenerator integrated system in FCC process. (in preparation)

## International conferences

1. **Chuachuensuk, A.**, Paengjuntuek, W., Kheawhom, S. and Arpornwichanop, A. Performance of a Downer-Type Regenerator of Fluid Cracking Process. In The 20th European Symposium on Computer Aided Process Engineering (ESCAPE-20), June 6-9, 2010, Ischia, Naples, Italy.

2. **Chuachuensuk, A.**, Paengjuntuek, W., Kheawhom, S. and Arpornwichanop, A. Numerical study of the FCC catalyst regeneration via steam gasification and burning reactions in downer-type regenerator. In 6th Asia Pacific

Chemical Reaction Engineering Symposium (APCRE'11), September 18-21, 2011, Beijing, China.

3. **Chuachuensuk, A.**, Zhu, J., and Arpornwichanop, A. Theoretical Analysis of a Downer Reactor and Riser Regenerator Integrated System in FCC process. In Pure and Applied Chemistry International Conference 2013 (PACCON 2013), January 23-25, 2013, Chon Buri, Thailand.

# VITA

Mr. Anon Chuachuensuk was born on October 6, 1985 in Bangkok, Thailand. He received the Bachelor Degree in Chemical Engineering (with first class honours) from Department of Chemical Engineering, Faculty of Engineering, Srinakharinwirot University in 2007. He continued his graduate study in doctoral degree at Control and Systems Engineering Research Center, Department of Chemical Engineering, Faculty of Engineering, Chulalongkorn Universiy in June 2007 and received scholarship from PTT public company limited for four years. During his graduate study, he got the Ph.D. Scholarship for research abroad from the Graduate School of Chulalongkorn University for spending a period of six months at the Particle Technology Research Center (PTRC), Department of Chemical and Biochemical Engineering, Faculty of Engineering, The University of Western Ontario, Canada.